Ângela Marisa Pereira Carvalho

Microfabricated Surfaces for Guided Tissue Regeneration

Dissertação submetida à Faculdade de Engenharia da Universidade do Porto para obtenção do grau de Doutor em Engenharia Biomédica

2018

Supervision:

Professor Doutor Fernando Jorge Monteiro
Faculdade de Engenharia da Universidade do Porto (FEUP);
Instituto de Investigação e Inovação em Saúde, Universidade do Porto (i3S);
Instituto de Engenharia Biomédica, Universidade do Porto (INEB).

Advisor:

Professora Doutora Maria Helena Fernandes
Laboratory for Bone Metabolism and Regeneration, Faculdade de Medicina Dentaria da Universidade do Porto, Portugal (FMDUP)

The work described in this thesis was performed at:

FEUP - Faculdade de Engenharia da Universidade do Porto, Portugal;
INEB - Instituto de Engenharia Biomédica, Universidade do Porto, Portugal;
i3S - Instituto de Investigação e Inovação em Saúde, Universidade do Porto, Portugal;
FMDUP - Laboratory for Bone Metabolism and Regeneration, Faculdade de Medicina Dentaria da Universidade do Porto, Portugal;
OSU - Nanotech West Lab, The Ohio State University, USA;
ICV - Instituto de Cerámica y Vidrio, CSIC, Spain;
IST – Instituto Superior Técnico, Universidade de Lisboa, Portugal.

Financial Support:

This work was supported by FEDER funds through the Programa Operacional Factores de Competitividade (COMPETE) (POCI/01/0145/FEDER/007265) and by Portuguese funds through FCT (Fundação para a Ciência e a Tecnologia) under the Partnership Agreement PT2020 UID/QUI/50006/2013 and in the framework of project BONAMIDI (PTDC/CTM/100120/2008) and A. Carvalho grant (SFRH/BD/87624/2012).

ACKNOWLEDGMENTS

I would like to start by acknowledging my supervisor, Professor Fernando Jorge Monteiro, for his valuable and constructive guidance, encouragement, positivity and contagious good mood.

To Professor Maria Helena Fernandes, from Faculdade de Medicina Dentária da Universidade do Porto, whom without, a great part of my work wouldn't be possible. Thank you for your huge contribution, countless advices and letting me do a great part of my work in your lab. A thank you also to Dr. Pedro Gomes and Dr. João Rodrigues.

To the all Biocomposites team that I thank for all the companionship and joy they brought to work every day. A special thank you to Liliana, Joana and Marta R., for the constant help, cheerfulness and support, from day one ("Nada se cria, nada se perde, tudo se conquista", right?!). My special thanks also to the new friends out of i3S: Catarina, Tatiana, Ana and Filipa.

To Dr. Alejandro Pelaez-Vargas, whom I thank for my preparation for the lab work and for encouraging me to pursue this opportunity.

I would like to express my very great appreciation to Professor Derek Hansford for welcoming me in his team, for all the support and encouragement with my work. And to all the people from the Nanotech West Lab at The Ohio State University, for all the support throughout my stay. Special thanks to Colin for all the help in and out of the lab.

Everyone from Instituto de Cerámica y Vidrio (ICV), who really helped me with during a busy month of work, and a special thanks to Antonio de Aza for being kind enough to receive me in is group for such a short period.

I would also like to thank all the people who assisted me in the course of this work: Ricardo Vidal (BN), Maria Lazaro (b.IMAGE), Paula Magalhães and Tânia Meireles (CCGEN) and Rui Rocha (CEMUP).

To FEUP, INEB and i3S, I wish to acknowledge all the conditions that allowed me to perform my work. To the i3S colleagues and friends, thank you for being present at all the important moments.

I am equally grateful to Fundação para a Ciência e a Tecnologia (FCT) for my FCT grant (SFRH/BD/87624/2012) and project BONAMIDI (PTDC/CTM/100120/2008), that financed a considerable part of my work.

To my FF friends Xana, Vera, Prazeres, Calisto and Cátia, thank you for always being there.

To my family, especially my mother and my godmother, thank you for all the unconditional love, support and encouragement.

To Leonardo for all the love and constant support, thank you for always being there. It wouldn't have been the same without you.

PUBLICATIONS

The work performed in the frame of this thesis resulted in the following publications:

A. Carvalho, A. Pelaez-Vargas, D.J. Hansford, M.H. Fernandes, F.J. Monteiro. Effects of Line and Pillar Array Microengineered SiO_2 Thin Films on the Osteogenic Differentiation of Human Bone Marrow-Derived Mesenchymal Stem Cells. ***Langmuir,*** 2016; 32 (4): 1091– 1100.

A. Carvalho, T. Esteves, P. Quelhas, F.J. Monteiro. MobilityAnalyser: An automatic quantification of cells mobility on line and pillar array micropatterned surfaces. (***Submitted)***

A. Carvalho, L. Cangueiro, V. Oliveira, R. Vilar, M.H. Fernandes, F.J. Monteiro. Femtosecond laser microstructured Alumina toughened Zirconia: A new strategy to improve osteogenic differentiation of hMSCs. ***Applied Surface Science***, 2018; 435: *1237-1245.*

ABSTRACT

Despite the considerable evolution on bone tissue engineering strategies, currently used bone implants can have a limited lifespan in the body and several still exhibit high failure rates due to lack of osteointegration. Nowadays, clinical practices still rely vastly on bone grafts, a procedure still associated with high risks. Hence, designing a biomaterial that induces bone regeneration while providing the adequate mechanical support is still a great challenge. Improving the surface functionality of load bearing biomaterials could lead to enhanced implant-tissue interaction and consequently improved osteointegration.

Although Titanium continues to be the gold-standard material for bone replacement where high mechanical strength is required, several reports have shown limitations to the use of Ti, including poor osteointegration, allergic reactions, particles diffusion and bacterial infections. The need for new strategies has focused the attention on ceramics with high mechanical strength, such as Alumina toughened Zirconia (ATZ), which has an osteointegration rate comparable to Titanium. Still, its bioinertness demand the need for surface modifications to enhance the biological performance. Ceramic materials can be difficult to process due to their brittleness and chemical inertness, but appropriate surface topographic features can be developed with the application of coatings or direct modification with high-energy lasers.

It is widely accepted that surface topography plays a predominant role in controlling the material-host tissue interactions after implantation. Surface topography can modulate the biological response at macro-, micro- and nano- scales. Extensive research has been conducted using patterned surfaces that show a modulation of cell behaviour, improved cellular activity, and enhancement of osteogenic differentiation. Such topographical features provide a faster and more reliable osteointegration response, validating that cell adhesion, proliferation, organization and phenotype can be modulated at the micro- and nano-scale levels.

In this work, we developed two topographical surface modifications to improve the biological response to alumina toughened zirconia. The first modification was based on the application of a bioactive Silica coating onto the ceramic surface, by combining two well-known techniques, sol-gel and soft-lithography. The films were characterized in terms of chemistry, morphology, surface topography and roughness. The *in vitro* biological characterization was performed with human bone marrow derived

mesenchymal stem cells, that were cultured over line and pillar microtopographic features to evaluate the degree of osteogenic differentiation induced by the topographical stimuli. The micropatterned films induced higher osteogenic differentiation and expression of osteoblast-associated markers, compared to a flat control. In terms of the microfeatures, the pillar patterns caused a greater response of hMSCs osteogenic differentiation with increased expression of osteoblast-associated markers, ALP activity, and extracellular matrix mineralization after 21 days of culture.

In addition, the initial contact of hMSCs with the surface topographic features was evaluated. Cells showed to be modulated by the surface topography since the initial contacts with the microfeatures. Cell mobility was significantly higher on the micropatterned films, when compared to the cell mobility on flat films of the same material. In addition, in the presence of the micropatterns, cells were capable of migrating through longer distances, with higher velocities.

Even though the application of a bioactive coating may be a suitable modification to certain bone implant applications, it may happen that the addition of another layer may decrease the applicability of the implant, namely if high mechanical load or torque are applied during implantation. Thus, a second approach to surface modification was developed, making use of a femtosecond laser to generate texture on the Alumina toughened Zirconia surfaces, both at micro- and nanoscale levels.

Microfeatures were successfully developed with overlapping of high-frequency laser induced periodic surface structures (LIPSS), that nanotextured the ceramic surface in a direction perpendicular to those of the micropattern features. The ceramic was characterized in terms of morphology, structure, chemistry and roughness before and after laser treatment. Regarding the biological response to the developed micro/nano textured surfaces, cells alignment and proliferation showed to be modulated mostly by the microtopography. The laser treated surfaces displayed significantly higher expression of osteogenic-related markers, and a mineralized extracellular matrix, when compared to untreated ATZ, the control surface.

The surface topographical modifications described in this work constitute simple processes that can be applied to create precise and reproducible micro- and nano-texturized surfaces on ATZ ceramics. The obtained results point towards the possibility of developing hard ceramic-based biomaterials with improved surface bioactivity, which can be used for load-bearing applications, being capable of inducing guided tissue regeneration and improved osteointegration.

RESUMO

Apesar da evolução considerável que tem ocorrido na área da medicina regenerativa, os implantes ósseos atualmente utilizados apresentam uma vida útil limitada quando implantados, e vários ainda apresentam altas taxas de insucesso devido à fraca osteointegração dos implantes.

Atualmente é ainda comum a utilização de enxertos ósseos, um procedimento associado a riscos elevados. Desta forma, o desenvolvimento de biomateriais que sejam capazes de induzir regeneração óssea enquanto fornecem suporte mecânico é ainda um grande desafio. Melhorar a funcionalidade de superfície de biomateriais mecanicamente resistentes (de suporte e transmissão de carga) pode levar a um aumento da interação implante-tecido e, consequentemente, a uma osteointegração melhorada.

Apesar de o Titânio continuar a ser a referência por excelência para substituição de osso com alta resistência mecânica, vários estudos têm demonstrado limitações no uso deste material, associando-o por vezes a fraca osteointegração, reações alérgicas, difusão de partículas e infeções bacterianas.

A necessidade de novas estratégias tem direcionado a atenção para cerâmicos com alta resistência mecânica, como a Zircónia reforçada com Alumina (ATZ), que apresenta uma taxa de osteointegração comparável à do Titânio. Ainda assim, as suas características bioinertes requerem modificações de superfície que melhorem o seu desempenho biológico. Devido à sua fragilidade e inércia química, os materiais cerâmicos podem ser difíceis de processar. Porém, a sua topografia da superfície pode ser alterada com a aplicação de revestimentos ou modificação direta com lasers de alta energia.

É amplamente aceite que a topografia de superfície desempenha um papel predominante no controlo das interações entre o biomaterial e o tecido hospedeiro, após a implantação, modulando assim a resposta biológica. A topografia de superfície pode modular a resposta biológica à escala macro, micro e nanométrica. Vários estudos realizados com superfícies padronizadas mostram uma modulação do comportamento celular com aumento da atividade celular e da diferenciação osteogénica.

Tais topografias proporcionam uma osteointegração mais rápida e fiável, confirmando que a adesão, proliferação, organização e fenótipo celular podem ser modulados à escala micro- e nanométrica.

Neste trabalho, foram desenvolvidas duas modificações de topografia de superfície para melhorar a resposta biológica à zircónica reforçada com alumina. A primeira modificação baseou-se na aplicação de um revestimento bioactivo de sílica na superfície do material cerâmico, através da combinação de duas técnicas bem conhecidas, sol-gel e litografia-suave. Os filmes foram caracterizados em termos de química, morfologia, topografia de superfície e rugosidade. A caracterização biológica *in vitro* foi realizada com células mesenquimais derivadas da medula óssea, que foram colocadas em cultura com revestimentos com microtopografias em forma de linhas ou pilares, para avaliar o grau de diferenciação osteogénica induzida apenas pelos estímulos topográficos.

Os filmes micropadronizados induziram maior diferenciação osteogénica e expressão de marcadores associados a osteoblastos, em comparação com um controlo liso. Em termos de comparação de ambos os micropadrões, os padrões de pilares originaram uma resposta mais intensa da diferenciação osteogénica de hMSCs, com maior expressão de marcadores associados a osteoblastos, atividade da fosfatase alcalina e mineralização de matriz extracelular, após 21 dias em cultura.

Além disso, a avaliação do comportamento celular mostrou que a mobilidade celular foi significativamente maior nos revestimentos micropadronizados, quando comparada com a mobilidade celular nos revestimentos lisos do mesmo material. As células foram capazes de migrar ao longo de distâncias superiores e com velocidades mais elevadas.

Embora a aplicação de um revestimento bioactivo possa ser uma modificação adequada para certos implantes de substituição óssea, pode acontecer que a adição de um revestimento possa diminuir a aplicabilidade do implante, como por exemplo quando são aplicadas cargas mecânicas elevadas. Assim, a segunda modificação testada foi desenvolvida através do recurso a um laser de femtosegundo para texturar a superfície de Zircónica reforçada com Alumina, tanto à escala micro- como à escala nanométrica.

As microtexturas foram desenvolvidas com sucesso com sobreposição de estruturas periódicas induzidas por laser (LIPSS) de alta frequência, que nanotexturaram a superfície do cerâmico, numa direção perpendicular à das microtexturas. O material cerâmico foi caracterizado em termos de morfologia, estrutura, química e rugosidade antes e após o tratamento por laser. Em relação à resposta biológica às superfícies micro-/nano- texturadas, o alinhamento e proliferação das células mostraram ser fortemente modulados pela microtopografia. As superfícies tratadas com laser apresentaram expressão significativamente maior de marcadores osteogénicos e uma matriz

extracelular mineralizada, quando comparadas com as superfícies controlo, de ATZ não tratada.

As modificações de topografia de superfície descritas neste trabalho constituem processos simples, que podem ser aplicados para criar micropadrões e texturas manométricas de uma forma precisa e reprodutível em cerâmicos de ATZ. Os resultados obtidos apontam para a possibilidade de desenvolver biomateriais baseados em cerâmicos duros que apresentem bioatividade da superfície melhorada para ser utilizados em aplicações de suporte de carga, sendo capazes de induzir regeneração guiada de tecido e osteointegração melhorada.

TABLE OF CONTENTS

LIST OF ABBREVIATIONS

3Y-TZP - 3mol % Yttria-stabilized zirconia

AFM - Atomic force microscopy

ALP - Alkaline phosphatase

ATR - Attenuated total reflection

ATZ - Alumina toughened Zirconia

BMPs - Bone morphogenetic proteins

BMU - Basic multicellular unit

BSA - Bovine serum albumin

BSP - Bone sialoprotein

cDNA - Complementary DNAs

COL-I - Type I collagen

ECM - Extracellular matrix

EDS - X-ray dispersive spectroscopy

ESB - European Society for Biomaterials

FBS - Fetal bovine serum

FTIR - Fourier Transform Infrared

GAPDH - Glyceraldehyde- 3-phosphate dehydrogenase

HA - Hydroxyapatite

HBMSCs - Human bone marrow stromal cells

HCA - Hydroxycarbonate apatite

HDMEC - Human dermal microvascular endothelial cells

HDMS - Hexamethyldisilazane

HGF - Human gingival fibroblasts

hMSCs - Human bone marrow derived mesenchymal stem cells

HSFL - High spatial frequency

LIPSS - Laser induced periodic surface structures

LoG - Laplacian of Gaussian filter

LTD - Low-temperature degradation

MCR - MATLAB™ Component Runtime

M-CSF - Macrophage colony-stimulating factor

MSD - Mean square displacement

MTES - Methyltriethoxisilane

OC - Osteocalcin

ON - Osteonectin

OPG - Osteoprotegerin

OPN - Osteopontin

OSX - Osterix

PBS - Phosphate buffered saline

PDMS - Polydimethylsiloxane

qRT-PCR - Quantitative real-time polymerase chain reaction

Ra - Roughness average

RANKL - Receptor for activation of nuclear factor kappa B ligand

RFU - Relative fluorescence units

Rq - Root-mean-square

RT-PCR - Reverse transcriptase polymerase chain reaction

RUNX2 - Runt-related transcription factor 2

SEM - Scanning electron microscope

TCPS - Tissue culture polystyrene

TEOS - Tetraethylorthosilicate

WCA - Water contact angle

XRD - X-ray diffraction

ZTA - Zirconia toughened alumina

α-MEM - Alpha-minimum essential medium

β-TCP - Beta tricalcium phosphate

μATZ - Microtextured ATZ

CHAPTER I

INTRODUCTION

1. BONE

Bone is a unique, hierarchically structured and metabolically active organ, that undergoes remodeling throughout life. This capability of self-renewal has motivated extensive research on bone healing and bone tissue engineering.

Still, healing of a large bone defect, above a critical limiting size, can only be achieved with either bone grafts or the implantation of a biomaterial that might integrate in bone and induce new bone formation. [1]

Despite the continuous innovation on biomaterials and bone tissue engineering strategies, the repair of critical-size bone defects is still a challenge and, in such applications, autografts are still considered by many as the best option for bone healing.

In maxillofacial surgery, the use of autologous bone grafts from the iliac crest to reconstruct bone defects deriving from trauma, tumours, inflammation and jaw atrophy is still a common practice. [2]

However, autografts can't meet the demand for orthopedic implants since bone harvesting is a complicated process that can lead to several post-surgery complications at the harvest site. Additionally, the amount of bone that can be collected is limited, in a way to limit the risks of morbidity at the donor site.

Allografts and xenografts can be an alternative, since these grafts can be harvested from the same anatomic location, and therefore display similar mechanical properties, but both are still associated with risks of immune-rejection and disease transmission. [3]

With the increase in life expectancy, there is a naturally increasing need for bone substitutes. Bone implants should become the primary option to achieve the demand for orthopaedic implants and bone regeneration strategies, thus becoming necessary to improve the current strategies and develop implants with superior longevity and improved osteointegration. [4]

In order to develop specific biomaterials that might accomplish these requirements, detailed knowledge concerning bone biology, structure and mechanisms is crucial.

1.1. BONE STRUCTURE AND COMPOSITION

Bones primary roles are to provide structural and mechanical support for locomotion, to provide protection to vital organs and to regulate mineral homeostasis. In addition to structural support, they provide an adequate environment for the bone marrow and are the main reservoir for minerals, as well as for a variety of growth factors.

Bone has a complex **organic-inorganic architecture** that comprises macro-, micro- and nano-scale components and a diversified cellular composition.

At the macro-scale, two types of bone tissue can be identified: cortical and cancellous. Both have the same matrix composition and structure with the main difference residing in bone density. Cortical bone is dense, with a porosity of approximately 10% while cancellous bone can present porosity between 50 and 90%. [5]

Therefore, cortical bone forms the cortex of most bones, while cancellous bone, which is more brittle, is found at the ends of long bones, the centre of flat bones (ribs, skull, and pelvis) and the vertebral column.

Both cortical and trabecular bone are composed of osteons, the basic structural unit of bone. Cortical bone osteons are termed harversian systems, which consist of concentric layers of lamellae surrounding the haversian canals, where nerves and blood vessels that supply the bone pass through. On the other hand, the porous network of cancellous bone is made of trabeculae, comprising the bone marrow in its pores. [6]

Bone **chemical composition** consists of a mineralized extracellular matrix composed by an organic phase of predominantly collagen and an inorganic phase of calcium phosphate, in the form of hydroxyapatite (HA). Other remaining components like non-collagenous proteins, lipids and glycosaminoglycans are also present.[7]

Type I collagen is the most abundant organic component of bone and is organized into hierarchical structures, where the lowest hierarchical level consists of triple helical collagen molecule.

At the micro and nano-scales, hydroxyapatite crystals, oriented in a periodic array, reinforce aggregated type-I collagen and form the collagen fibrils. The reinforced collagen fibre is a universal building block for both cortical and trabecular bones (Figure 1). These are normally formed in a lamellar pattern, in which collagen fibrils are laid down in alternating orientations. [8-9]

The precise combination of collagen and hydroxyapatite define bone strength, toughness and flexibility to withstand bending strains. Type I collagen provides viscoelasticity and toughness, while the mineral phase of HA is responsible for stiffness and structural reinforcement.

In figure 1, a schematic representation of bone architecture and its organic-inorganic composition is presented.

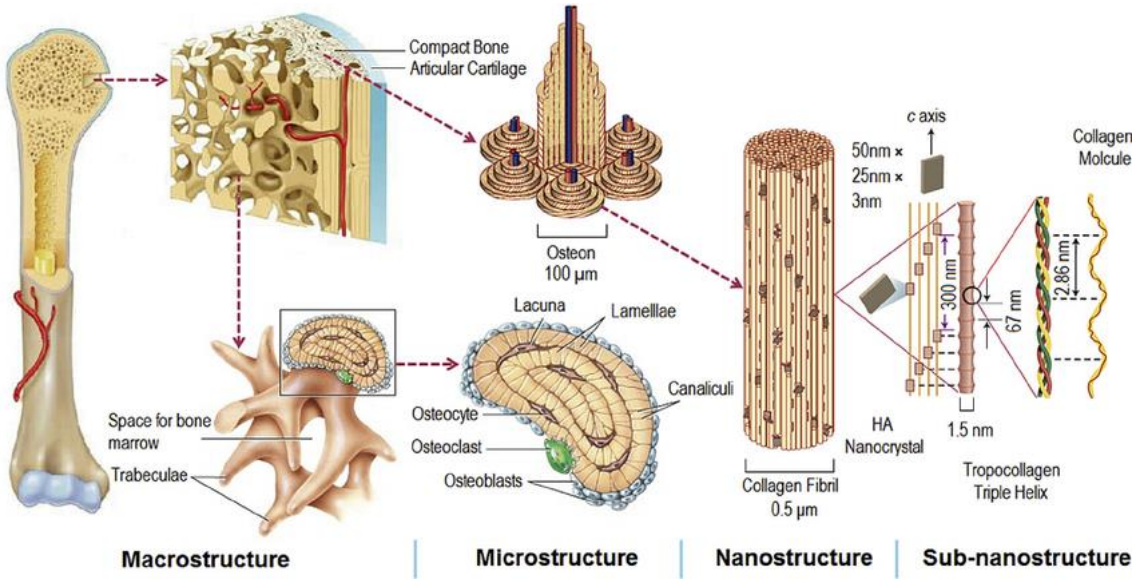

Figure 1.1 – Bone structure and organic-inorganic composition. Adapted from [6]

1.2. BONE CELLS AND MOLECULAR MECHANISMS

A heterogeneous group of cells can be found in bone, each one with a specific function related to bone formation, bone resorption, mineral homeostasis and bone repair, being distinguished through different morphologies and characteristic locations in bone (Figure 1.2). Bone cells originate from two cell lines: Cells from mesenchymal stem-cell origin form the bone and consist, sequentially, of pre-osteoblasts, osteoblasts, bone-lining cells and osteocytes. On the other hand, the cells from hematopoietic stem-cell origin are responsible for bone resorption and consist of marrow monocytes, pre-osteoclasts and osteoclasts. [5, 10]

Osteoblasts are the cell type responsible for bone formation. Four maturational stages are identified in the osteoblastic lineage, as described previously. With the appropriate conditions, mesenchymal stem cells initiate their differentiation along a linear sequence first to pre-osteoblast and then mature osteoblasts.

Pre-osteoblasts are considered to be all cells in the transition process from progenitor cells to osteoblasts and are, consequently, a heterogeneous group. Still, one characteristic assumed to distinguish these cells from the progenitors is the expression of transcription factor RUNX2 and, at a more advanced stage, osterix (OSX). [11]

Transcription factors RUNX2 and OSX are known to regulate osteoblasts differentiation. Specifically, Runt-related transcription factor 2 (RUNX2) is assumed to be the control

gene within the osteoblasts phenotype, essential for osteogenic differentiation of mesenchymal stem cells and to inhibit their differentiation into adipocytes and chondrocytes. [12]

Moreover, RUNX2 has been found to stimulate gene expression of osteocalcin (OC), type I collagen (COL-I), alkaline phosphatase (ALP), osteopontin (OPN) and bone sialoprotein (BSP). [13]

Osx is a downstream gene of RUNX2, as it been shown that this transcription factor was not expressed in *in vivo* models were RUNX2 was inhibited. Osterix is also believed to act in the regulation of certain osteogenesis-related markers such as osteonectin (ON), OC, OPN, COL-I and BSP. [12-13]

Osteoblasts are basophilic and mononuclear cells, composed by a large nuclei, enlarged Golgi apparatus and extensive endoplasmic reticulum, typical features of cells that produce large amount of extracellular proteins.

Osteoblasts form a continuous layer at sites of active bone formation. These cells are responsible for the synthesis and mineralization of the organic bone matrix, also known as osteoid. Osteoblasts synthesize predominantly type-I collagen, the main component of the osteoid, but also glycoproteins like ON, OPN and BSP, enzymes such as ALP and collagenase, γ-carboxyglutamic acid containing proteins, like OC, proteoglycans, proteolipids and several growth factors [14]

Matrix proteins as ALP, COL-I and OPN are not bone specific and have been identified in different types of cells. Even so, all have been found to be early indicators of osteoblasts differentiation. In turn, BSP and OC are osteoblast specific genes. Osteocalcin specifically is the second most abundant protein in bone and is considered a late osteogenic marker, highly expressed by mature osteoblasts, mostly during bone matrix mineralization. [13]

Active osteoblasts are polarized, meaning the cell membrane that is in direct contact with the bone surface possesses many cytoplasmic processes that extend into the newly deposited matrix. [11]

These cells also regulate mineralization by releasing small vesicles that concentrate calcium and phosphate and play a role in bone remodelling by expressing osteoclastogenic factors, namely the macrophage colony-stimulating factor (M-CSF) and the receptor for activation of nuclear factor kappa B ligand (RANKL) and an inhibitor of osteoclastogenesis, osteoprotegerin (OPG). [15-16]

OPG is produced by osteoblasts, binds to RANKL and acts as a blocker to osteoclastic bone resorption, thus enhancing bone matrix synthesis. [13]

Mature osteoblasts can follow one of three paths: terminally differentiate into osteocytes, become inactive bone lining cells or undergo apoptosis.

Osteoblasts become **bone lining cells** at the end of the formation phase by reducing their cytoplasm and organelles and becoming quiescent. In an inactive state, these cells cover the bone surface and play a role in the regulation of bone fluid composition, circulation and ion homeostasis. Bone lining cells also assist in the regulation of bone resorption and formation by communicating with osteoblasts and osteoclasts progenitors cells in the marrow. [14]

Osteocytes are formed by a subpopulation of osteoblasts that undergoes terminal differentiation upon being incorporated in the bone matrix and experiencing mineralization. These are the most abundant bone cells, about 90 to 95%, and can have a lifespan of decades. During the incorporation in the bone matrix, osteoblasts lose a considerable percentage of their typical cell organelles and cytoplasm and acquire a stellar shape with 50 or more thin extensions, designated as osteocyte processes. [11, 17]

Osteocytes are spatially isolated but maintain connections between each other, as well as with bone lining cells, osteoblasts and the bone surface via their osteocyte processes, multiple long fillopodial extensions rich in actin cytoskeleton. Osteocytes contain lysosomes and so, are active and may function as phagocytic cells during osteolysis. [17-18]

Osteoclasts originate from the hematopoietic lineage and are uniquely specialized in resorbing the mineralized bone matrix. Their cellular morphology differs from the osteoblast lineage, as they are large, multinucleated cells, originated from the fusion of mononuclear cells. [14, 19] Osteoclasts differentiation is induced by a variety of factors produced mostly by osteoblast or marrow stromal cells. The most known factors necessary to promote osteoclastogenesis, are M-CSF and RANKL. [18]

When activated to resorb, osteoclasts become highly polarised and form distinct membrane domains, including the sealing zone and the ruffle border, the cell membrane in the area facing the bone matrix. [20]

Lysosomal enzymes synthesized by osteoclasts are secreted through the ruffle border membrane into the bone-resorption compartment for the dissolution of the inorganic component of old bone matrix. [21-22]

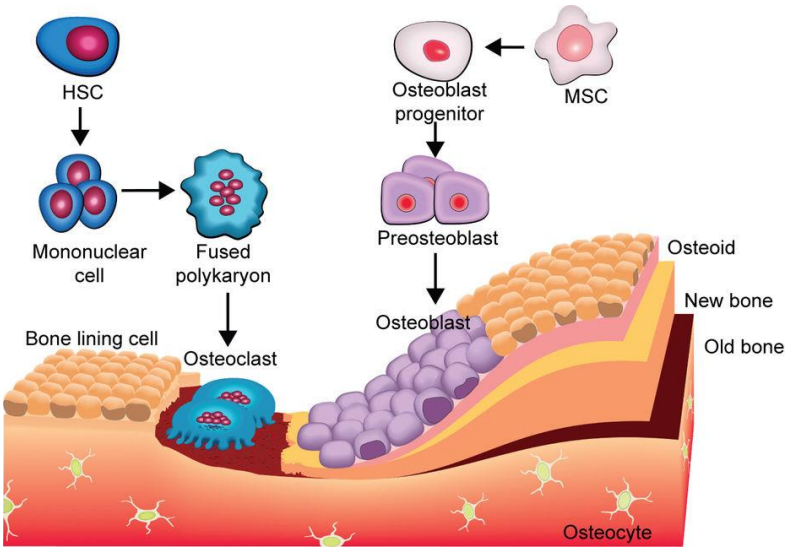

Figure 1.2 – Bone cells origin and stages. [23]

1.3. BONE REMODELLLING

Bone undergoes continuous remodelling to optimally adapt its structure to changing functional demands such as physiologic influences or mechanical loading.

The balance between bone formation and bone resorption is precisely regulated by the bone remodelling cycle throughout life. All bone cells are involved in the process, forming the basic multicellular unit (BMU) that ensures the coordination of the different phases of bone remodelling: activation, resorption, reversal and formation. [9, 17]

The remodeling cycle is initiated by the ***activation*** of the quiescent bone surface, covered with bone lining cells and by osteoblasts expressing osteoclastogenic factors such as RANKL, initiating the fusion of pre-osteoclasts to form multinucleated ostoclasts [21]

In the ***resorption*** phase, osteoclasts attach to the bone surface through integrin receptors in the cellular membrane that bind to RGD containing peptides in the bone matrix, creating an isolated sealing zone beneath the cell. Through the sealed zone, resorbing osteoclasts secrete hydrogen ions through proton pumps in the cell membrane to lower the pH and dissolve the mineralized matrix. The inorganic matrix is then degraded by lysosomal enzymes tartrate-resistant acid phosphatase and cathepsin K. [14, 16]

As bone resorption subsides and resorption pits remain, osteoclasts disappear and mononuclear cells prepare the surface for bone formation. This is the ***reversal*** phase.

Matrix debris is removed and the resorption lacuna is leveled. Although not yet fully understood, it is believed that during the reversal phase the mononuclear cells may release factors that can play a role in guiding osteoblasts during the bone formation phase. [17]

The bone remodeling cycle is finished with the synthesis and deposition of bone matrix by osteoblasts, the bone ***formation*** phase. Functional osteoblasts synthesize a collagenous organic matrix and regulate its mineralization, by releasing small, membrane-bound vesicles that concentrate calcium and phosphate. During this phase, the more mature osteoblasts are entrapped in the organic matrix and become osteocytes, while others can terminally differentiate into bone lining cells, building a canopy covering the surface and keeping the bone in a quiescent state until the next cycle. [19-20]

2. BIOCERAMICS

Biomaterials have been constantly evolving as a result of a multidisciplinary approach from materials science, biology, chemistry, physics and medicine, with the final goal of developing an adequate biological interaction between material and host. [24]

At the first Consensus Conference of the European Society for Biomaterials (ESB) a biomaterial was defined as "a non-viable material used in a medical device, intended to interact with biological systems". However, the ESB current definition has been updated to "a material intended to interface with biological systems to evaluate, treat, augment or replace any tissue, organ or function of the body" a change in definition that shows how the concept of Biomaterials has evolved in the recent decades. [25]

The interest in ceramics for medical applications started during the 1960's and these materials have been extensively researched ever since. Biocompatible ceramics that are used with the intent of clinical and research applications are termed bioceramics.

Bioceramic implants have been mostly used for replacement and regeneration of the skeletal system, such as bone, joints and teeth and the constant advances in bioceramics have been directly related with significant progresses in bone tissue engineering. [26-28]

Bioceramics are a large class of inorganic, non-metallic materials, including also glasses and glass-ceramics, that can be produced as crystalline and amorphous materials, and be processed either in dense or porous structures, as bulk blocks, granules, cements or coatings. [29-30]

In general, ceramics can be characterized by high chemical resistance and high melting temperatures, low impact and tensile strength and inherent brittleness. However, bioceramics are a complex and heterogeneous group of materials, being usually categorized according to the type of interaction with the host tissue, dividing them into two categories: bioactive or bioinert. Additionally, bioactive ceramics can be classified as resorbable or non-resorbable. [31]

Bioactive ceramics include various groups of calcium phosphate ceramics (hydroxyapatite, beta-TCP), glasses and glass-ceramics, that are chemically reactive, being capable of binding to the host tissues but lack adequate mechanical strength. This is why they are mostly applied as scaffolds, bone cements and as coatings to mechanically resistant substrate biomaterials. [32]

Resorbable ceramics can be resorbed by common bone homeostatsis and slowly replaced with new tissue, when implanted. Common examples of bioresorbable ceramics include tricalcium phosphates (beta-TCP) and calcium carbonate.

Bioinert ceramics like Alumina (Al_2O_3) and Zirconia (ZrO_2) present high mechanical strength, and show stable physicochemical properties, undergoing little or no chemical changes when exposed to physiological conditions. Specifically, hard ceramics like Al_2O_3 and ZrO_2 show high compression strength, excellent corrosion resistance, low friction coefficient, and low electrical and thermal conductivities.[33-35] Due to these excellent mechanical properties and their inertness, they are mostly used in load-bearing applications and when mechanical support is required, such as in dental and orthopedic implants, femoral heads and acetabular cups.

However, the constant advances in manufacturing techniques have improved the development of high performance ceramics, which can broaden their use, as an alternative to metals, in several bone implants. [36]

2.1. BIOINERT CERAMICS

For years, Titanium and its alloys have been used in numerous orthopedic implants, being the gold standard for dental implants. However, several problems have been reported on the use of titanium, such as allergic reactions, discoloration and tarnishing of soft tissues, infections and the diffusion of metal particles, found close to the implant-site, in lymph nodes and systemically. [37-40]

When compared to metals, hard ceramics display superior mechanical and tribological properties with excellent biocompatibility.

Alumina (Al_2O_3) was introduced as an alternative biomaterial to titanium due to its biocompatibility, high mechanical strength, low friction and low wear coefficients and excellent corrosion resistance. [41]

Common clinical applications of Alumina include dental implants, maxillofacial reconstructions, and components in joints prostheses, namely for shoulder, hip and knee. The main drawback of alumina ceramics are its brittleness under tensile strength, with a low fracture toughness. These particular characteristics have limited a wider application of this ceramic on other bone implants, where higher bending strength is required.

Zirconia (ZrO_2) also gained popularity as a structural bioceramic due to its excellent mechanical properties. As opposed to Alumina, Zirconia shows high fracture toughness. Additionally, it has well reported biocompatibility, high hardness and wear resistance, low friction coefficient and exhibits osteointegration comparable to titanium. Zirconia exists in three phases: monoclinic, tetragonal and cubic, which are stable at increasingly higher temperatures [42-43]

ZrO_2 experiences phase transition from monoclinic to tetragonal at 1000~1200ºC, and from tetragonal to cubic at 2370ºC. The monoclinic form is stable at room temperature, however, the tetragonal phase shows superior mechanical properties.

When changing from tetragonal to monoclinic, zirconia undergoes a martensitic transformation, associated with an increase in volume of approximately 4.5 %, which is enough to exceed the material strength and results in cracks propagation, which can lead to fracture.

However, the tetragonal or cubic phases of zirconia can be retained as metastable phases at room temperatures by stabilizing it with cubic oxides, thus preventing the failure of pure Zirconia upon cooling. These oxides were termed as "stabilizers". [44-45]

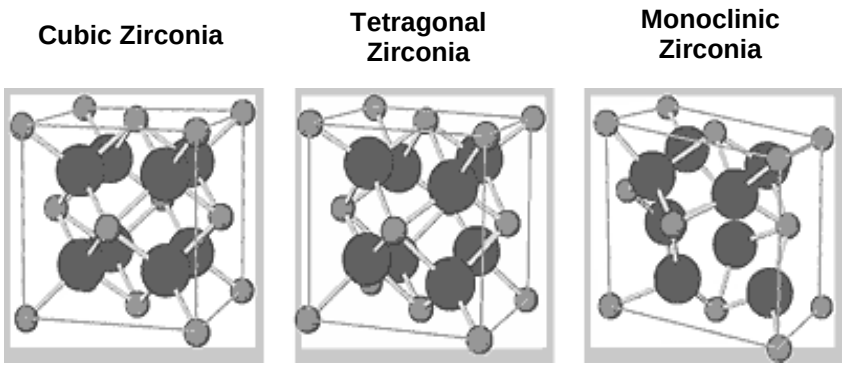

Figure 2.1 - Structure of the three Zirconia phases. [31]

Due to the volume expansion in the tetragonal to monoclinic (t→m) phase transformation, pure ZrO_2 is normally doped with oxide stabilizers such as MgO, Y_2O_3, or CeO_2, that are used to maintain the metastable tetragonal structure, metastable at room temperature. Alloying zirconia with cubic oxides results in an increase in fracture toughness of the material, efficiently arresting crack propagation, a process designated as transformation toughening. [46-47]

Transformation toughening is a mechanism that can be used to improve the toughness of zirconia by controlling the transformation process in the stress field ahead of the crack tip. [48] During transformation toughening, the volume expansion associated with the transformation from tetragonal to monoclinic phase acts on the crack to reduce its potential to propagate, as shown in figure 2.2. The metastable tetragonal particles transform into the more stable monoclinic phase, at the same time helping to close the crack, by shielding it with the compressive stresses associated with the transformed particles. The crack energy is effectively absorbed, thus arresting further crack growth and toughening the material. [36, 48]

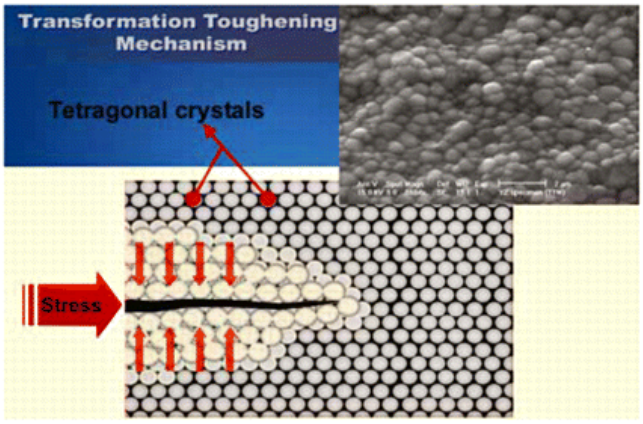

Figure 2.2 - Resistance to cracking in transformation-toughened zirconia. This phenomenon occurs as tetragonal phase transforms to the larger monoclinic phase under stress. The stress field advancing ahead of a propagating crack transforms the small tetragonal particles to larger monoclinic particles. The larger particles exert a crack-closing force in the process zone behind the crack tip, effectively resisting propagation of the crack. [49]

The most commonly used stabilizer is Yttria (Y_2O_3). 3 mol% yttria stabilized polycrystalline tetragonal zirconia (3Y-TZP) is the most common form of zirconia used for biomedical applications, with some advantages. One is the fine grain size and well-controlled microstructure with minimum residual porosity, resulting in a material with excellent tribological and mechanical properties. Another one is the higher fracture strength and toughness derived from the transformation toughening process. [49]

Despite this positive ability for transformation toughening, zirconia also exhibits a downside characteristic of low-temperature degradation (LTD). LTD is characterized by the leaching of the ceramic matrix and Ytrrium ions, when in contact with water and particularly in physiological environment under stress. Leaching may lead to losing its transformational toughening, causing a slow tetragonal-to-monoclinic phase

transformation of grains that leads to surface roughening, grain pull-out and micro-cracking. [50-51]

With the ageing process still being a limiting factor for zirconia use in implants, several researchers have focused on studying composites of Alumina and Zirconia that may help to overcome the limits of both monolithic ceramics.

2.1.1. ALUMINA TOUGHENED ZIRCONIA (ATZ)

Corresponding to the relative fractions of alumina and zirconia, there is zirconia toughened alumina (ZTA) with alumina as matrix component and alumina toughened zirconia (ATZ) with zirconia as matrix component. An ATZ ceramic combines the main advantages of both ceramics with the hardness and wear resistance of alumina and the fracture toughness as well as biaxial bending strength of zirconia. [52-53] The presence of alumina in a zirconia matrix has a positive influence on the phase stability resulting in the formation of a highly ageing-resistant material by the dispersion of alumina particles within the zirconia matrix. Several studies have reported that the addition of Al_2O_3 to 3Y-TZP, in different percentages and up to 20%, could suppress the propagation of the tetragonal to monoclinic phase transformation upon ageing in water. [54-55]

According to the results reported by De Aza *et al* [56] and Ruhle *et al* [57], when compared to the single ceramics, the fracture toughness of the ATZ increases, which in turn influences the mechanical properties of the ceramic. Compared to alumina, a composite of 20% Al_2O_3 + 80% 3Y-TZP also exhibits a relatively lower hardness, which can be an advantage since the final shape of the implants can be easily processed by machining. [46]

The use of these ceramics has been limited to bone support applications, due to their excellent mechanical properties and relative inert properties. The development of novel surface modifications could improve the success rate of these materials, by increasing the implants osteointegration, consequently increasing the interest in these ceramics for several applications such as dental, maxillofacial and craniofacial implants, where high mechanical strength is needed.

3. BIOMATERIALS SURFACE FUNCTIONALIZATION

Tissue engineering strategies have recently focused on biomaterials that can elicit specific responses from the host tissues. The events that normally lead to integration of an implant into bone and determine its performance take place mainly at the tissue-implant interface. [58] In that sense, surface modifications can provide exceptional control of the host tissue response to the implanted biomaterial. By altering the surface of a biomaterial, it is possible to provide improved surface functionalities, while still maintaining the properties of the bulk material. [59]

A range of surface properties is known to influence cells response to the implant, such as ionic composition, charge, hydrophobicity and roughness.

Over the years, several biochemical and topographical features have been explored to improve the biological response to bioinert materials. Surface modifications are material-dependent, in the sense that not all techniques can be applied to certain substrate materials and the most suitable modifications can be selected accordingly, from chemical, topographical or coatings.

Surface topography has long been proved to influence the response of several cell types, with effects on adhesion, morphology, migration and differentiation of mesenchymal stem cells. [60-61]

A variety of methods has been developed in order to create topographical features on implants surfaces but some have the disadvantage of altering the surface chemistry and degrading the bulk material. [62]

Improved technologies to modify ceramic implants are an open field for intensive research. The development of combined strategies, able to modify bioinert ceramics surface without affecting their mechanical properties are still required.

3.1. MICROPATTERNING APPROACH

Surface microfabrication techniques have been widely used for the spatial control of cells. Its combination with surface chemistry and material science has provided new tools to further explore, *in vitro* and *in vivo*, the effects of surface properties on cell functionality and control.[63-65]

Among the microfabrication strategies to modify implant surfaces, **micropatterning** has been widely applied to several biomaterials surfaces, with the intent of studying and modulating cells response.

It usually refers to the soft-lithography technique, although other techniques can be used for different micropatterning approaches. Microengineered surfaces are powerful platforms to evaluate cells reaction to different chemistries and microenvironments with varying complexities.

Our group developed an approach of micropatterning to modify glass and 3Y-TZP surfaces by combining two widely used techniques: soft-lithography for preparation of stamping molds and sol-gel to prepare silica. [66-67] With this method it is possible to apply a coating to a substrate material and the initial liquid/gel prepared by sol-gel acquires its final geometry by solidifying in a mold. [68] This synergy allows the production of micropatterned surfaces with controlled chemistry, roughness, thickness and texture.

3.2. SOFT-LITHOGRAPHY

Soft-lithography technique was designed as an alternative to the most commonly used patterning method, photolithography. Photolithography is an expensive technique, it cannot be easily applied to non-planar surfaces and provides almost no control over the chemistry of the patterned surfaces. [69-71]

Soft-lithography was developed by Xia and Whitesides, who fabricated patterns and structures with feature sizes ranging from 30 nm to 100 μm on the surface of an elastomeric material for pattern transfer or modifications. [70] The name soft-lithography covers a group of techniques, all of them employing an elastomeric, generally polydimethylsiloxane (PDMS) mold to develop patterns on a surface (Figure 3.1). [71-72]

Soft-lithography is an exceptional approach to develop micropatterns since it is simple and inexpensive, with potential to develop a variety of topographical alterations on different surfaces and using different materials to prepare them. Soft-lithography techniques can be used to develop both two-dimensional surface patterns as thin films or SAMs, as well as to generate quasi three-dimensional topographical features. [64]

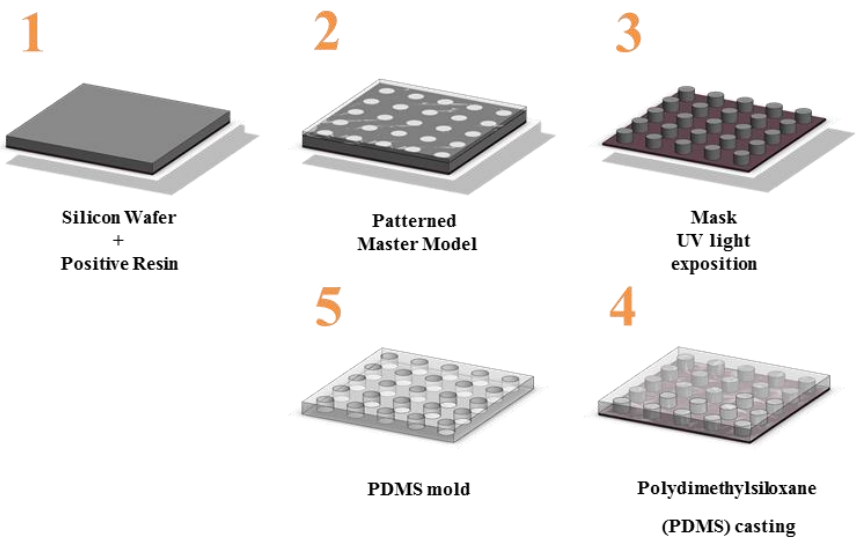

Figure 3.1 – Scheme of the micropatterned molds production. Soft-Lithography is used to obtain polymeric molds with microscale features via a two steps process. First, photolithography is used to produce a master pattern with micro-scale dimensions (steps 1-3). The master is then used to create polydimethylsiloxane (PDMS) negative molds (steps 4-5).

3.3. SOL-GEL

The sol-gel process is a wet-chemical technique widely used in materials science and ceramic engineering. This method is an attractive alternative for the synthesis of glasses due to its low processing temperatures, simple equipments required and operation schemes, relatively low cost, low environmental impact and the properties of the obtained material. [73]

In recent years, sol–gel process has been increasingly employed for the preparation of bioactive glasses, including silica (SiO_2) glasses, since it leads to the formation of gels from mixtures of liquid reagents, close to room temperature. It involves several steps: the development of inorganic networks, formation of colloidal suspensions (sol) and gelation of the sol to form a network in a continuous liquid phase (gel). Drying of the gel, gives rise to glass-like materials called xerogels.[74-75]

The process starts when one or two silicate precursors (two for hybrid glasses) are mixed with a solvent and a catalyst and stirred for a few hours, close to room temperature. This is then followed by the hydrolysis, a reaction that can be catalyzed by acids or alkalis. Afterwards, in the gelation step, the sol transforms into a gel. This step consists in the establishment of bonds between the solution molecules to form a three-dimensional

network. It is important to stand out that this process is different from the solidification of a mixture, since the solid structure remains completely impregnated within the sol. [76] During the aging step, the sol-gel derived material expels the liquid phase (solvent) in a process called syneresis. [74, 77] During the drying process the gel volume decreases several times and a glasslike material is obtained, named xerogel. [74]
Finally, the material is heat-treated in order to favor further polycondensation and to obtain a glass with more adequate mechanical properties, smaller pore size and structural stability via sintering and densification of the material.

As mentioned in section 3.1, the developed micropatterning approach allows to modify the surface of ceramics by combining the two described methods, sol-gel and soft-lithography. During the sol stage, the silica solution is applied onto the ceramic and the PDMS negative mold is pressed against de substrate. After a few hours, the silica sol dries and the PDMS mold can be removed, leaving a microfabricated coating on top of the ceramic. [66, 78] Figure 3.2 illustrates the process to stamp silica coatings.

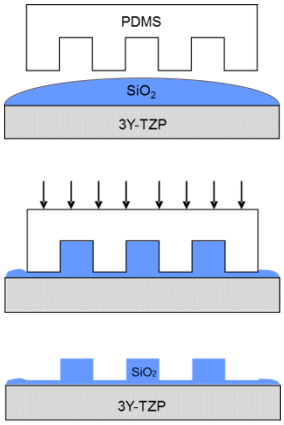

Figure 3.2 – Final preparation step of micropatterned SiO_2 coatings. [78]

3.4. SILICA PROPERTIES

Silica glasses have been widely studied for bone regeneration strategies due to their high biocompatibility and biological effects upon implantation. [42] SiO_2 is bioactive, meaning that it binds to and interacts with living bone without inducing the formation of fibrous tissue around it, thus not promoting excessive inflammatory reaction nor citotoxicity.[79-81] Additionally, silica glasses prepared by sol-gel have been shown to exhibit high bone

bonding and osteointegration rates with excellent degradation/bioresorption properties and ionic degradation products from silica have shown osteoconductive properties. [82]
A common characteristic of all bioactive materials is the formation of a biologically active hydroxycarbonate apatite (HCA) layer, due to surface dissolution in physiological environment. This formation of HCA on bioactive glasses and the release of soluble silica ions $(SiO_4)^{4-}$ to the surrounding tissue are key factors in the rapid bonding of these glasses to tissue, stimulating its growth. [76, 81, 83]

Adding a bioactive coating to a bioinert biomaterial may be a good approach to optimize the biological response to an implant. Still, the development of strategies that allow a modification directly on the biomaterial would make its production easier, without the need of adding another element to the final product. Additionally, if high mechanical forces are considered, a coating that cannot withstand high mechanical loading may be a liability to the final product, thus the need for direct surface modification strategies.

3.5. ULTRAFAST LASER IRRADIATION

So far, the main techniques used to modify implants surface were mostly developed for application in metals. Specifically, the most common methods used to modify commercial titanium are plasma or HVOF spraying, grid blasting, acid etching, laser ablation and anodizing. [60]
Since hard ceramics were later introduced as suitable materials for bone regeneration and replacement, the know-how developed for titanium surface modification has reduced applicability for ceramics.
The available methods can affect the stability of the tetragonal phase of Y-TZP by low temperature degradation in the presence of water and yttria leaching due to chemical attack. Methods like sandblasting can also cause small flaws in the structure of the ceramics, which will affect the mechanical performance in the long-term.[84-85]
The use of ultrafast lasers to create micro- and nano-texturing may be a good approach for surface modifications to improve osteointegration processes, such as protein adsorption and cell/surface interactions. Laser micromachining is a relatively fast and non-contact process that does not require tooling, thus eliminating tool wear and cutting forces on the material. [86] Commonly, CO_2 and Nd/YAG lasers have been applied to treat ceramics; however, they can cause chemical decomposition, thermal stresses and

microcracking due to the thermal nature of the radiation interaction of these lasers with the material. [87-88] Due to these limitations in processing ceramic materials, the use of femtosecond UV laser-ablation has been recently investigated. [87, 89-90] The interaction between the UV light pulses with the ceramics surface is manly electronic, with a direct band–band excitation, which leads to a higher accuracy of machining and smoother surfaces. [88]

Femtosecond laser treatment allows achieving a wide range of surface textures while minimizing damage to the material. Its main advantage is the fact that it operates with extremely short pulse duration, so a very high peak power is achieved leading to intense non-linear effects, which allows processing almost every type of materials without undesirable collateral thermal effects. [91]

Recent work has shown that, with appropriate processing methods, desired patterns can be imprinted on materials surfaces in a very short timescale of a ultrafast laser pulse duration and at the laser pulse frequency (up to 100 MHz), allowing for fast surface patterning by laser direct writing. The systems allows creating isotropic or anisotropic patterns with roughness varying between ~10 nm and 10 μm and periodicity between ~200 nm and 200 μm by adjusting optical parameters. [91-92]

Previous work developed by Oliveira, *et al* established the ability to produce micro-, nano- and multiscales topographies consisting of micropillars, nanopillars and combinations of both. [92]

Considering specifically Alumina and Zirconia, some work has been developed regarding its modification with femtosecond lasers, but few results are available with periodic surface patterning or biological characterization of such surfaces. [93-95]

4. BIOLOGICAL RESPONSE TO SURFACE TOPOGRAPHY

The field of dentistry played an important role in promoting and establishing research on modified surface implants, especially with Titanium. Surface roughness is now well known to affect the rate of osteointegration and biomechanical fixation of dental implants and can be classified in terms of macro-, micro- and nano- sized topography. The macro-sized topography can range from millimeters to hundreds of micrometers, and is directly related to the implant geometry, having a major role in the primary stability of the implants during the early phases of implantation. [60-61]

On the other hand, both micro- and nano- sized topographies have shown to play a more crucial role in terms of cellular and molecular responses, by enhancing protein adsorption, cell adhesion and consequently, improving osteointegration.

Specifically, the effects of microtopography on cell behavior has been widely studied and previous research has shown that micropatterned surfaces, independently of their surface chemistry, exhibit a strong influence on *in vitro* and *in vivo* cell behavior. [95-97]

Cell responses to topography can differ based on the pattern topography. Uniformly or randomly textured surfaces on the micro-and nano-scale have been used to study cell adhesion, spreading, migration and phenotype expression. Anisotropic topographic patterns have shown to induce cell alignment and dictate the degree of migration along grooves and ridges. In turn, isotropic surfaces tend to show a more random cells orientation, with cell spreading and contact to several patterns. [47]

Cells respond to surface features by adjusting their morphology and/or orientation. This cellular reaction is usually termed as **contact guidance**, an important morphogenetic mechanism where traction forces exerted by cells might create fiber orientation that then serves to guide their migration. [98-99] When responding to surface topography, changes in cell morphology, including cell alignment, can be regarded as one of the early indicators for cell differentiation and gene expression. There are several reports using patterned surfaces that show that there is a range of micro-scale surface topographies that improve cellular activity and extracellular matrix formation/mineralization, thus leading to a faster and more reliable osteointegrative response. [63, 100]

Numerous studies developed in the last years, performed *in vitro* and *in vivo,* also suggest that micro-scale features enhanced cell adhesion and proliferation, cell orientation and organization along the direction of the microfeatures, altered migration and motility patterns. Up-regulation of certain cytoskeletal and extracellular matrix proteins was also

induced, as well as reduced immune response, increased mitochondrial activity and augmented differentiation. It was established that these effects are both cell and topography-dependent. [101-104]

The effects of nanotextured surfaces on cell behavior have also been the subject of several studies. [105-106] Dalby, *et al*. have shown that circular nanostructures can induce osteogenic differentiation of mesenchymal stem cells without osteogenic factors on the cell culture medium. [107] Also, micro- and nanostructured material surfaces have shown to provide a greater number of nucleation sites for the precipitation of calcium and phosphorus from blood plasma, which results in the formation of an amorphous apatite layer on the surface of the implant that could potentiate osteointegration. [108]

The effect of micro- and nano- surface textures and arrangements on cells organization, proliferation and differentiation is still an open field to extensive research. Continuous research can lead to the development of specific surface topographies that can guide tissue regeneration and consequently achieve full osteointegration.

REFERENCES

1. Olszta, M. J.; Cheng, X.; Jee, S. S.; Kumar, R.; Kim, Y.-Y.; Kaufman, M. J.; Douglas, E. P.; Gower, L. B. Bone Structure and Formation: A New Perspective. *Materials Science and Engineering: R: Reports* **2007,** *58*, 77-116.
2. Schaaf, H.; Lendeckel, S.; Howaldt, H. P.; Streckbein, P. Donor Site Morbidity after Bone Harvesting from the Anterior Iliac Crest. *Oral surgery, oral medicine, oral pathology, oral radiology, and endodontics* **2010,** *109*, 52-8.
3. Sarkar, S. K.; Lee, B. T. Hard Tissue Regeneration Using Bone Substitutes: An Update on Innovations in Materials. *Korean J Intern Med* **2015,** *30*, 279-293.
4. Mantripragada, V. P.; Lecka-Czernik, B.; Ebraheim, N. A.; Jayasuriya, A. C. An Overview of Recent Advances in Designing Orthopedic and Craniofacial Implants. *J Biomed Mater Res A* **2013,** *101*, 3349-3364.
5. Buckwalter, J. A.; Glimcher, M. J.; Cooper, R. R.; Recker, R. Bone Biology .1. Structure, Blood-Supply, Cells, Matrix, and Mineralization. *J Bone Joint Surg Am* **1995,** *77A*, 1256-1275.
6. Wang, X.; Xu, S.; Zhou, S.; Xu, W.; Leary, M.; Choong, P.; Qian, M.; Brandt, M.; Xie, Y. M. Topological Design and Additive Manufacturing of Porous Metals for Bone Scaffolds and Orthopaedic Implants: A Review. *Biomaterials* **2016,** *83*, 127-41.
7. Henkel, J.; Woodruff, M. A.; Epari, D. R.; Steck, R.; Glatt, V.; Dickinson, I. C.; Choong, P. F. M.; Schuetz, M. A.; Hutmacher, D. W. Bone Regeneration Based on Tissue Engineering Conceptions - a 21st Century Perspective. *Bone Res* **2013,** *1*, 216-248.
8. Garnero, P. The Role of Collagen Organization on the Properties of Bone. *Calcified tissue international* **2015,** *97*, 229-40.
9. Henkel, J.; Woodruff, M. A.; Epari, D. R.; Steck, R.; Glatt, V.; Dickinson, I. C.; Choong, P. F.; Schuetz, M. A.; Hutmacher, D. W. Bone Regeneration Based on Tissue Engineering Conceptions - a 21st Century Perspective. *Bone Res* **2013,** *1*, 216-48.
10. Marks, S. C., Jr.; Popoff, S. N. Bone Cell Biology: The Regulation of Development, Structure, and Function in the Skeleton. *The American journal of anatomy* **1988,** *183*, 1-44.
11. Long, F. Building Strong Bones: Molecular Regulation of the Osteoblast Lineage. *Nature reviews. Molecular cell biology* **2011,** *13*, 27-38.
12. Komori, T. Regulation of Osteoblast Differentiation by Transcription Factors. *Journal of cellular biochemistry* **2006,** *99*, 1233-9.
13. Kirkham, G.; Cartmell, S. Genes and Proteins Involved in the Regulation of Osteogenesis. *Ashammakhi N, Reis R, Chiellini E, editores. Topics in Tissue Engineering* **2007,** *3*.
14. Fernandes, M. H.; Gomes, P. S. Bone Cells Dynamics During Peri-Implantitis: A Theoretical Analysis. *Journal of oral & maxillofacial research* **2016,** *7*, e6.
15. Kular, J.; Tickner, J.; Chim, S. M.; Xu, J. K. An Overview of the Regulation of Bone Remodelling at the Cellular Level. *Clin Biochem* **2012,** *45*, 863-873.
16. Raggatt, L. J.; Partridge, N. C. Cellular and Molecular Mechanisms of Bone Remodeling. *J Biol Chem* **2010,** *285*, 25103-25108.
17. Clarke, B. Normal Bone Anatomy and Physiology. *Clinical journal of the American Society of Nephrology : CJASN* **2008,** *3 Suppl 3*, S131-9.
18. Kular, J.; Tickner, J.; Chim, S. M.; Xu, J. An Overview of the Regulation of Bone Remodelling at the Cellular Level. *Clin Biochem* **2012,** *45*, 863-873.
19. Raggatt, L. J.; Partridge, N. C. Cellular and Molecular Mechanisms of Bone Remodeling. *J Biol Chem* **2010,** *285*, 25103-8.

20. Crockett, J. C.; Rogers, M. J.; Coxon, F. P.; Hocking, L. J.; Helfrich, M. H. Bone Remodelling at a Glance. *Journal of cell science* **2011,** *124*, 991-8.
21. Hadjidakis, D. J.; Androulakis, II Bone Remodeling. *Annals of the New York Academy of Sciences* **2006,** *1092*, 385-96.
22. Feng, X. Chemical and Biochemical Basis of Cell-Bone Matrix Interaction in Health and Disease. *Current chemical biology* **2009,** *3*, 189-196.
23. Rahman, M. S.; Akhtar, N.; Jamil, H. M.; Banik, R. S.; Asaduzzaman, S. M. Tgf-Beta/Bmp Signaling and Other Molecular Events: Regulation of Osteoblastogenesis and Bone Formation. *Bone Res* **2015,** *3*, 15005.
24. Vallet-Regi, M. Evolution of Bioceramics within the Field of Biomaterials. *Cr Chim* **2010,** *13*, 174-185.
25. O'Brien, F. J. Biomaterials &Amp; Scaffolds for Tissue Engineering. *Materials Today* **2011,** *14*, 88-95.
26. Vallet-Regi, M.; Izquierdo-Barba, I.; Colilla, M. Structure and Functionalization of Mesoporous Bioceramics for Bone Tissue Regeneration and Local Drug Delivery. *Philosophical transactions. Series A, Mathematical, physical, and engineering sciences* **2012,** *370*, 1400-21.
27. Kokubo, T. *Bioceramics and Their Clinical Applications*. Elsevier: **2008**.
28. Manzano, M.; Vallet-Regi, M. Revisiting Bioceramics: Bone Regenerative and Local Drug Delivery Systems. *Prog Solid State Ch* **2012,** *40*, 17-30.
29. Huang, J.; Best, S. 1 - Ceramic Biomaterials for Tissue Engineering. In *Tissue Engineering Using Ceramics and Polymers (Second Edition)*, Woodhead Publishing: **2014**, pp 3-34.
30. Best, S. M.; Porter, A. E.; Thian, E. S.; Huang, J. Bioceramics: Past, Present and for the Future. *J Eur Ceram Soc* **2008,** *28*, 1319-1327.
31. Park, J. B.; Bronzino, J. D. *Biomaterials: Principles and Applications*. crc press: **2002**.
32. Burdick, J. A.; Mauck, R. L. *Biomaterials for Tissue Engineering Applications: A Review of the Past and Future Trends*. Springer Science & Business Media: **2010**.
33. Moraes, M. C. C. d. S. e. B. d.; Elias, C. N.; Duailibi Filho, J.; Oliveira, L. G. d. Mechanical Properties of Alumina-Zirconia Composites for Ceramic Abutments. *Materials Research* **2004,** *7*, 643-649.
34. Shackelford, J. F. *Bioceramics*. CRC Press: **2004**; Vol. 1.
35. Sáenz, A.; Rivera, E.; Brostow, W.; Castano, V. M. Ceramic Biomaterials: An Introductory Overview. *Journal of Materials Education* **1999,** *21*, 267-276.
36. Narayan, R. *Biomedical Materials*. Springer: **2009**.
37. Evrard, L.; Waroquier, D.; Parent, D. [Allergies to Dental Metals. Titanium: A New Allergen. *Revue medicale de Bruxelles* **2010,** *31*, 44-9.
38. Urban, R. M.; Jacobs, J. J.; Tomlinson, M. J.; Gavrilovic, J.; Black, J.; Peoc'h, M. Dissemination of Wear Particles to the Liver, Spleen, and Abdominal Lymph Nodes of Patients with Hip or Knee Replacement. *The Journal of bone and joint surgery. American volume* **2000,** *82*, 457-76.
39. Sicilia, A.; Cuesta, S.; Coma, G.; Arregui, I.; Guisasola, C.; Ruiz, E.; Maestro, A. Titanium Allergy in Dental Implant Patients: A Clinical Study on 1500 Consecutive Patients. *Clinical oral implants research* **2008,** *19*, 823-35.
40. Jacobs, J. J.; Skipor, A. K.; Patterson, L. M.; Hallab, N. J.; Paprosky, W. G.; Black, J.; Galante, J. O. Metal Release in Patients Who Have Had a Primary Total Hip Arthroplasty. A Prospective, Controlled, Longitudinal Study. *The Journal of bone and joint surgery. American volume* **1998,** *80*, 1447-58.

41. Beckmann, N. A.; Gotterbarm, T.; Innmann, M. M.; Merle, C.; Bruckner, T.; Kretzer, J. P.; Streit, M. R. Long-Term Durability of Alumina Ceramic Heads in Tha. *BMC musculoskeletal disorders* **2015,** *16*, 249.
42. Kohal, R. J.; Att, W.; Bachle, M.; Butz, F. Ceramic Abutments and Ceramic Oral Implants. An Update. *Periodontology 2000* **2008,** *47*, 224-43.
43. Schierano, G.; Mussano, F.; Faga, M. G.; Menicucci, G.; Manzella, C.; Sabione, C.; Genova, T.; von Degerfeld, M. M.; Peirone, B.; Cassenti, A.; Cassoni, P.; Carossa, S. An Alumina Toughened Zirconia Composite for Dental Implant Application: In Vivo Animal Results. *BioMed research international* **2015,** *2015*, 157360.
44. Denry, I.; Kelly, J. R. State of the Art of Zirconia for Dental Applications. *Dental materials : official publication of the Academy of Dental Materials* **2008,** *24*, 299-307.
45. Lughi, V.; Sergo, V. Low Temperature Degradation -Aging- of Zirconia: A Critical Review of the Relevant Aspects in Dentistry. *Dental materials : official publication of the Academy of Dental Materials* **2010,** *26*, 807-20.
46. Nevarez-Rascon, A.; Aguilar-Elguezabal, A.; Orrantia, E.; Bocanegra-Bernal, M. H. On the Wide Range of Mechanical Properties of Zta and Atz Based Dental Ceramic Composites by Varying the Al2o3 and Zro2 Content. *Int J Refract Met H* **2009,** *27*, 962-970.
47. Jeon, H.; Hidai, H.; Hwang, D. J.; Healy, K. E.; Grigoropoulos, C. P. The Effect of Micronscale Anisotropic Cross Patterns on Fibroblast Migration. *Biomaterials* **2010,** *31*, 4286-95.
48. Park, J. B. *Bioceramics: Properties, Characterizations, and Applications*. Springer New York: **2008**; Vol. 218.
49. Giordano, R. Materials for Chairside Cad/Cam-Produced Restorations. *J Am Dent Assoc* **2006,** *137 Suppl*, 14S-21S.
50. Kohal, R. J.; Wolkewitz, M.; Hinze, M.; Han, J. S.; Bachle, M.; Butz, F. Biomechanical and Histological Behavior of Zirconia Implants: An Experiment in the Rat. *Clinical oral implants research* **2009,** *20*, 333-9.
51. Deville, S.; Chevalier, J.; Fantozzi, G.; Bartolome, J. F.; Requena, J.; Moya, J. S.; Torrecillas, R.; Diaz, L. A. Low-Temperature Ageing of Zirconia-Toughened Alumina Ceramics and Its Implication in Biomedical Implants. *J Eur Ceram Soc* **2003,** *23*, 2975-2982.
52. Daguano, J. K. M. F.; Santos, C.; Souza, R. C.; Balestra, R. M.; Strecker, K.; Elias, C. N. Properties of Zro2-Al2o3 Composite as a Function of Isothermal Holding Time. *Int J Refract Met H* **2007,** *25*, 374-379.
53. Schneider, J.; Begand, S.; Kriegel, R.; Kaps, C.; Glien, W.; Oberbach, T. Low-Temperature Aging Behavior of Alumina-Toughened Zirconia. *J Am Ceram Soc* **2008,** *91*, 3613-3618.
54. Faga, M. G.; Vallee, A.; Bellosi, A.; Mazzocchi, M.; Thinh, N. N.; Martra, G.; Coluccia, S. Chemical Treatment on Alumina-Zirconia Composites Inducing Apatite Formation with Maintained Mechanical Properties. *J Eur Ceram Soc* **2012,** *32*, 2113-2120.
55. Elshazly, S.; Elshazly, E. S.; Ali, M. E.-S.; El-Hout, S. Alumina Effect on the Phase Transformation of 3y-Tzp Ceramics. *Journal of Materials Sciences and Technology* **2009,** *24*, 873-877.
56. De Aza, A. H.; Chevalier, J.; Fantozzi, G.; Schehl, M.; Torrecillas, R. Crack Growth Resistance of Alumina, Zirconia and Zirconia Toughened Alumina Ceramics for Joint Prostheses. *Biomaterials* **2002,** *23*, 937-945.
57. Ruhle, M. In Situ Observations of Stress-Induced Phase Transformations in Zro 2-Containing Ceramics. *Advances in ceramics* **1984,** *12*, 256.
58. Puleo, D. A.; Nanci, A. Understanding and Controlling the Bone-Implant Interface. *Biomaterials* **1999,** *20*, 2311-21.

59. Treccani, L.; Yvonne Klein, T.; Meder, F.; Pardun, K.; Rezwan, K. Functionalized Ceramics for Biomedical, Biotechnological and Environmental Applications. *Acta biomaterialia* **2013,** *9*, 7115-50.
60. Le Guehennec, L.; Soueidan, A.; Layrolle, P.; Amouriq, Y. Surface Treatments of Titanium Dental Implants for Rapid Osseointegration. *Dental Materials* **2007,** *23*, 844-54.
61. Junker, R.; Dimakis, A.; Thoneick, M.; Jansen, J. A. Effects of Implant Surface Coatings and Composition on Bone Integration: A Systematic Review. *Clinical oral implants research* **2009,** *20 Suppl 4*, 185-206.
62. Govindarajan, T.; Shandas, R. A Survey of Surface Modification Techniques for Next-Generation Shape Memory Polymer Stent Devices. *Polymers-Basel* **2014,** *6*, 2309-2331.
63. Ito, Y. Surface Micropatterning to Regulate Cell Functions. *Biomaterials* **1999,** *20*, 2333-2342.
64. Mendonca, G.; Mendonca, D. B.; Aragao, F. J.; Cooper, L. F. Advancing Dental Implant Surface Technology--from Micron- to Nanotopography. *Biomaterials* **2008,** *29*, 3822-35.
65. Falconnet, D.; Csucs, G.; Grandin, H. M.; Textor, M. Surface Engineering Approaches to Micropattern Surfaces for Cell-Based Assays. *Biomaterials* **2006,** *27*, 3044-63.
66. Carvalho, A.; Pelaez-Vargas, A.; Gallego-Perez, D.; Grenho, L.; Fernandes, M. H.; De Aza, A. H.; Ferraz, M. P.; Hansford, D. J.; Monteiro, F. J. Micropatterned Silica Thin Films with Nanohydroxyapatite Micro-Aggregates for Guided Tissue Regeneration. *Dental Materials* **2012,** *28*, 1250-1260.
67. Pelaez-Vargas, A.; Gallego-Perez, D.; Magallanes-Perdomo, M.; Fernandes, M. H.; Hansford, D. J.; De Aza, A. H.; Pena, P.; Monteiro, F. J. Isotropic Micropatterned Silica Coatings on Zirconia Induce Guided Cell Growth for Dental Implants. *Dental Materials* **2011,** *27*, 581-589.
68. Marzolin, C.; Smith, S. P.; Prentiss, M.; Whitesides, G. M. Fabrication of Glass Microstructures by Micro-Molding of Sol-Gel Precursors. *Adv Mater* **1998,** *10*, 571-+.
69. Lam, M. T.; Clem, W. C.; Takayama, S. Reversible on-Demand Cell Alignment Using Reconfigurable Microtopography. *Biomaterials* **2008,** *29*, 1705-1712.
70. Xia, Y. N.; Whitesides, G. M. Soft Lithography. *Annu Rev Mater Sci* **1998,** *28*, 153-184.
71. Sakka, S. *Handbook of Sol-Gel Science and Technology. 1. Sol-Gel Processing*. Springer: **2005**; Vol. 1.
72. Yu, B. Y.; Chou, P. H.; Sun, Y. M.; Lee, Y. T.; Young, T. H. Topological Micropatterned Membranes and Its Effect on the Morphology and Growth of Human Mesenchymal Stem Cells (Hmscs). *J Membrane Sci* **2006,** *273*, 31-37.
73. Guleryuz, H.; Kaus, I.; Filiàtre, C.; Grande, T.; Einarsrud, M.-A. Deposition of Silica Thin Films Formed by Sol–Gel Method. *Journal of sol-gel science and technology* **2010,** *54*, 249-257.
74. Podbielska, H.; Ulatowska-Jarza, A. Sol-Gel Technology for Biomedical Engineering. *Technical Sciences* **2005,** *53*.
75. Arcos, D.; Vallet-Regi, M. Sol-Gel Silica-Based Biomaterials and Bone Tissue Regeneration. *Acta biomaterialia* **2010,** *6*, 2874-88.
76. Pierre, A. C. *Introduction to Sol-Gel Processing*. Springer: **1998**; Vol. 1.
77. McDonagh, C.; Sheridan, F.; Butler, T.; MacCraith, B. D. Characterisation of Sol-Gel-Derived Silica Films. *J Non-Cryst Solids* **1996,** *194*, 72-77.
78. Pelaez-Vargas, A.; Carvalho, A.; Grenho, L.; Monteiro, F. J.; Gallego-Perez, D.; Higuita-Castro, N.; Hansford, D. J.; Arismendi, J. A.; Fernandes, M. H.; Ferraz, M. P. *Micropatterned Coatings for Guided Tissue Regeneration in Dental Implantology*. **2012**.
79. Catauro, M.; Melisi, D.; Curcio, A.; Rimoli, M. G. Sol-Gel Processing of Anti-Inflammatory Entrapment in Silica, Release Kinetics, and Bioactivity. *J Biomed Mater Res A* **2008,** *87*, 843-9.

80. López, A.; Ureña, A.; Rams, J. Laser Densification of Sol–Gel Silica Coatings on Aluminium Matrix Composites for Corrosion and Hardness Improvement. *Surface and Coatings Technology* **2009,** *203*, 1474-1480.
81. Hench, L. L. Sol-Gel Materials for Bioceramic Applications. *Curr Opin Solid St M* **1997,** *2*, 604-610.
82. Hamadouche, M.; Meunier, A.; Greenspan, D. C.; Blanchat, C.; Zhong, J. P.; La Torre, G. P.; Sedel, L. Long-Term in Vivo Bioactivity and Degradability of Bulk Sol-Gel Bioactive Glasses. *Journal of biomedical materials research* **2001,** *54*, 560-566.
83. Hench, L. L.; Jones, J. R. *Biomaterials, Artificial Organs and Tissue Engineering*. CRC Press Boca Raton, FL, United States: **2005**.
84. Zhang, Y.; Lawn, B. R.; Rekow, E. D.; Thompson, V. P. Effect of Sandblasting on the Long-Term Performance of Dental Ceramics. *J Biomed Mater Res B Appl Biomater* **2004,** *71*, 381-6.
85. Zhang, Y.; Lawn, B. R.; Malament, K. A.; Van Thompson, P.; Rekow, E. D. Damage Accumulation and Fatigue Life of Particle-Abraded Ceramics. *Int J Prosthodont* **2006,** *19*, 442-8.
86. Samant, A. N.; Dahotre, N. B. Laser Machining of Structural Ceramics-a Review. *J Eur Ceram Soc* **2009,** *29*, 969-993.
87. Oliveira, V.; Vilar, R.; Conde, O.; Freitas, P. Laser Micromachining of Al2o3-Tic Ceramics. *Journal of materials research* **1997,** *12*, 3206-3209.
88. Cappelli, E.; Orlando, S.; Sciti, D.; Montozzi, M.; Pandolfi, L. Ceramic Surface Modifications Induced by Pulsed Laser Treatment. *Appl Surf Sci* **2000,** *154*, 682-688.
89. Ihlemann, J.; WolffRottke, B. Excimer Laser Micro Machining of Inorganic Dielectrics. *Appl Surf Sci* **1996,** *106*, 282-286.
90. Ihlemann, J.; Scholl, A.; Schmidt, H.; Wolffrottke, B. Nanosecond and Femtosecond Excimer-Laser Ablation of Oxide Ceramics. *Appl Phys a-Mater* **1995,** *60*, 411-417.
91. Oliveira, V.; Polushkin, N. I.; Conde, O.; Vilar, R. Laser Surface Patterning Using a Michelson Interferometer and Femtosecond Laser Radiation. *Opt Laser Technol* **2012,** *44*, 2072-2075.
92. Oliveira, V.; Ausset, S.; Vilar, R. Surface Micro/Nanostructuring of Titanium under Stationary and Non-Stationary Femtosecond Laser Irradiation. *Appl Surf Sci* **2009,** *255*, 7556-7560.
93. Perrie, W.; Rushton, A.; Gill, M.; Fox, P.; O'Neill, W. Femtosecond Laser Micro-Structuring of Alumina Ceramic. *Appl Surf Sci* **2005,** *248*, 213-217.
94. Erdur, E. A.; Basciftci, F. A. Effect of Ti:Sapphire-Femtosecond Laser on the Surface Roughness of Ceramics. *Lasers in surgery and medicine* **2015,** *47*, 833-8.
95. Dinca, V.; Sima, L. E.; Rusen, L.; Bonciu, A.; Lippert, T.; Dinescu, M.; Farsari, M. Bio-Interfaces Engineering Using Laser-Based Methods for Controlled Regulation of Mesenchymal Stem Cell Response in Vitro. In *Recent Advances in Biopolymers*, Perveen, F. K., Ed. InTech: Rijeka, **2016**, p Ch. 09.
96. Flemming, R. G.; Murphy, C. J.; Abrams, G. A.; Goodman, S. L.; Nealey, P. F. Effects of Synthetic Micro- and Nano-Structured Surfaces on Cell Behavior. *Biomaterials* **1999,** *20*, 573-88.
97. Wilkinson, C. D. W.; Riehle, M.; Wood, M.; Gallagher, J.; Curtis, A. S. G. The Use of Materials Patterned on a Nano- and Micro-Metric Scale in Cellular Engineering. *Materials Science and Engineering: C* **2002,** *19*, 263-269.
98. Guido, S.; Tranquillo, R. T. A Methodology for the Systematic and Quantitative Study of Cell Contact Guidance in Oriented Collagen Gels. Correlation of Fibroblast Orientation and Gel Birefringence. *J Cell Sci* **1993,** *105 (Pt 2)*, 317-31.

99. Sun, J.; Ding, Y.; Lin, N. J.; Zhou, J.; Ro, H.; Soles, C. L.; Cicerone, M. T.; Lin-Gibson, S. Exploring Cellular Contact Guidance Using Gradient Nanogratings. *Biomacromolecules* **2010,** *11*, 3067-3072.
100. Schwartz, Z.; Nasazky, E.; Boyan, B. D. Surface Microtopography Regulates Osteointegration: The Role of Implant Surface Microtopography in Osteointegration. *Alpha Omegan* **2005,** *98*, 9-19.
101. Curtis, A.; Wilkinson, C. Topographical Control of Cells. *Biomaterials* **1997,** *18*, 1573-83.
102. Clark, P. Cell Behaviour on Micropatterned Surfaces. *Biosensors and Bioelectronics* **1994,** *9*, 657-661.
103. von Recum, A. F.; van Kooten, T. G. The Influence of Micro-Topography on Cellular Response and the Implications for Silicone Implants. *J Biomater Sci Polym Ed* **1995,** *7*, 181-98.
104. Singhvi, R.; Stephanopoulos, G.; Wang, D. I. Effects of Substratum Morphology on Cell Physiology. *Biotechnol Bioeng* **1994,** *43*, 764-71.
105. Curtis, A.; Gadegaard, N.; Dalby, M.; Riehle, M.; Wilkinson, C.; Aitchison, G. Cells React to Nanoscale Order and Symmetry in Their Surroundings. *NanoBioscience, IEEE Transactions on* **2004,** *3*, 61-65.
106. Zhu, B.; Lu, Q.; Yin, J.; Hu, J.; Wang, Z. Alignment of Osteoblast-Like Cells and Cell-Produced Collagen Matrix Induced by Nanogrooves. *Tissue engineering* **2005,** *11*, 825-834.
107. Dalby, M. J.; Gadegaard, N.; Tare, R.; Andar, A.; Riehle, M. O.; Herzyk, P.; Wilkinson, C. D.; Oreffo, R. O. The Control of Human Mesenchymal Cell Differentiation Using Nanoscale Symmetry and Disorder. *Nature materials* **2007,** *6*, 997-1003.
108. Wang, C.-C.; Hsu, Y.; Hsieh, M.; Yang, S.; Su, F.; Lee, T. Effects of Nano-Surface Properties on Initial Osteoblast Adhesion and Ca/P Adsorption Ability for Titanium Alloys. *Nanotechnology* **2008,** *19*, 335709.

CHAPTER II

The effects of line and pillar array microengineered SiO_2 thin films on the osteogenic differentiation of human bone marrow derived mesenchymal stem cells

Angela Carvalho [1,2,3,*], Alejandro Pelaez-Vargas [4], Derek J. Hansford [5], Maria H. Fernandes [6], Fernando J. Monteiro [1,2,3]

[1] *i3S - Instituto de Investigação e Inovação em Saúde, Universidade do Porto, Rua Alfredo Allen, 208 4200-135, Porto, Portugal;*

[2] *INEB - Instituto de Engenharia Biomédica, Universidade do Porto, Rua Alfredo Allen, 208 4200-135, Porto, Portugal;*

[3] *Faculdade de Engenharia, Departamento de Engenharia Metalúrgica e Materiais, Universidade do Porto, Rua Dr Roberto Frias, s/n, 4200-465 Porto, Portugal;*

[4] *Universidad Cooperativa de Colombia, Faculty of Dentistry, Carrera 47 # 37sur-18, Medellín, Colombia;*

[5] *Department of Biomedical Engineering, The Ohio State University, 1080 Carmack Rd., Columbus, OH, USA*

[6] *Laboratory for Bone Metabolism and Regeneration, Faculdade de Medicina Dentária, Universidade do Porto, Rua Dr. Manuel Pereira da Silva, 4200-393 Porto, Portugal*

Langmuir 2016, 32, 1091−1100

ABSTRACT

A primary goal in bone tissue engineering is the design of implants that induce controlled, guided, and rapid healing. The events that normally lead to the integration of an implant into bone and determine the performance of the device occur mainly at the tissue-implant interface. Topographical surface modification of a biomaterial might be an efficient tool to induce stem cell osteogenic differentiation and replace the use of biochemical stimuli. The main goal of this work was to develop micropatterned bioactive silica thin films to induce the osteogenic differentiation of human bone marrow derived mesenchymal stem cells (hMSCs) only through topographical stimuli. Line and pillar micropatterns were developed by a combination of sol-gel/soft-lithography and characterized by SEM, AFM, and contact angle measurements. hMSCs were cultured onto the microfabricated thin films and flat control up to 21 days in basal conditions. The micropatterned groups induced higher osteogenic differentiation and expression of osteoblast-associated markers, compared to the flat controls. Comparing the micropatterns, the pillars caused a greater response of hMSCs osteogenic differentiation with higher expression of osteoblast-associated markers, ALP activity, and extracellular matrix mineralization after 21 days of culture. These findings suggest that specific microtopographic cues can direct hMSCs towards osteogenic differentiation.

Keywords: Biomaterials micropatterning, soft-lithography, microtopographic cues, osteogenic differentiation

1. Introduction

It is well established that the cell-surface interaction is a major determinant for successful biomaterials implantation. Cells react to topographic stimuli through mechanotransduction, a process in which physical stimuli are sensed through the cell membrane and transduced into intracellular signalling that causes changes in cells' functions.[1-4]

Cell reactions to physical cues have been classified based on the topographical patterns. Line topographies are known to cause cell alignment and guide cell migration, while pillar cues have shown to induce a random cellular orientation with high fiber stress.[5, 6] This modification of cell morphology dependent of the surface pattern can be considered as an early indicator for cell differentiation and gene expression.[4]

Even though topographical control of cells has been a well-exploited field, few authors have evaluated MSC differentiation based only on the impact of surface topography, without the potentially masking effects from osteogenic supplements.[7-11] Currently, the most common method of stimulating the osteogenic differentiation pathways in MSCs is through supplemented media or soluble factors. In most reports that evaluate the effects of topography, authors have chosen to stimulate osteogenic differentiation using combinations of both surface topography and soluble factors.[12-17]

However, the stimulation of MSCs into an osteogenic pathway through topographic stimuli has many advantages over other techniques commonly used to induce differentiation. Topographic modifications are much more stable *in vivo* than surface chemistry modifications and control the cell differentiation at a specific site of action. Also, the high dosages of chemicals used to achieve efficacy *in vitro* may cause adverse effects, such as tumorigenicity, and the obtained results are difficult to translate to *in vivo* situations.[8, 18, 19]

Currently, there is a lack of studies simultaneously characterizing the effects of different geometric patterns at micron scale on MSCs adhesion, proliferation, and osteogenic differentiation with no chemical stimulus. The existing studies tend to focus on cell response with variation on the scale, density or organization of a specific pattern.[20, 21, 22]

There is a range of micro-scale surface topographies that has proven to improve cellular activity and extracellular matrix formation/mineralization with a faster osteointegration response. Studies performed *in vitro* and *in vivo* indicated that micro-scale features enhanced cell adhesion and proliferation, orientation, and organization along the microfeatures, altered migration and motility patterns, up-regulation of certain cytoskeletal and extracellular matrix proteins, reduced immune response, and increased differentiation.[1, 23-26] The identification of topographic cues that precisely control MSCs differentiation would greatly improve the current tissue engineering strategies and implant efficacy.

Advances in microfabrication have allowed the development of well-defined topographical features to study the behavior of a wide range of cells.[16, 27-29] The combination of sol-gel processing and soft-lithography to create micropatterned bioactive silica thin films has been introduced in previous works by our group, to modify the surfaces of glass and zirconia.[30-32] Formerly, we focused mainly on modifying the surface of Zirconia in order to improve its bioactivity without compromising the mechanical properties**.** This approach makes it possible to produce micropatterned surfaces with

controlled chemistry, roughness, thickness, and textures that may be applied to several substrates.[33, 34]

Previous reports have shown that these micropatterned silica surfaces have the ability to modulate early cell attachment, proliferation and induce alignment of human dental pulp derived mesenchymal stem cells (hDP-MSCs), osteoblast-like cells, human gingival fibroblasts (HGF) and human dermal microvascular endothelial cells (HDMEC).[22, 31, 35]

In the current work a simple strategy is presented, based on sol-gel/soft-lithography combination, to fabricate controlled surface microtopographies with bioactive silica. With these thin films we propose to evaluate the effect of line and pillar microtopographies on the osteogenic differentiation of hMSC derived from human bone marrow. It was hypothesized that the microtopography itself might modulate and accelerate a MSC osteogenic response and the different geometric patterns would trigger different levels of osteogenic differentiation.

2. Experimental Section

2.1. Micropatterned thin films

A combined methodology of sol-gel and soft-lithography was used to produce micropatterned SiO_2 thin films. Glass coverslips (15mm, Marienfeld) were used as the substrate for the thin films. First, hybrid SiO_2 sols were produced via a sol-gel process with acid catalysis in a single stage, using tetraethylorthosilicate (TEOS, Sigma-Aldrich, USA) and methyltriethoxisilane (MTES, Sigma-Aldrich) as SiO_2 precursors at a 4:6 molar ratio. Alcohol and nitric and acetic acids served as solvent and catalysts, respectively. The sol was aged for 24 h at 4ºC prior to use. Flat SiO_2 thin films were prepared via spin-coating (SCS G3P-8 Specialty Thin film Systems, Cookson Electronics, USA) at 3000rpm for 45s.

The soft-lithography method was used to create line and pillar micropatterned silica surfaces. Initially, UV photolithography was used to produce a master mold with desirable microfeatures (lines and pillars, 5 µm in width with 10µm interspacing) in a Class 100 clean room facility. Afterwards, negative molds of polydimethylsiloxane (PDMS, Silastic T-2, Dow Corning, USA) were obtained by mixing the base with the curing agent and pouring it over the master molds. The SiO_2 sols were then stamped on the glass coverslips using the PDMS molds. Finally, the samples were heat-treated at

500ºC for 60 minutes using a 5°C/min ramp rate. All the thin films were later visualized by SEM.

2.2. Materials Characterization

Morphology and topography analysis were carried out using a scanning electron microscope (SEM, FEI Quanta 400FEG ESEM/EDAX Genesis X4M), sputter thin film all samples were with palladium–gold. The surface topography of the thin films was evaluated using Atomic Force Microscopy (AFM, Veeco Metrology Multimode/ Nanoscope IVA) in tapping mode. AFM images were acquired after the sintering treatment. 3D topographic images of the thin films were obtained using commercial software (NanoScope, Digital Instruments/Veeco). Nanoroughness was calculated in terms of roughness average (Ra) and root-mean-square (Rq) on six boxes of 3μm × 3μm on the top of the patterns and the flat control.

Surface hydrophobicity was quantified using a contact angle measurement device (OCA 15, DataPhysics Instruments GmbH). The sessile drop method was applied with ultrapure water at 25 ºC and the contact angle was calculated by the Laplace–Young function (SCA 20 software, DataPhysics Instruments GmbH). All the patterned surfaces were similarly oriented. Other relevant material characterizations had been previously performed.[22, 31]

2.3. Biological characterization

2.3.1. hBMSCs harvest and culture

Human Mesenchymal Stem Cells (hMSCs) from human bone marrow were obtained from orthopaedic surgery procedures, with patient's informed consent. The bone was broken into small pieces and washed with alpha-minimum essential medium (α-MEM, Sigma) supplemented with 10 % fetal bovine serum (FBS, Gibco) and 1 % penicillin-streptomycin (3×10^{-4} mol/L and 5×10^{-4} mol/L, Gibco), basal culture medium. The resultant cell suspensions were seeded in Petri dishes for 10 days. Afterwards, cell monolayers were washed with PBS twice and the media was changed.

A flow cytometry analysis confirmed that cells were positive for MSC markers CD105, CD146 and CD90, and negative for CD45.

When a high degree of confluence was reached in the primary culture, the adherent cells were washed with PBS, enzymatically released with 0.04% trypsin at 37 ºC, and subcultured. Cells of passage 4 were used in the experiments. As MSCs have the ability

to differentiate into several lineages, a preliminary experiment was performed to evaluate the favoured differentiation pathway of these cells in the experimental conditions used to address the cell response to the developed micropatterned films. Cells were seeded at a density of 2×10^4 cells/cm^2 on tissue culture polystyrene (TCPS) and cultured for 21 days in the basal medium described above. After, histochemical staining was performed with ALP stain for osteogenesis, Oil red stain for adipogenesis and safranin O for chondrogenesis. Cells stained positively for osteoblasts and negative for both chondrocytes and adipocytes.

Micropatterned thin films (Lines and Pillars) and the flat SiO_2 thin film control (Flat) were seeded with MSCs at a density of 2×10^4 cells/cm^2, and cultured for 21 days in the basal medium. In a parallel experiment, MSCs were also cultured on tissue culture polystyrene (TCPS), used as a control of the cell culture.

The cultures were incubated in a humidified atmosphere of 5% CO_2 at 37 ºC, with the culture medium being changed twice a week. Cultures were characterized throughout the culture time as follows.

2.3.2. Cells metabolic activity/proliferation

Cell metabolic activity was evaluated by the resazurin assay. Fresh medium with 10% of resazurin was added to the cells and incubated for 3 hours. Afterwards, 100µl was transferred to a 96-well plate and the fluorescence was quantified in a microplate reader (Synergy HT, BioTek) at 535 nm excitation wavelength and 590 nm emission wavelength. The results were expressed in relative fluorescence units (RFU).

DNA content was measured using the Quant-iT^{TM} Picogreen® DNA assay (Invitrogen) according to the manufacturer's instructions. Briefly, 100 µL of each cell lysate solution was added to 100 µL of PicoGreen reagent and incubated in the dark at room temperature for 5 min. Finally, the fluorescence intensity was measured with a microplate spectrofluorometer (Synergy HT, BioTek) at 530 and 590 nm (480-520 nm) emission (excitation), respectively. The results were expressed in ng of DNA per mL.

2.3.3. Cell Morphology

For focal adhesion immunostaining, fixed samples (3.7% paraformaldehyde, 15 min) were incubated for 5 min with 0.1% v/v Triton X-100 (Sigma) and 30 min with 1 wt% bovine serum albumin (BSA, Merck) at room temperature, to block nonspecific binding. Samples were then incubated with mouse anti-human vinculin mAb clone hVIN-1

(Sigma) at 1:100 for 1h at room temperature and then washed with PBS and stained with Alexa Fluor 488 rabbit anti-mouse IgG, F(ab')2 fragment (Molecular Probes) at 1:200 for 30 min at room temperature. Samples were subsequently washed three times and nuclei were counterstained with 1 μg ml^{-1} DAPI (Molecular Probes) for 10 min at RT. Cells were observed with a Spectral Confocal Microscope Leica TCS-SP5 AOBS (Leica) after staining. Immunostained cells were analysed in three replicates of each surface that were divided in 5 quadrants. In the obtained images, contrast was enhanced with Corel Photo-Paint X7 in order to accentuate focal adhesions from non-specific staining of the cells actin. For the morphology evaluation via SEM (FEI Quanta 400 FEG/ESEM), the cells were dehydrated in graded ethanol and hexamethyldisilazane (HMDS, Sigma) solutions from 50% to 100%, respectively. The samples were then sputter-coated (SPI-Module) with palladium-gold.

2.3.4. ALP activity

For the alkaline phosphatase (ALP) activity and total protein content measurements, cells were washed with PBS, frozen at -20ºC and later thawed at 37ºC to carry out the measurements. Cells were permeabilized by adding 200 μl of 0.1% v/v Triton X-100 for 30 minutes. Total protein was quantified by Lowry's method using bovine serum albumin as a standard. The ALP activity of cells was analyzed by substrate hydrolysis (p-nitrophenyl phosphate, Sigma) in alkaline buffer solution (2-amino-2-methyl-1-propanol, Sigma) at pH 10.5. The plate was incubated at 37ºC for 1h and consecutively NaOH (5M, Sigma) was added to stop the hydrolysis reaction and the product p-nitrophenol was measured in a plate reader at 405 nm of absorbance. The ALP results were normalized to total protein content and were expressed in nanomoles of p-nitrophenol produced per microgram of protein (nmol μg $protein^{-1}$).

2.3.5. Reverse transcriptase polymerase chain reaction (RT-PCR)

At day 21 of culture, total RNA was isolated from the cell culture on the materials using the RiboPure™ kit according to the manufacturer's instructions and quantified by measuring the absorbance of the samples at 260 nm. RT-PCR was performed using the Titan One Tube RT-PCR System (Roche Applied Science, USA), according to the manufacturer's instructions with a total volume of 25 μl for each reaction mixture. Total RNA (200 ng) was reverse transcribed at 50ºC for 30 min, followed by 2 min at 94ºC for

denaturation. Complementary DNAs (cDNAs) were then amplified with recombinant Taq-DNA polymerase with 30 cycles of denaturation at 94ºC for 30 s, annealing at 55ºC for 30 s, elongation at 68ºC for 45 s, followed by a prolonged elongation of 7 min at 68ºC. The primer sequences used for PCR amplification are shown in Table 1. In order to obtain a semiquantitative assessment of gene expression, data were expressed as normalized ratios by comparing the integrated density values for all genes tested with those for glyceraldehyde- 3-phosphate dehydrogenase (GAPDH). The PCR products were separated by 1% (w/v) agarose gel electrophoresis and visualized by ethidium bromide staining. The images of the gel were captured with a camera and the densitometric analysis of the bands obtained was performed with ImageJ 1.41 software.

Table 1 - Primers for PCR amplification

Gene	Primer sequence (forward)	Primer sequence (reverse)
GAPDH	5'-CAGGACCAGGTTCACCAACAAGT-3'	5'-GTGGCAGTGATGGCATGGACTGT-3'
RUNX2	5'-CAGTTCCCAAGCATTTCATCC-3'	5'-TCAATATGGTCGCCAAACAG-3'
COL-I	5'-TCCGGCTCCTGCTCCTCTTA-3'	5'-ACCAGCAGGACCAGCATCTC-3'
ALP	5'-ACGTGGCTAAGAATGTCATC-3'	5'-CTGGTAGGCGATGTCCTTA-3'
BMP-2	5'-GCAATGGCCTTATCTGTGAC-3'	5'-GCAATGGCCTTATCTGTGAC-3'
OC	5'-CATGAGAGCCCTCACA-3'	5'-AGAGCGACACCCTAGAC-3'

2.3.6. Histochemical assays

For histochemical analyses, fixed cultures (1.5% glutaraldehyde, 10 min) were stained for phosphate and calcium deposits. Phosphate deposits were assessed by the von Kossa assay. The cultures were covered with a 1.0% silver nitrate solution and kept for 1 h under UV light. After washing with distilled water, a 5.0% sodium thiosulphate solution was added for 2 min and cultures were washed again. Phosphate deposits stained black.

Alizarin red staining was used to assess calcium-rich deposits produced by cells in culture. A pH 6.3 solution was produced by mixing 3 mg of Alizarin Red S with 3 ml of NH_4OH 0.28%. This solution was filtered and applied to the fixed cells for 2 min. Afterwards, cells were washed with distilled water and a solution of acidic ethanol was added for 15 s. Cells were again washed and left to dry. The reaction stained the calcium deposits in orange/red.

2.4. Statistical analysis

Triplicate experiments were performed for all experiments. The results were expressed as the arithmetic mean ± standard deviation. The statistical analysis of the results was done using the one-way analysis of variance (One-way ANOVA) followed by the Tukey HSD *post hoc* test. Levels of $p \leq 0.05$ were considered to be statistically significant. The statistical analysis was performed using the SPSS statistical software (Statistical Package for the Social Sciences Inc., USA).

3. Results

3.1. Materials characterization

SEM observation showed that both thin films with line and pillar arrays were successfully fabricated. The thin films faithfully reproduced the mold features with micropatterns of ~5 μm width and ~10 μm interspacing, as shown in Figure 1.

The 3D topographic images of the micropatterned and flat silica thin films obtained by AFM are shown in Figure 1. The nanoroughness analysis (Ra and Rq parameters) revealed that the top of the lines had a statistically significant higher average roughness (Ra = 78.98 ± 1.54 nm) when compared to both the top of the pillars (Ra = 9.43 ± 2.20 nm) and the flat control (Ra = 0.71 ± 0.06 nm). Also, the roughness of the micropatterned pillars surface was statistically significantly higher than that of the flat silica control. The same results were obtained for the measurements of root mean square (Rq) where the micropatterned lines presented the highest values (Rq = 92.88 ± 1.95 nm), followed by the micropatterned pillars surface (Rq = 16.55 ± 5.03 nm), while the flat silica thin film presented statistically significantly lower Rq values (Rq = 0.87 ± 0.05 nm).

The results of water contact angle (WCA) measurements (Figure 1) revealed that the silica produced by sol-gel is a hydrophilic material, as it is shown by the contact angle of the flat control. The contact angle increased significantly with the presence of the patterned features, with the pillar array surface presenting a hydrophilic behaviour on the verge of hydrophobic values while the line array thin film revealed high hydrophobicity values.

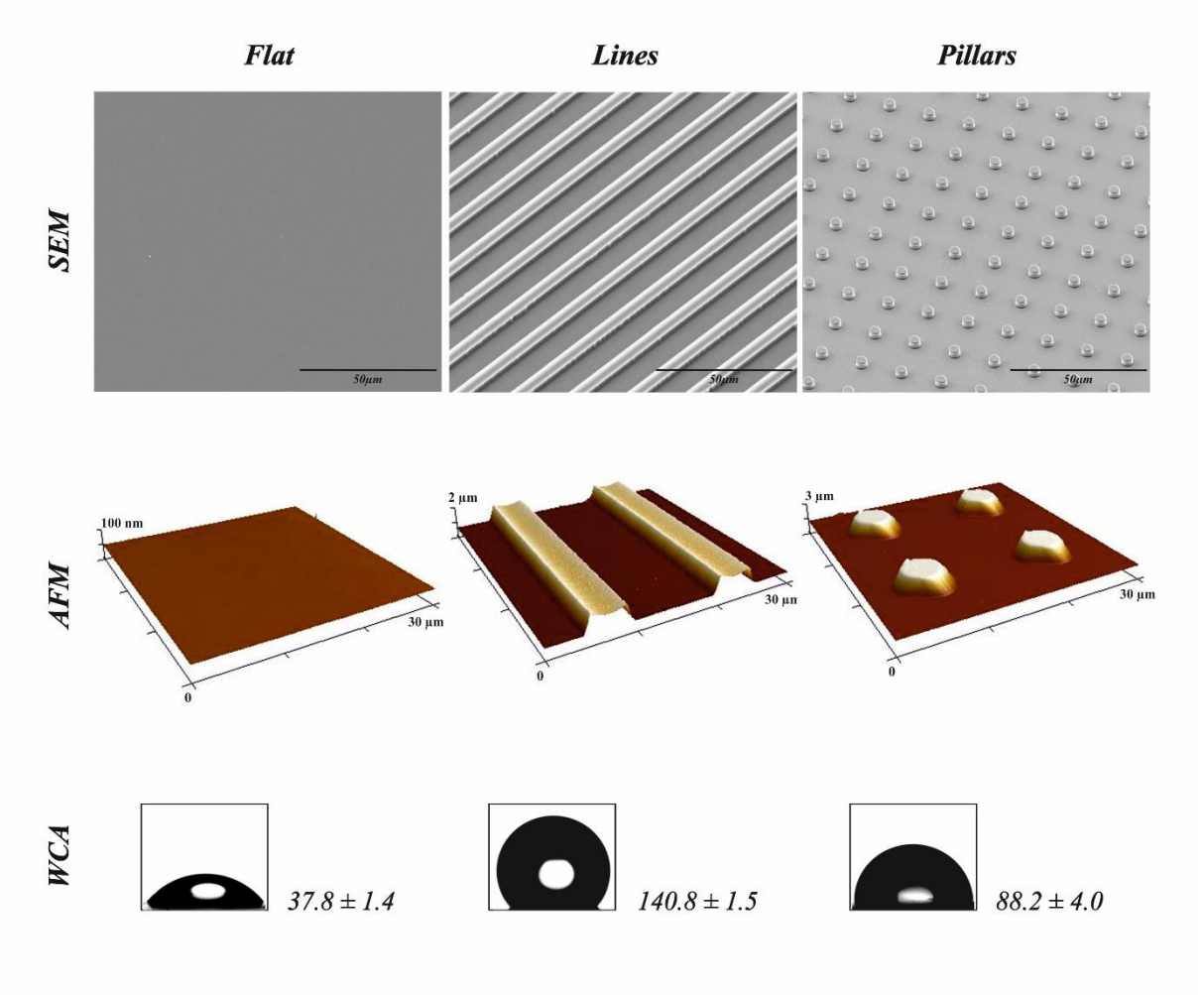

Figure 1 – SEM, AFM and WCA characterization of the flat and micropatterned silica thin films.

3.2. Biological characterization

3.2.1. Cells metabolic activity and proliferation

Figure 2 shows the results of the rezasurin and DNA quantification assays. The rate of cell growth increased with the time of culture for all SiO_2 thin films, with a low growth rate between days 1 and 7, a lag-phase characteristic of hMSCs cultures. From this time-point onwards, the cell growth rate increased up to the 21st day of culture for all tested materials. In terms of metabolic activity, the flat silica group exhibited a statistically significant increase at day 14, compared to both micropatterned groups. No statistical differences were observed between the microstructured surfaces for all time-points. Similar results were obtained for cell proliferation through DNA quantification (Figure 2): a higher cell proliferation at day 14 for the flat surface group and no differences between both micropatterned thin films at any time points.

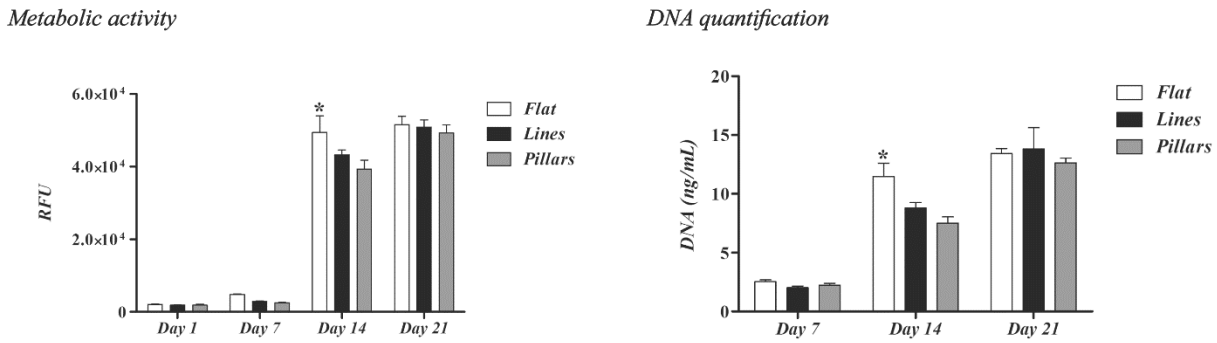

Figure 2 – Cell metabolic activity/proliferation of hBMSCs cultured on the three silica thin films. * represents statistically significant differences ($p \leq 0.05$) between the thin films, at each time-point.

3.2.2. Morphology

Cells focal adhesions at day 1 were observed by confocal microscopy (Figure 3). Cells are well adhered to the silica films and more spread out on the micropatterned thin films, generally following to the patterns. The cells adhered to the flat silica thin films show less focal adhesions than those adhered to the micropatterned silica thin films. On both micropatterned films, cells showed a higher number of focal adhesions mainly following and connecting to the patterns. The focal adhesions formed on the lines patterns are also anisotropically oriented according to the features on the surface. On the micropatterned pillars it was possible to observe a high number of focal adhesions connected to several patterns on the film surface, located mainly on the cell periphery, which exhibited a stretched morphology throughout the surface of the thin films.

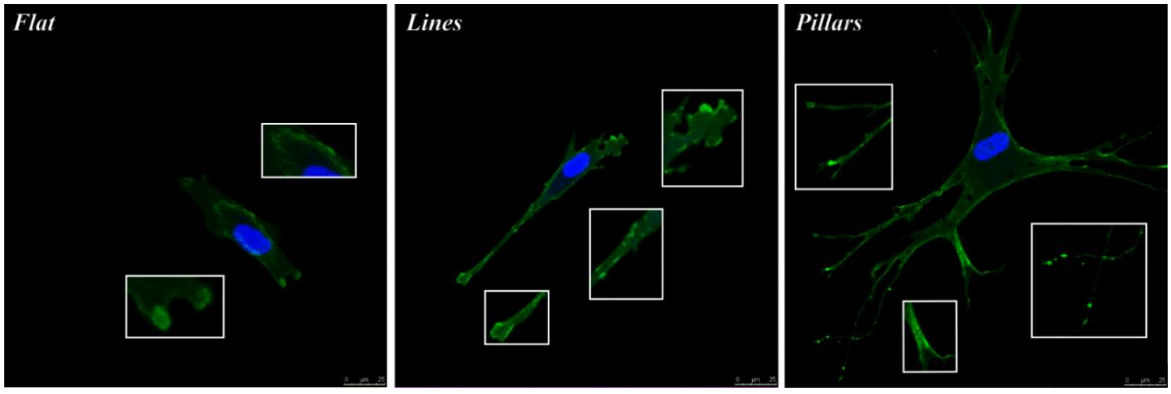

Figure 3 - Immunostaining of focal adhesions and cells morphology at day 1 of culture on the flat, lines micropatterned and pillars micropatterned thin films. hMSCs focal adhesions were stained with phalloidin (green) and nuclei with DAPI (blue).

SEM evaluation of cells morphology at day 7 and 14 is presented in Figure 4. At day 7, the hMSCs on the flat films were randomly oriented and spread. On the lines surfaces, cells maintained their alignment according to the features, while on the pillars surface, cells were well spread and stretched with filopodia connecting several pillars through the surface, as shown in the immunostaining of focal adhesions. After 14 days, the flat silica thin films were completely covered by a layer of cells. The surfaces of both micropatterned thin films were mainly covered by a layer of hMSCs that still exhibited filopodia connected with the micropatterns and neighboring cells. On the lines patterns thin films, cells were completely oriented according to the patterns while in the case of the micropatterned pillars group the cells are randomly oriented while exhibiting an extended morphology (Figure 4).

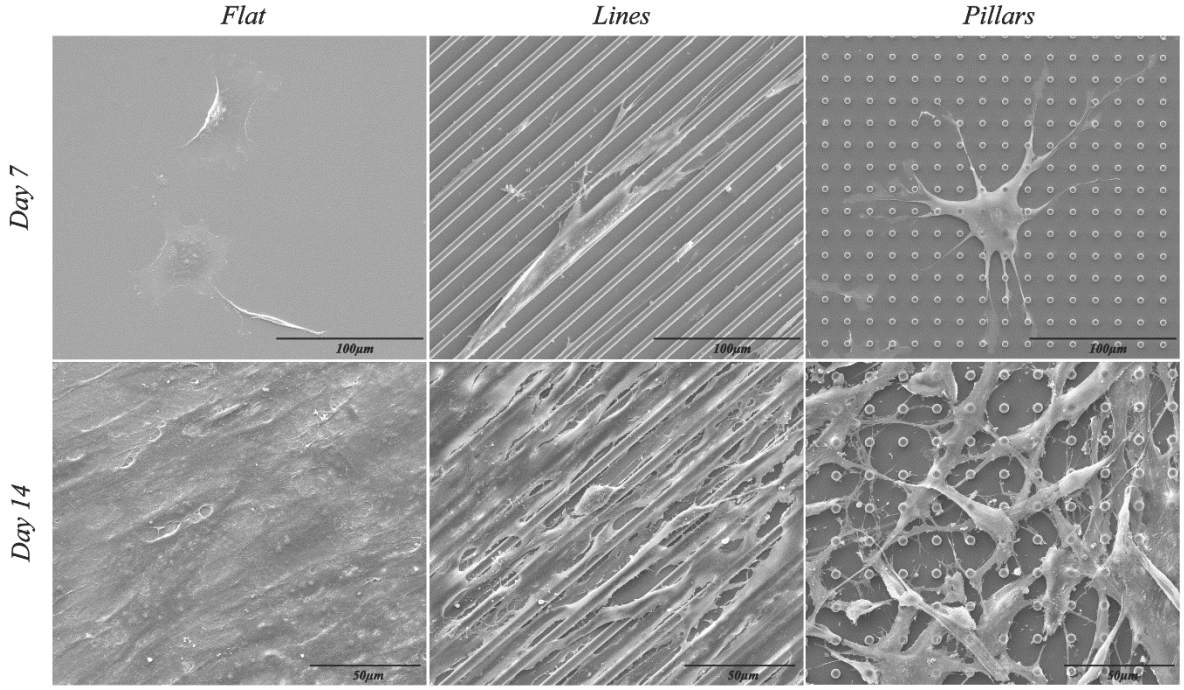

Figure 4 – SEM images of hMSCs morphology while adhered to the flat control and the micropatterned thin films, at 7 and 14 days of culture.

3.2.3. ALP activity and RT-PCR

The ALP activity increased with the time of culture for all tested silica thin films (Figure 6). At the 14 and 21 days of culture, the micropatterned pillars group induced a statistically significant higher enzyme activity, compared with both the flat and the lines groups.

Regarding the RT-PCR results, all surfaces expressed osteoblast-associated markers after 21 days of culture. Osteoprotegerin (OPG) was expressed by the cells cultured on all silica thin films with no differences. The micropatterned surfaces showed a significantly higher expression of RUNX2, BMP-2, and ALP when compared to the flat surfaces. On the other hand, the cells on flat controls expressed more collagen type I (COL-I) than on the pillars surfaces.

The micropatterned pillars surfaces stand out with a greater expression of osteocalcin (OC) compared to both the other groups. No other differences were found between cells on both micropatterned groups in the expression of the remaining osteoblast marker genes.

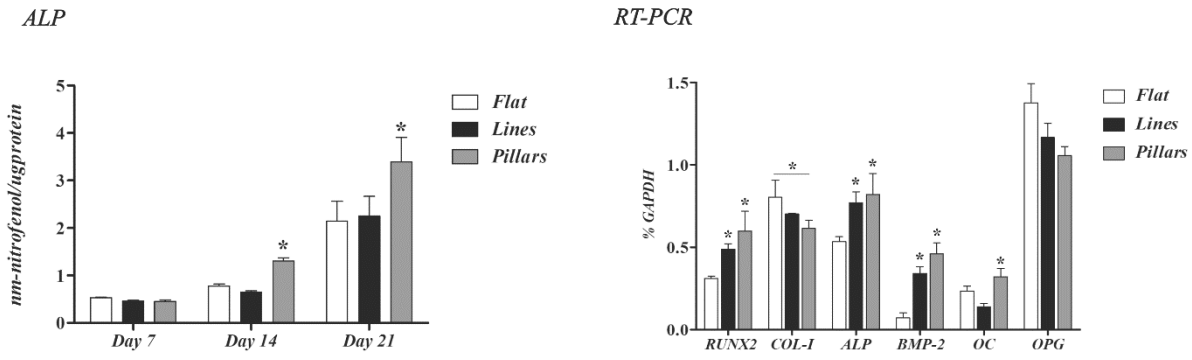

Figure 5 - Alkaline Phosphatase Activity and RT-PCR analysis, at 21 days of culture, of the osteoblastic-associated markers: RUNX2, COL-I, ALP, BMP-2, OC and OPG. * represents statistically significant differences ($p \leq 0.05$) between all SiO_2 films at each time-point.

3.2.4. Matrix Mineralization

At day 21, mineralization of the ECM by the hMSCs was assessed by SEM (Figure 6). Cells presented a continuous cell layer and calcium phosphate deposits were found in all the silica thin films, however, mineralization was much more evident on the pillars patterns surfaces, with deposits dispersed through the continuous layer of cells. In both the flat and lines patterns materials, there were fewer calcium phosphate deposits which were clearly smaller. Through EDS analysis it was calculated a Ca/P ratio of 1.58, within the range expected for calcium phosphate.

Figure 6 also shows the results from the Von Kossa reaction for the presence of phosphate deposits in hMSCs cultures. These demonstrated a positive staining at day 21. The micropatterned thin films showed a stronger positive reaction for the presence of

phosphate deposits with clear formation of three-dimensional nodules, more noticeable for the microstructured pillars surfaces. In addition, it was observed that on the microstructured surfaces, the phosphate deposits were aligned with the micropatterns.

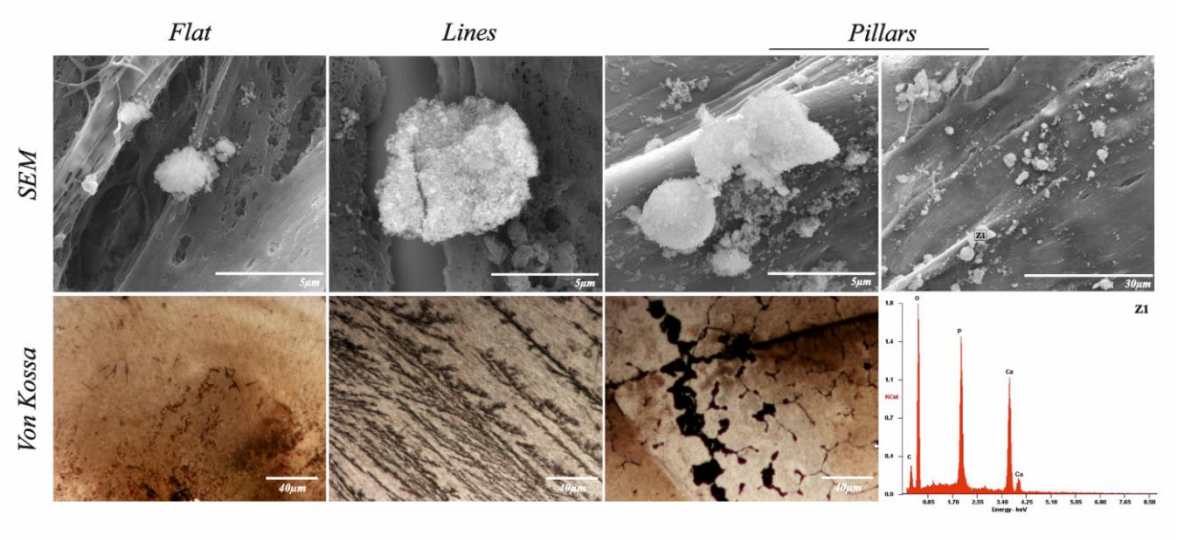

Figure 6 – SEM and Von Kossa images of the cells mineralization deposits after 21 days of culture. A representative EDS analysis of the calcium phosphate deposits is shown (bottom right).

4. Discussion

Line and pillar topographies are known to cause different responses from cells. While line patterns are known to induce cell alignment and guide cell migration along the patterned features, pillar patterns induce a more random orientation of cells, which tend to spread to interact with multiple features. [5, 36] It has been noted that stem cell differentiation into different lineages is accompanied by significant changes in cell morphology and that cell shape also has an effect on MSCs biological processes such as proliferation and differentiation. McBeath, *et al*., observed that MSC that adhered and spread were more likely to undergo osteogenesis, while unspread round cells commonly became adipocytes. [37, 38]

In this work hMSCs were cultured in basal conditions on two micropatterned surfaces with a chemically identical but flat surface used as control. Cell osteogenic differentiation was evaluated in terms of the effects of microtopography. We hypothesized that human mesenchymal stem cells can undergo osteogenic differentiation triggered solely by microtopographic stimuli, and different geometric shapes may trigger different levels of osteogenesis.

Line and pillar micropatterned silica thin films were successfully obtained through the combination of sol-gel and soft-lithography. The hydrophobicity studies of the silica thin films revealed that the wettability is affected by the micropatterning. The flat silica film presented a hydrophilic behavior and so did the pillars micropatterned surface, with a higher contact angle value, but still within hydrophilic limits. The lines surface, however, presented a highly hydrophobic value. The surface chemistry of both the micropatterned materials and the flat silica has been shown to be the same, therefore the quite different contact angle values are caused by the different nano/micro roughness of the surfaces. This phenomenon of microtopography influencing the wettability of a surface has already been observed by our group and also by other authors. [22, 31, 39, 40] The higher hydrophobicity value of the lines patterns surface may also be related with air gaps, which are more easily formed in this type of pattern.

These findings were complemented by the AFM results, that showed that the microtextured surfaces presented higher nanoroughness values than the flat film. In addition, the line pattern presented the highest values both for Rq and Ra analyses. This combinatory effect of micro/nanoroughness affecting the surfaces hydrophobicity has been previously reported. [41, 42]

It is thought that cells response to the underlying material was mainly modulated by surface topography/roughness and chemistry. The patterned surfaces may have strengthened cells adhesion, as shown by the higher number of focal adhesions on these surfaces.

Surface-cell and cell-cell interactions activate specific pathways that regulate stem cell fate [43]. However, the underlying biological phenomena that take place within cells when responding to surface topography have not yet been clearly unravelled. It is known that cells adhere to substrates through integrin-mediated focal adhesions and transfer information about the cell environment towards the cell interior, triggering a cellular response to the underlying surface topography that may influence processes such as adhesion, alignment, migration, differentiation, etc. [43, 44, 45, 46]

The cells adhering to the flat films displayed the lowest number of focal adhesions while the cells cultured on the micropatterned films presented more dot-like vinculin structures, supporting the hypothesis that the presence of the microfeatures enables the establishment of more cell-surface interactions. On the microstructured thin films the focal adhesions were mainly present in the lamellipodia and filopodia connecting to the patterns at the cells boundaries. This effect of focal adhesion arrangement according to surface

topography on cell actin organization and alignment has also been reported previously. [47, 48, 49, 50]

The *in vitro* culture showed that all the thin films were cytocompatible and capable of maintaining viable cells that proliferated throughout the culture period. Cells showed a well spread morphology on the pillar patterns thin films and a more elongated one on the line patterns. On the flat film, cells were randomly spread and elongated. From day 1 to day 7 of culture, the lag-phase, characteristic of MSCs is represented in both the metabolic activity and the proliferation values. The period of higher proliferation/expansion took place between day 7 and day 14, where both metabolic activity and proliferation were increased on all materials. Cells cultured on the flat control showed a significantly higher metabolic activity and proliferation for this time-point. These results suggest that while cells on the flat surface were still undergoing proliferation, MSCs on the micropatterned surfaces were already entering the stage of osteoblastic differentiation, therefore showing lower cell proliferation and metabolic activity. From day 14 to day 21 of culture, the proliferation remained almost the same and no differences were found between all the SiO_2 thin films. This indicates that from day 14 till day 21 cells on all the materials were decreasing proliferation and increasing differentiation. At days 14 and 21 of culture, cells on the micropatterned pillars showed a significantly increased ALP activity comparatively to both the flat and line patterned samples. When cells undergo differentiation, their proliferation is decreased. Previous studies have shown that cells with enhanced differentiation presented lower cell numbers, decreased proliferation and increased ALP activity and osteocalcin (OC) expression. [51, 52, 53] The RT-PCR results show that, at the 21st day of culture, hMSCs showed a commitment towards the osteoblastic lineage with expression of all osteoblast associated markers for all the thin films. The micropatterned surfaces displayed a significantly higher RUNX2, ALP and BMP-2 expression when compared to the flat control. The pillar array surfaces showed statistically significant increased OC gene expression when compared with both the flat and line array groups and a lower expression of COL-I than the flat control.

RUNX2 expression is necessary for multipotent MSC to differentiate into the osteoblastic lineage. This transcription factor plays an important role in osteogenesis and its expression is known to increase during osteoblast differentiation, in the mineralization phase. It is also known that its overexpression up-regulates ALP activity and the expression of osteoblast-specific genes such as OC, which is considered an essential marker of the mineralization state. [54, 55, 56, 57, 58, 59]

The pillar patterns samples, that demonstrated the most advanced osteogenic differentiation, exhibited a lower COL-I expression at day 21. These results are in accordance with the findings by zur Nieden, *et al*., indicating that type I collagen is mainly expressed at the end of cell proliferation and during matrix deposition. [55] ALP was up-regulated on both micropatterned surfaces, in accordance with RUNX2 results. Bone morphogenetic proteins (BMPs) have potent osteoinductive properties and have shown to regulate the differentiation of MSCs into bone cells and are essential in bone repair. BMP-2, specifically, promotes RUNX2 expression and strongly promotes MSC osteogenic differentiation. [59, 60, 61] In this work, the micropatterned surfaces with high BMP-2 expression also revealed higher levels of RUNX2. The significantly higher expression of OC, a late osteogenic marker, by the microstructured pillars group showed that MSC cultured on this surface were more advanced in the osteogenic differentiation, with mature osteoblasts and matrix mineralization.

The similar expression of OPG, a key gene regulating osteoclastogenesis, may indicate that the micropatterns would not affect normal osteoclastic activity.

The RT-PCR results are in agreement with the observation of mineralization through SEM and histochemical assays, in which the micro-pillars group presented the highest levels of ECM mineralization. Particularly, from the Von Kossa experiments it was possible to observe large nodules aligned with the characteristic cell morphology on these surfaces. This effect was also visible in the case of the lines surfaces, but with less pronounced and smaller nodules. The formation of a calcified extracellular matrix is a relevant indication of osteogenic differentiation.

Overall, osteogenic differentiation was more evident on the micropatterned surfaces. The results indicate that the hMSCs cultured on the pillars surfaces were at the most advanced state of osteoblast maturation with higher levels of extracellular matrix mineralization, as confirmed by the lower expression of COL-I, higher ALP activity, increased expression of OC, and larger area of mineralized matrix.

On the other hand, the hMSCs cultured on both the flat and micropatterned lines groups appeared to be still in ECM maturation stage in a transient evolution to the mineralization phase, with a higher COL-I expression, lower OC, and smaller mineralization nodules than those observed for the surfaces with the micro-pillars. Still, the micropatterned lines surface showed an earlier switch to the mineralization state, with more mineralization than the flat surface group and ALP, BMP-2, and RUNX2 expression at the same levels as the micro-pillars films.

Previous studies reported that the osteogenic differentiation of hMSCs could be enhanced when cultured on pits and pillar shaped patterns, due to the actin distribution and stretching to random directions. [9, 15] Our results from the pillars micro-scale patterns are in accordance with both studies, carried out with nanostructures. Dalby, *et al*., also showed that 120 nm circular disordered nanopits can induce osteogenic differentiation in the absence of chemical stimuli. [9]

Another study developed by Dalby's team showed that MSCs cultured on the same 120nm pits but with no disorder are capable of maintaining MSCs growth and multipotency for long periods of culture (28 days) [62]. This discovery shows that slight variations within the same patterns can produce very different outcomes of MSCs fate. These findings also show, although indirectly, that it is challenging to make comparisons with different studies, because even the smallest changes can produce quite different results.

The results obtained with the micro-pillars structures, when compared to the other two test surfaces, may be due to the fact that this surface geometry allows cells to organize more similarly to natural bone structure. The design of surface topography capable of inducing an earlier hMSCs commitment and differentiation into the osteoblastic lineage may trigger the formation of a stable mineralized ECM earlier in the healing process *in vivo*. The obtained results support our hypothesis that a precisely engineered micropatterned SiO_2 thin film could potentially be used to induce osteogenic differentiation and an earlier formation of a calcified extracellular matrix.

5. Conclusion

The results show that a specific range of microtopographic features could promote osteogenic differentiation of hMSCs and that this stimulation is dependent on the geometric pattern arrangement. Such microengineered surfaces modulated the behaviour of hMSCs in terms of adhesion, orientation, guided proliferation, and osteogenic differentiation. Both micropatterned thin films induced higher osteogenic differentiation than the flat control. The microstructured pillars thin films presented a higher potential to induce hMSCs differentiation into an osteogenic lineage through topographic stimuli with higher expression of mature osteoblast genes, higher ALP activity, and higher ECM calcification. Still, the micro-lines surface modulated cell proliferation and induced higher osteogenic differentiation than the flat control. These micropatterned surfaces may

be a good approach to be used when specific guided bone regeneration is required. Topography-mediated fate determination of hMSC has enormous potential to allow the design of specific implant surfaces capable of promoting rapid and more effective osteointegration.

Acknowledgements

This work was financed by *FEDER funds through the Programa Operacional Factores de Competitividade – COMPETE* and by *Portuguese funds through FCT – Fundação para a Ciência e a Tecnologia* in the framework of Ângela Carvalho's PhD grant (SFRH/BD/87624/2012) whose support is acknowledged.

References

1. Ito, Y. Surface micropatterning to regulate cell functions. *Biomaterials* **1999,** *20* (23-24), 2333-42.
2. Nikkhah, M.; Edalat, F.; Manoucheri, S.; Khademhosseini, A. Engineering microscale topographies to control the cell-substrate interface. *Biomaterials* **2012,** *33* (21), 5230-5246.
3. Guido, S.; Tranquillo, R. T. A Methodology for the Systematic and Quantitative Study of Cell Contact Guidance in Oriented Collagen Gels - Correlation of Fibroblast Orientation and Gel Birefringence. *J Cell Sci* **1993,** *105*, 317-331.
4. Sun, J. R.; Ding, Y. F.; Lin, N. J.; Zhou, J.; Ro, H.; Soles, C. L.; Cicerone, M. T.; Lin-Gibson, S. Exploring Cellular Contact Guidance Using Gradient Nanogratings. *Biomacromolecules* **2010,** *11* (11), 3067-3072.
5. Jeon, H.; Hidai, H.; Hwang, D. J.; Healy, K. E.; Grigoropoulos, C. P. The effect of micronscale anisotropic cross patterns on fibroblast migration. *Biomaterials* **2010,** *31* (15), 4286-95.
6. Lim, J. Y.; Donahue, H. J. Cell sensing and response to micro- and nanostructured surfaces produced by chemical and topographic patterning. *Tissue Eng* **2007,** *13* (8), 1879-1891.
7. Watari, S.; Hayashi, K.; Wood, J. A.; Russell, P.; Nealey, P. F.; Murphy, C. J.; Genetos, D. C. Modulation of osteogenic differentiation in hMSCs cells by submicron topographically-patterned ridges and grooves. *Biomaterials* **2012,** *33* (1), 128-36.
8. Zhao, L.; Liu, L.; Wu, Z.; Zhang, Y.; Chu, P. K. Effects of micropitted/nanotubular titania topographies on bone mesenchymal stem cell osteogenic differentiation. *Biomaterials* **2012,** *33* (9), 2629-41.
9. Dalby, M. J.; Gadegaard, N.; Tare, R.; Andar, A.; Riehle, M. O.; Herzyk, P.; Wilkinson, C. D. W.; Oreffo, R. O. C. The control of human mesenchymal cell differentiation using nanoscale symmetry and disorder. *Nat Mater* **2007,** *6* (12), 997-1003.
10. Oh, S.; Brammer, K. S.; Li, Y. S.; Teng, D.; Engler, A. J.; Chien, S.; Jin, S. Stem cell fate dictated solely by altered nanotube dimension. *Proceedings of the National Academy of Sciences of the United States of America* **2009,** *106* (7), 2130-5.
11. Olivares-Navarrete, R.; Hyzy, S. L.; Hutton, D. L.; Erdman, C. P.; Wieland, M.; Boyan, B. D.; Schwartz, Z. Direct and indirect effects of microstructured titanium substrates on the induction of mesenchymal stem cell differentiation towards the osteoblast lineage. *Biomaterials* **2010,** *31* (10), 2728-2735.

12. Kim, E. J.; Boehm, C. A.; Mata, A.; Fleischman, A. J.; Muschler, G. F.; Roy, S. Post microtextures accelerate cell proliferation and osteogenesis. *Acta biomaterialia* **2010,** *6* (1), 160-9.
13. Bitar, M.; Benini, F.; Brose, C.; Friederici, V.; Imgrund, P.; Bruinink, A. Evaluation of early stage human bone marrow stromal proliferation, cell migration and osteogenic differentiation on mu-MIM structured stainless steel surfaces. *Journal of materials science. Materials in medicine* **2013,** *24* (5), 1285-92.
14. Brammer, K. S.; Choi, C.; Frandsen, C. J.; Oh, S.; Jin, S. Hydrophobic nanopillars initiate mesenchymal stem cell aggregation and osteo-differentiation. *Acta biomaterialia* **2011,** *7* (2), 683-90.
15. You, M. H.; Kwak, M. K.; Kim, D. H.; Kim, K.; Levchenko, A.; Kim, D. Y.; Suh, K. Y. Synergistically enhanced osteogenic differentiation of human mesenchymal stem cells by culture on nanostructured surfaces with induction media. *Biomacromolecules* **2010,** *11* (7), 1856-62.
16. Hamilton, D. W.; Wong, K. S.; Brunette, D. M. Microfabricated discontinuous-edge surface topographies influence osteoblast adhesion, migration, cytoskeletal organization, and proliferation and enhance matrix and mineral deposition in vitro. *Calcified tissue international* **2006,** *78* (5), 314-25.
17. Engel, E.; Martinez, E.; Mills, C. A.; Funes, M.; Planell, J. A.; Samitier, J. Mesenchymal stem cell differentiation on microstructured poly (methyl methacrylate) substrates. *Annals of Anatomy-Anatomischer Anzeiger* **2009,** *191* (1), 136-144.
18. Logan, N.; Brett, P. The Control of Mesenchymal Stromal Cell Osteogenic Differentiation through Modified Surfaces. *Stem Cells Int* **2013**.
19. Murphy, W. L.; McDevitt, T. C.; Engler, A. J. Materials as stem cell regulators. *Nat Mater* **2014,** *13* (6), 547-557.
20. Kim, D. H.; Seo, C. H.; Han, K.; Kwon, K. W.; Levchenko, A.; Suh, K. Y. Guided Cell Migration on Microtextured Substrates with Variable Local Density and Anisotropy. *Advanced functional materials* **2009,** *19* (10), 1579-1586.
21. Zinger, O.; Zhao, G.; Schwartz, Z.; Simpson, J.; Wieland, M.; Landolt, D.; Boyan, B. Differential regulation of osteoblasts by substrate microstructural features. *Biomaterials* **2005,** *26* (14), 1837-47.
22. Pelaez-Vargas, A.; Gallego-Perez, D.; Carvalho, A.; Fernandes, M. H.; Hansford, D. J.; Monteiro, F. J. Effects of density of anisotropic microstamped silica thin films on guided bone tissue regeneration--in vitro study. *Journal of biomedical materials research. Part B, Applied biomaterials* **2013,** *101* (5), 762-9.
23. Schwartz, Z.; Nasazky, E.; Boyan, B. D. Surface microtopography regulates osteointegration: the role of implant surface microtopography in osteointegration. *The Alpha omegan* **2005,** *98* (2), 9-19.
24. Curtis, A.; Wilkinson, C. Topographical control of cells. *Biomaterials* **1997,** *18* (24), 1573-1583.
25. Vonrecum, A. F.; Vankooten, T. G. The Influence of Micro-Topography on Cellular-Response and the Implications for Silicone Implants. *J Biomat Sci-Polym E* **1995,** *7* (2), 181-198.
26. Yu, B. Y.; Chou, P. H.; Sun, Y. M.; Lee, Y. T.; Young, T. H. Topological micropatterned membranes and its effect on the morphology and growth of human mesenchymal stem cells (hMSCs). *J Membrane Sci* **2006,** *273* (1-2), 31-37.
27. Ghibaudo, M.; Trichet, L.; Le Digabel, J.; Richert, A.; Hersen, P.; Ladoux, B. Substrate topography induces a crossover from 2D to 3D behavior in fibroblast migration. *Biophys J* **2009,** *97* (1), 357-68.

28. Csaderova, L.; Martines, E.; Seunarine, K.; Gadegaard, N.; Wilkinson, C. D.; Riehle, M. O. A biodegradable and biocompatible regular nanopattern for large-scale selective cell growth. *Small* **2010,** *6* (23), 2755-61.
29. Falconnet, D.; Csucs, G.; Grandin, H. M.; Textor, M. Surface engineering approaches to micropattern surfaces for cell-based assays. *Biomaterials* **2006,** *27* (16), 3044-3063.
30. Pelaez-Vargas, A.; Gallego-Perez, D.; Magallanes-Perdomo, M.; Fernandes, M. H.; Hansford, D. J.; De Aza, A. H.; Pena, P.; Monteiro, F. J. Isotropic micropatterned silica coatings on zirconia induce guided cell growth for dental implants. *Dental Materials* **2011,** *27* (6), 581-589.
31. Carvalho, A.; Pelaez-Vargas, A.; Gallego-Perez, D.; Grenho, L.; Fernandes, M. H.; De Aza, A. H.; Ferraz, M. P.; Hansford, D. J.; Monteiro, F. J. Micropatterned silica thin films with nanohydroxyapatite micro-aggregates for guided tissue regeneration. *Dental materials : official publication of the Academy of Dental Materials* **2012,** *28* (12), 1250-60.
32. Pelaez-Vargas, A.; Gallego-Perez, D.; Ferrell, N.; Fernandes, M. H.; Hansford, D.; Monteiro, F. J. Early spreading and propagation of human bone marrow stem cells on isotropic and anisotropic topographies of silica thin films produced via microstamping. *Microscopy and microanalysis : the official journal of Microscopy Society of America, Microbeam Analysis Society, Microscopical Society of Canada* **2010,** *16* (6), 670-6.
33. Marzolin, C.; Smith, S. P.; Prentiss, M.; Whitesides, G. M. Fabrication of glass microstructures by micro-molding of sol-gel precursors. *Adv Mater* **1998,** *10* (8), 571-+.
34. Qin, D.; Xia, Y.; Whitesides, G. M. Soft lithography for micro- and nanoscale patterning. *Nature protocols* **2010,** *5* (3), 491-502.
35. Laranjeira, M. S.; Carvalho, A.; Pelaez-Vargas, A.; Hansford, D.; Ferraz, M. P.; Coimbra, S.; Costa, E.; Santos-Silva, A.; Fernandes, M. H.; Monteiro, F. J. Modulation of human dermal microvascular endothelial cell and human gingival fibroblast behavior by micropatterned silica coating surfaces for zirconia dental implant applications. *Sci Technol Adv Mat* **2014,** *15* (2).
36. Lim, J. Y. Topographic Control of Cell Response to Synthetic Materials. *Tissue Eng Regen Med* **2009,** *6* (1-3), 365-370.
37. McBeath, R.; Pirone, D. M.; Nelson, C. M.; Bhadriraju, K.; Chen, C. S. Cell shape, cytoskeletal tension, and RhoA regulate stem cell lineage commitment. *Developmental cell* **2004,** *6* (4), 483-95.
38. Kilian, K. A.; Bugarija, B.; Lahn, B. T.; Mrksich, M. Geometric cues for directing the differentiation of mesenchymal stem cells. *Proceedings of the National Academy of Sciences of the United States of America* **2010,** *107* (11), 4872-7.
39. Mills, C. A.; Fernandez, J. G.; Martinez, E.; Funes, M.; Engel, E.; Errachid, A.; Planell, J.; Samitier, J. Directional alignment of MG63 cells on polymer surfaces containing point microstructures. *Small* **2007,** *3* (5), 871-9.
40. Navarro, M.; Aparicio, C.; Charles-Harris, M.; Ginebra, M. P.; Engel, E.; Planell, J. A. Development of a biodegradable composite scaffold for bone tissue engineering: Physicochemical, topographical, mechanical, degradation, and biological properties. *Adv Polym Sci* **2006,** *200*, 209-231.
41. Barthlott, W.; Neinhuis, C. Purity of the sacred lotus, or escape from contamination in biological surfaces. *Planta* **1997,** *202* (1), 1-8.
42. Jung, Y. C.; Bhushan, B. Contact angle, adhesion and friction properties of micro- and nanopatterned polymers for superhydrophobicity. *Nanotechnology* **2006,** *17* (19), 4970-4980.
43. Nava, M. M.; Raimondi, M. T.; Pietrabissa, R. Controlling Self-Renewal and Differentiation of StemCells via Mechanical Cues. *J Biomed Biotechnol* **2012**.

44. Matsuzaka, K.; Walboomers, F.; de Ruijter, A.; Jansen, J. A. Effect of microgrooved poly-l-lactic (PLA) surfaces on proliferation, cytoskeletal organization, and mineralized matrix formation of rat bone marrow cells. *Clinical oral implants research* **2000,** *11* (4), 325-33.
45. Uttayarat, P.; Toworfe, G. K.; Dietrich, F.; Lelkes, P. I.; Composto, R. J. Topographic guidance of endothelial cells on silicone surfaces with micro- to nanogrooves: Orientation of actin filaments and focal adhesions. *J Biomed Mater Res A* **2005,** *75A* (3), 668-680.
46. Seo, C. H.; Furukawa, K.; Montagne, K.; Jeong, H.; Ushida, T. The effect of substrate microtopography on focal adhesion maturation and actin organization via the RhoA/ROCK pathway. *Biomaterials* **2011,** *32* (36), 9568-75.
47. Teixeira, A. I.; Abrams, G. A.; Bertics, P. J.; Murphy, C. J.; Nealey, P. F. Epithelial contact guidance on well-defined micro- and nanostructured substrates. *J Cell Sci* **2003,** *116* (10), 1881-1892.
48. Yim, E. K. F.; Darling, E. M.; Kulangara, K.; Guilak, F.; Leong, K. W. Nanotopography-induced changes in focal adhesions, cytoskeletal organization, and mechanical properties of human mesenchymal stem cells. *Biomaterials* **2010,** *31* (6), 1299-1306.
49. Matsuzaka, K.; Walboomers, X. F.; Yoshinari, M.; Inoue, T.; Jansen, J. A. The attachment and growth behavior of osteoblast-like cells on microtextured surfaces. *Biomaterials* **2003,** *24* (16), 2711-9.
50. Rani, V. V. D.; Vinoth-Kumar, L.; Anitha, V. C.; Manzoor, K.; Deepthy, M.; Shantikumar, V. N. Osteointegration of titanium implant is sensitive to specific nanostructure morphology. *Acta biomaterialia* **2012,** *8* (5), 1976-1989.
51. Lincks, J.; Boyan, B. D.; Blanchard, C. R.; Lohmann, C. H.; Liu, Y.; Cochran, D. L.; Dean, D. D.; Schwartz, Z. Response of MG63 osteoblast-like cells to titanium and titanium alloy is dependent on surface roughness and composition. *Biomaterials* **1998,** *19* (23), 2219-2232.
52. Boyan, B. D.; Batzer, R.; Kieswetter, K.; Liu, Y.; Cochran, D. L.; Szmuckler-Moncler, S.; Dean, D. D.; Schwartz, Z. Titanium surface roughness alters responsiveness of MG63 osteoblast-like cells to 1 alpha,25-(OH)(2)D-3. *J Biomed Mater Res* **1998,** *39* (1), 77-85.
53. Schwartz, Z.; Lohmann, C. H.; Oefinger, J.; Bonewald, L. F.; Dean, D. D.; Boyan, B. D. Implant surface characteristics modulate differentiation behavior of cells in the osteoblastic lineage. *Advances in dental research* **1999,** *13*, 38-48.
54. Stein, G. S.; Lian, J. B.; van Wijnen, A. J.; Stein, J. L.; Montecino, M.; Javed, A.; Zaidi, S. K.; Young, D. W.; Choi, J. Y.; Pockwinse, S. M. Runx2 control of organization, assembly and activity of the regulatory machinery for skeletal gene expression. *Oncogene* **2004,** *23* (24), 4315-4329.
55. zur Nieden, N. I.; Kempka, G.; Ahr, H. J. In vitro differentiation of embryonic stem cells into mineralized osteoblasts. *Differentiation* **2003,** *71* (1), 18-27.
56. Choi, J. Y.; Lee, B. H.; Song, K. B.; Park, R. W.; Kim, I. S.; Sohn, K. Y.; Jo, J. S.; Ryoo, H. M. Expression patterns of bone-related proteins during osteoblastic differentiation in MC3T3-E1 cells. *J Cell Biochem* **1996,** *61* (4), 609-618.
57. Mikami, Y.; Omoteyama, K.; Kato, S.; Takagi, M. Inductive effects of dexamethasone on the mineralization and the osteoblastic gene expressions in mature osteoblast-like ROS17/2.8 cells. *Biochem Bioph Res Co* **2007,** *362* (2), 368-373.
58. Ducy, P.; Zhang, R.; Geoffroy, V.; Ridall, A. L.; Karsenty, G. Osf2/Cbfa1: A transcriptional activator of osteoblast differentiation. *Cell* **1997,** *89* (5), 747-754.
59. Datta, H. K.; Ng, W. F.; Walker, J. A.; Tuck, S. P.; Varanasi, S. S. The cell biology of bone metabolism. *J Clin Pathol* **2008,** *61* (5), 577-587.
60. Lee, M.-H.; Kim, Y.-J.; Kim, H.-J.; Park, H.-D.; Kang, A.-R.; Kyung, H.-M.; Sung, J.-H.; Wozney, J. M.; Ryoo, H.-M. BMP-2-induced Runx2 expression is mediated by Dlx5, and TGF-

β1 opposes the BMP-2-induced osteoblast differentiation by suppression of Dlx5 expression. *Journal of Biological Chemistry* **2003,** *278* (36), 34387-34394.
61. Carreira, A. C.; Alves, G. G.; Zambuzzi, W. F.; Sogayar, M. C.; Granjeiro, J. M. Bone Morphogenetic Proteins: Structure, biological function and therapeutic applications. *Arch Biochem Biophys* **2014,** *561*, 64-73.
62. McMurray, R. J.; Gadegaard, N.; Tsimbouri, P. M.; Burgess, K. V.; McNamara, L. E.; Tare, R.; Murawski, K.; Kingham, E.; Oreffo, R. O.; Dalby, M. J. Nanoscale surfaces for the long-term maintenance of mesenchymal stem cell phenotype and multipotency. *Nat Mater* **2011,** *10* (8), 637-44.

CHAPTER III

MobilityAnalyser: A novel approach for automatic quantification of cell mobility on periodic patterned substrates using brightfield microscopy images

Ângela Carvalho[1, 2, 3, *,#], Tiago Esteves[1, 2, 3,*], Pedro Quelhas[1, 2], Fernando Jorge Monteiro[1, 2, 3]

[1] i3S - Instituto de Investigação e Inovação em Saúde, U. Porto, Rua Alfredo Allen, 208, 4200-135, Porto, Portugal;

[2] INEB - Instituto de Engenharia Biomédica, U. Porto, Rua Alfredo Allen, 208, 4200-135, Porto, Portugal;

[3] Faculdade de Engenharia, U. Porto, Rua Dr. Roberto Frias, s/n, 4200-465 Porto, Portugal;

* These authors contributed equally to this work.

Submitted

ABSTRACT

Background and Objective: Surface topography of biomaterials has been shown to have an effect on cells behaviour. Cell-material interactions can be visually characterized by assessing both cell shape and spreading at initial time-points and, its migration patterns, as a response to the underlying topography. While many have reported the study of cells migration and shape with fluorescence labelling, the focus on evaluating cells response to surface topography is to observe, under real-time conditions, interactions between cells and surfaces. In this manuscript we present a novel approach to automatically detect and remove periodic background patterns in brightfield microscopy images, in order to perform automatic cell mobility analysis.

Methods: The developed software, MobilityAnalyser, performs the automatic tracking of unmarked cells, while allowing the user to manually correct any wrongfully detected or tracked cell. Human Mesenchymal Stem Cells (hMSCs) trajectory, migration distance, velocity and persistence were evaluated over line and pillar micropatterned SiO_2 films and on a flat SiO_2 control substrate.

Results: The developed tool proved to be effective in automatically removing background patterns of both line and pillar shapes and in performing cell detection and tracking. MobilityAnalyser accurately measured cells mobility in a fraction of the time required for manual analysis, while eliminating user's subjectivity.

The results obtained with the software confirmed how the different topographies affected cells trajectory, migration pathways and velocities, with a statistically significant increase for the micropatterned surfaces, when compared with the flat control. The persistence parameter also proved the influence of both patterns on the directionality of cell movement.

Conclusions: MobilityAnalyser is an automatic tool to remove periodic background patterns, detect and track cells, providing significant parameters of cell mobility that allow to characterize cells response to different surface topographies. The software is freely available at:
https://drive.google.com/open?id=1Fbb321ogLD19SlRjceMETNUqDHgpeBPl.

Keywords: Brightfield microscopy, Cell-surface interaction, MobilityAnalyser, micropatterned surfaces, software development.

1. Introduction

Over the years, several biomaterials with different microenvironments have been developed, resulting in countless platforms for studying cells behaviour. [1-3]

A successful cell-biomaterial interaction depends on the colonization of the implant surface by cells and is, in part, determined by cell adhesion and migration. [4-5] Surface topography is known to influence these cellular processes, which makes the monitoring of cells attachment, morphology and migration on structured substrates a key aspect to understand how different surface topographies can influence cells response. [5-7]

It has been reported that the effects of surface topography on MSCs arrangement, morphology and migration can modulate cell fate and differentiation pathway and lead to a higher level of osteogenic differentiation, when compared to flat substrates. [8-9]

Previously, we showed that hMSCs have a higher degree of osteoblastic differentiation when cultured on micropatterned surfaces than on flat ones. [10]

With the intent of evaluating the initial cell response to the surface topography, we developed an automatic tool for assessment of cell velocity, migration distance, pathway and persistence. The software was applied to time-lapse videos of human mesenchymal stem cell on SiO_2 surfaces with line and pillar micropatterns and a flat surface of the same material for control.

Currently, the automatic methods available are not suitable to perform measurements on patterned surfaces from brightfield microscopy images. To avoid manual analysis, which is time consuming and prone to be biased and induce subjective observations, the developed tool first identifies and perform the removal of the background pattern, in order to facilitate the automatic tracking of cells. Additionally, an interesting feature of the software is that the user can manually correct any detected error from the automatic tracking. It can either delete the tracking of a single cell or manually follow other cell and add it to the analysis.

Cell mobility and morphology analysis has already been performed on other studies where the background was flat. [11-15] Nevertheless, it is known that there is a dependency between segmentation and interferences or changes in the image background, like changes or distortions of image intensity or illuminance. [16] However, image background pre-processing steps are mainly concerned with intensity inhomogeneities and illumination. [17-19]

Several other works tried to address similar problems with background pattern removal. [20-21] Capel et al. performed the removal of unwanted, non-periodic patterns from forensic

images by registering the image under analysis with a control background pattern image [20]. This is not possible in our experimental case since a control image from the background pattern is not available and the existing pattern varies between images. Considering the case of periodic background patterns it is possible to perform image background removal by filtering in the Fourier domain [21]. However, this only works for periodic stripe patterns, which does not applies to the pillar patterned images. If we consider the existence of background pattern as texture, there are also several methods that can be used to address this problem [22]. Such methods perform texture classification and segmentation. Still, they do not provide a simple way to synthesize or remove the background image. In order to facilitate cell detection and tracking for mobility and morphology analysis we proposed a new approach to automatically detect the periodic background pattern, synthetize the full background, and remove it from the original image. The proposed approach consists of four steps: firstly, it is evaluated if whether or not there is a periodic background pattern or not; then, if it exists, the background pattern is detected based on its periodicity; afterwards the full background image is synthesized; and finally the background is subtracted from the original image, obtaining solely information related to the existing cells. The developed software consists of an easy to use, rapid and automatic tool that can be used to evaluate initial cell response to different surface topographies and is freely available for testing at: https://drive.google.com/open?id=1Fbb321ogLD19SlRjceMETNUqDHgpeBPl.

2. Methods

2.1. Micropatterned thin films

Hybrid SiO_2 sols were produced via a sol–gel process with acid catalysis in a single stage, using Tetraethylorthosilicate (TEOS, Sigma–Aldrich, USA) and Methyltriethoxisilane (MTES, Sigma–Aldrich) as SiO_2 precursors. Cover slips were used as a model substrate. The soft-lithography method was used to create line and pillar micropatterned silica surfaces. Initially, UV photolithography was used to produce a master mold with the desired microfeatures (lines and pillars, 5 μm in width with 10μm interspacing) in a (Class 100) clean room facility. Afterwards, negative molds of polydimethylsiloxane (PDMS, Silastic T-2, Dow Corning, USA) were obtained by mixing the base with the curing agent and pouring it over the master molds. The SiO_2 sols were then stamped on the glass coverslips using the PDMS molds. Flat SiO_2 coatings were fabricated via spin-coating

(SCS G3P-8 Specialty Coating Systems, Cookson Electronics, USA) at 3000 rpm for 45 s. Finally, the samples were heat-treated at 500ºC for 60 minutes using a 5°C/min ramp rate.

2.2. Cell harvesting and cultures

Human Mesenchymal Stem Cells (hMSCs) from human bone marrow were obtained from orthopaedic surgery procedures, after patient's informed consent. The bone sample was broken into small pieces and washed with alpha-minimum essential medium (α-MEM, Sigma) supplemented with 10 % fetal bovine serum (FBS, Gibco) and 1 % penicillin-streptomycin (3×10^{-4} mol/L and 5×10^{-4} mol/L, Gibco). The resultant cell suspensions were seeded in Petri dishes for 10 days. Subsequently, cell monolayers were washed with PBS twice and the media was changed. A flow cytometry analysis confirmed that cells were positive for MSC markers CD105, CD146, and CD90 negative for CD45. When a high degree of confluence was reached, the adherent cells were washed with PBS, enzymatically released with 0.04% trypsin at 37 ºC, and subcultured.

2.3. Time lapse microscopy

The cultures were incubated in a humidified atmosphere of 5% CO_2 at 37 ◦C and the medium was changed twice a week. Cells of passage 4 were used in the experiments. When high confluence was reached, the adherent cells were washed with PBS and enzymatically released with 0.04% trypsin at 37 ◦C. The resultant cells were seeded at a density of 4×10^4 cells/cm^2 on the thin films and placed inside an incubator at 37ºC and 5% CO_2 for 60 min to adhere.

The thin films were placed each in a u-dish with glass bottom (Ibidi, Germany) and mounted onto the stage of a motorized Spectral Confocal Microscope Leica TCS-SP5 AOBS (Leica. Germany) equipped with a camera. Brightfield images of the hMSCs were automatically recorded with the LAS AF Lite (Leica, Germany) every 5 min, for a period of 12h. Cells were maintained at 37ºC and 5% CO_2 during the experiment.

2.4. MobilityAnalyser software description

The **MobilityAnalyser** software was implemented in MATLAB™ and a MS Windows™ 32-bit version was compiled and it is available online at https://drive.google.com/open?id=1Fbb321ogLD19SlRjceMETNUqDHgpeBPl.

It requires the installation of MATLAB™ or of the MATLAB™ Component Runtime (MCR) installer. This software is a user-friendly application that performs the automatic quantification of cell mobility in time-lapse videos without the interference of the existing background patterns (removed automatically by the software). If a background pattern exists, the first step for its detection is to extract keypoints from the image that will allow to infer the pattern periodicity. Given the pattern periodicity, we are able to identify both background and foreground locations. Therefore, we first removed the foreground in order to fully reconstruct the background pattern. Secondly, we subtracted the reconstructed background pattern from the original input image obtaining only information regarding the existing cells without background interference. [11] The analysis of the cell mobility is based on a detection-association tracking approach that relies on the Laplacian of Gaussian filter (LoG) for the task of cell detection. The LoG filter is based on the image scale-space representation to enhance the blob like structure. The scale of the LoG filter is set to the expected range of cell radius dimensions. Cell detection is performed by detecting local maxima of LoG response in the input image. The detected maxima enable the estimation of cell location. [12] From this, the tracking of cells is performed using a detection association approach, based on the cell detections distance between consecutive frames and similarity measures between cells. The similarity analysis of SIFT descriptors was used as cell appearance descriptors to include more information and held the tracking process. The software allows the user to open time-lapse videos of the experiments, perform cell tracking through time and finally perform cell mobility analysis saving the results in an excel file together with image results related to cell trajectory and cell persistence.

2.5. Cell mobility measures

The direct result of applying tracking tools is a sequence of coordinates indicating the position of each tracked object at each time point. While this is as essential step and a tremendous data reduction, by itself this does not lead to new insights. The final step is the computation of biological meaningful quantitative metrics from these coordinates:

Distance travelled: distance travelled by a cell considering the entire cell trajectory.

Velocity: this metric is related with the rate of displacement.

Persistence: the persistence analysis gives a measure of the type of motion displayed by cells. [23]

The referred quantitative measures are used to characterize cells mobility and describe cell behaviour. This is the relevant information that is meaningful to assess the influence of the background patterns on the cells under analysis.

2.6. Statistical analysis

The results were expressed as the arithmetic mean ± standard error. When applicable, the statistical analysis of the results was performed using the Student's t-test. Levels of $p \leq 0.05$ were considered to be statistically significant.

3. Results and discussion

3.1. MobilityAnalyser performance and parameters evaluation

MobilityAnalyser was applied to time-lapse videos of hMSCs on all silica thin films: flat, micropatterned with lines and micropatterned with pillars, as shown on figure 1.

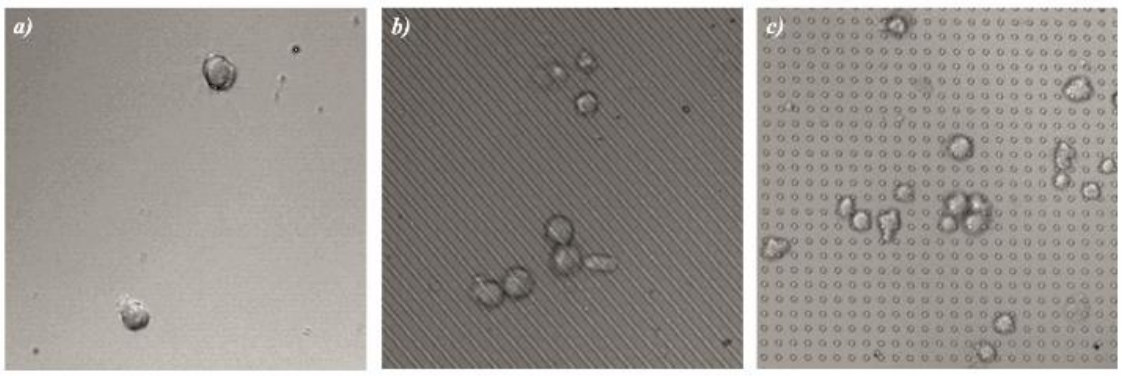

Figure 1 – Brightfield images of cells on the three types of SiO_2 thin films: a) flat; b) micropatterned lines; c) micropatterned pillars.

Each of the analysed time-lapse videos was composed of 150 individual frames and the time between frames acquisition was 5 minutes. This value (inserted by the user) is used by the software for the computation of the cells velocity. The cell size parameter used by the software for the cell detection task is based on the magnification of the time-lapse

video under analysis which is also given by the user. Finally, the scale is also user specified, and it is based on this value that it is possible to compute the travelled distance, as well as the persistence lines for each cell.

Given the input parameters, cells are automatically detected using the LOG filter. Different methodologies were proposed in the past for the task of cell detection, such as automatic thresholding segmentation [24], active contours [25], and watershed segmentation. [26] However, the application of the aforementioned methods to cell segmentation is not trivial, as it relies on the separation of individual cells that can be overlapping or touching each other. [27] Also, it is known that there is a dependency between segmentation and interferences or changes in the image background, such as changes or distortions of image intensity or illumination. [16] Since the proposed software automatically performs the removal of the existing background patterns, this problem is solved.

Relying on a detection-association approach, the tracking results are computed based on the detected cells. Given the cell tracking results, the software displays the location history for each cell. At this point it is possible for the user to correct any visually identified errors, delete the tracking result for a specific cell or perform the manual tracking again for a specific cell and add it to the analysis. The mobility analysis of the tracking results is only performed after visual inspection by the user. Most tools offer very little functionality for manual trajectory inspection and correction. [28] This functionality associated with the task of background pattern removal were the basis for the development of the MobilityAnalyser software. It was also possible to decide and include all the mobility measures that were considered relevant for our study, and were not available in a single tool, among the available tracking tools.

The developed software also allows for the user to perform a completely manually run analysis of the time lapse video. In this mode the user is expected to insert the cell location in each frame of the time lapse video for each specific cell. Figure 2 displays the running time of the software for the cell tracking task, performed manually and automatically. It is clear that the automatic cells tracking is faster than the manual approach, with statistically significant differences and, with a running time of around 3,80 minutes for the micropatterned lines, about 3,49 minutes for the micropatterned pillars and a lower time, of about 2,09 minutes for the flat film. In the case of incorrect detection or tracking during the automatic process that might need to be manually corrected, the total times of analysis may be increased. Manual correction is available, after the automatic tracking.

The cell number also plays an important role on the running time, since, when more cells are present, the time required for the analysis will also increase. For this specific test, there were 49 cells in the video with micro-lines, 46 cells in the video with micro-pillars and 34 cells in the video with flat silica thin films. Regarding the manual tracking results, for the different background patterns, it may be seen that for the flat thin film, the running time was also shorter. In the case of this specific background there were fewer cells and these were generally close to the same location, thus facilitating the task of manual tracking.

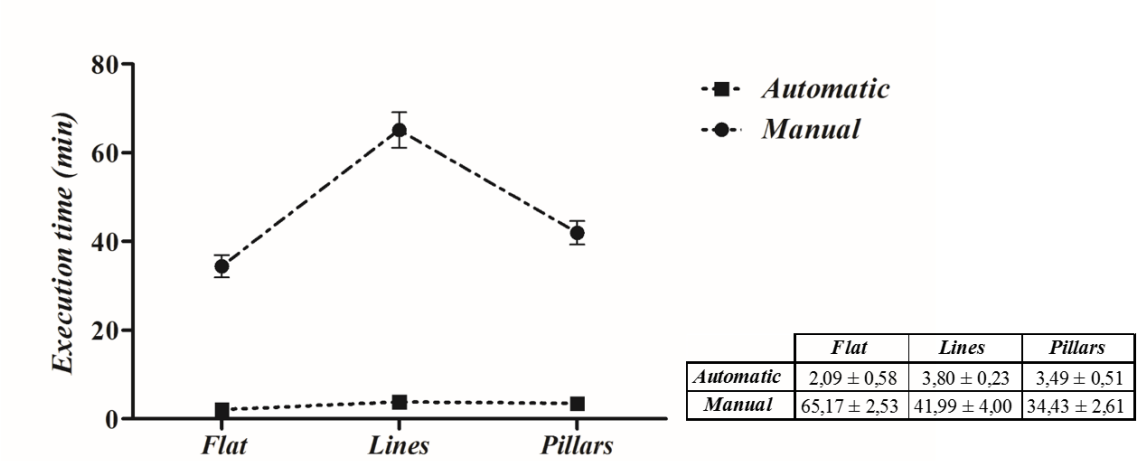

	Flat	*Lines*	*Pillars*
Automatic	2,09 ± 0,58	3,80 ± 0,23	3,49 ± 0,51
Manual	65,17 ± 2,53	41,99 ± 4,00	34,43 ± 2,61

Figure 2 – Running time comparison between the manual and the automatic mobility analysis.

3.2 Mobility measures computation

Consider C_i^n, a cell *i*, among all the detected cells, in frame *n*.

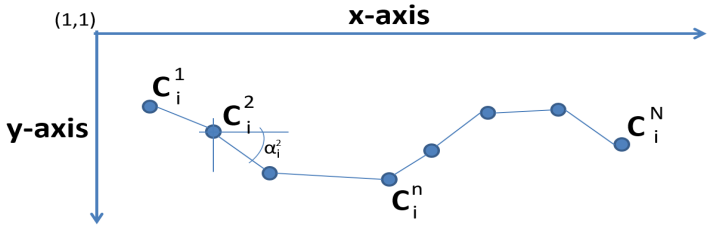

Figure 3 – Sample trajectory of a cell i, consisting of N time points where $C_i^n = (x_i^n, y_i^n)$ is the spatial position of the object i in each frame n.

3.2.1. Travelled Distance

This metric measures the distance travelled by a cell from its initial location from the beginning till the end of the time lapse video, considering the entire cell trajectory. Even if the final location of a cell in the last frame is close to its location in the first frame, this metric shows whether that specific cell was not moving during the entire time-lapse video (travelled distance result close to 0) or if the cell was moving and, by randomness, travelled back to the initial location (travelled distance should be longer in this situation). For each cell i, its travelled distance is computed as:

$$d_{trav}(i) = \sum_{n=i}^{N-1} d(C_i^n, C_i^{n+1})$$

The distance between any two locations between two cells, C_i^n and C_i^{n+1}, (figure 3) is assumed to be the Euclidean norm.

3.2.2. Velocity

Other measures that can be easily derived from a trajectory are those concerning the rate of displacement. Instantaneous velocity, for example, is computed as the displacement from one frame to the next (figure 3), divided by the time interval:

$$V(i) = \frac{d(C_i^n, C_i^{n+1})}{time(n, n+1)}$$

To compute this metric, the time interval ($time(n, n+1)$) between the acquisition of frames is required, in order to divide the travelled distance by the elapsed time.

3.2.3. Persistence

The persistence analysis gives a measure of the type of motion displayed by cells. It requires the computation of the mean square displacement (MSD) for each specific individual cell i, which is performed as [23]:

$$MSD_i(\tau) = \langle \delta(\tau)^2 \rangle = \langle C_i^{n+\tau} - C_i^n \rangle_n,$$

where the brackets indicate averages over all times *n* of the displacement between time intervals for each cell *i* according to the coordinates x_i^n, y_i^n of the cell C. τ is the time

interval between any two positions, and we considered several time intervals ($\tau = [1, 2, 4, 8, 16, 32, 64, 128]$) were considered. By plotting $\langle \delta(\tau)^2 \rangle \; vs \; \tau$ one may have an idea about the type of motion for each cell.

If a cell is moving always in the same direction, for all the time intervals, τ, the mean square displacement will always increase, originating a persistence line with high slope. On the other hand, if a cell is not moving and it remains all the time at the same location, no matter how much we increase the time interval τ is considered, the mean square displacement will always be the same since the cell is not moving, originating a line with low slope. In the case of existing a moving cell but always around the same location, for small time intervals τ the mean square displacement is high but as we increase the time interval τ the mean square displacement stabilizes or decreases (persistence line with high slope in the first part of the line and low/decreasing slope in the rest of the line). The computation of the persistence gives an overall information about the type of cell motion along the entire time-lapse video.

3.3 Biological Assessment

3.3.1. hMSCs migration distance and velocity

The results obtained from the MobilityAnalyser software allowed for a complete assessment of cell response to both micropatterned surfaces and the flat control, by providing different parameters for evaluation and comparison.

Cells on both micropatterned surfaces showed a longer migration distance with higher velocities, than cells on the flat substrate. Cells travelled distance in the horizontal and vertical directions is displayed in figure 4.

hMSCs on the flat surface revealed a mean travelled distance of around 58.9 ± 5.9 μm, where cell velocity was found to be around 0.079 ± 0.008 μm/min. As it can be seen on figure 4a, hMSCs travelled distance was shorter than on the micropatterned surfaces.

On the other hand, hMSCs over the micropatterned lines exhibited a statistically significant longer travelled distance (102.2 ± 7.9 μm) than on the flat surface, with a 0.136 ± 0.011 μm/min mean velocity (Figure 4b). The micro-pillars also influenced cell migration. Both the mean travelled distance (87 ± 5.6 μm) and the average velocity of cells (0.117 ± 0.007 μm/min) presented statistically significantly higher values than the flat substrate. There were no statistically significant differences between both micropatterned surfaces, in terms of migration distance and velocity.

The obtained average velocity results show that cell migration was accelerated due to the cell-pattern interactions.

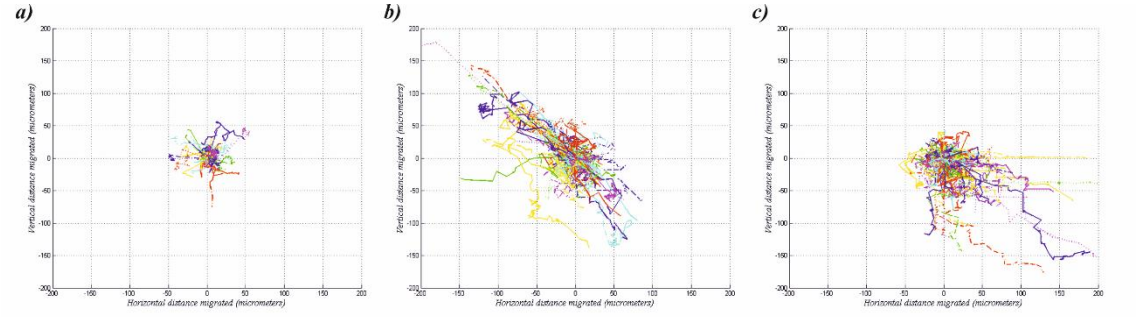

Figure 4 - Distance travelled by cells on all silica thin films: a) flat; b) micropatterned lines; c) micropatterned pillars.

3.3.2. Persistence

Even though the distance and velocity are key parameters, it is also relevant to evaluate the influence of patterns on the movement and directionality of cells. Performing the analysis of the cell persistence results (figure 5), the existing differences between cell mobility on the three surfaces are clear. The cell persistence results for the flat SiO_2 film (figure 5d) show persistence lines with a low, almost horizontal, slope, meaning that the cells were always moving around their initial location, as it may be seen in figure 5a, where cell trajectories are displayed. Considering the results of cells on the micropatterned lines (figure 5e), there is an high slope on most of the persistence lines, indicating that cells were moving within the same directionality, as it may be seen for most of the cells in figure 5b. The influence of patterns on cell movement and directionality is clear, as it may be observed that cells are moving mostly along the grooves between the line micropatterns. On figure 5f, the persistence results for cells over the micro-pillars are similar to those found for micro-lines, as the persistence lines have relatively high slopes indicating that cells are moving and migrating to different locations from their initial position. Nevertheless, it is evident that cell movement is not as one-directional as in the case for micropatterned lines (figure 5c).

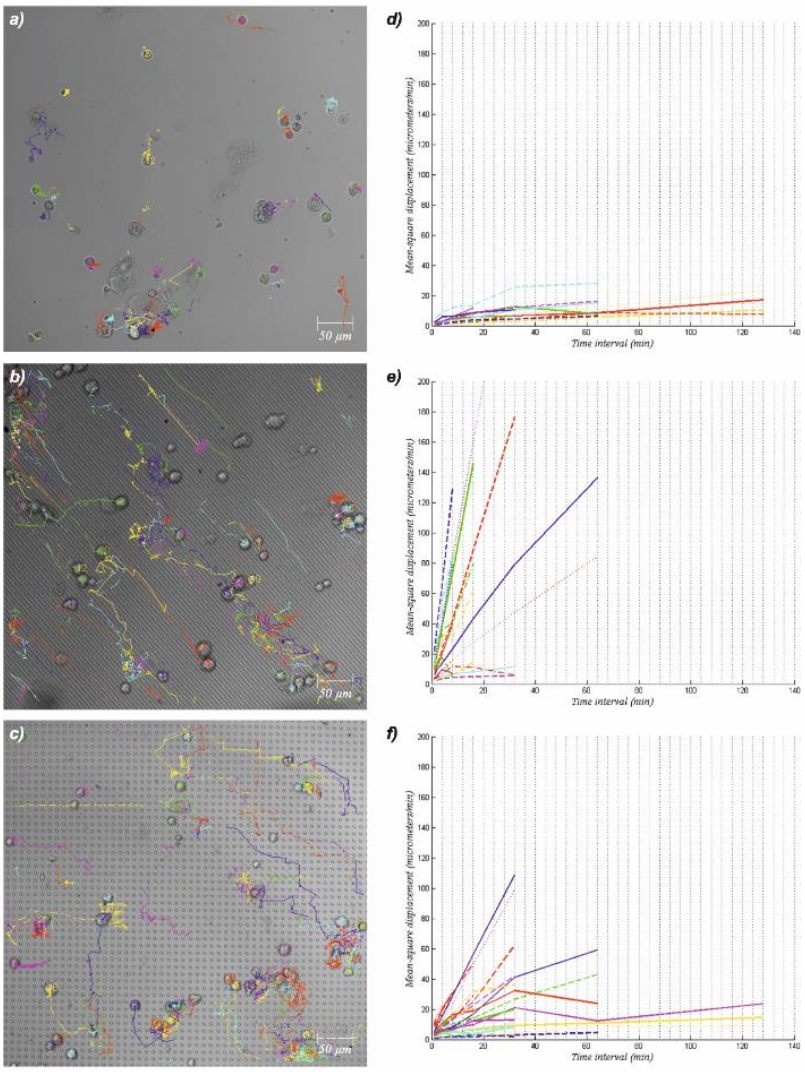

Figure 5 – Cell trajectory (a, b and c) and persistence analysis (d, e and f) of hMSCs on all the silica thin films: a,d) flat; b,e) micropatterned lines; c,f) micropatterned pillars.

4. Discussion

In this work we proposed a novel approach to detect and extract periodic background patterns in brightfield time-lapse images, for quantification of cellular mobility parameters. The approach is based on the analysis of keypoints periodicity obtained from each image. Once the existing periodic background pattern is found, this approach enables its removal from the original image, by image subtraction. Using the images from where the periodic background pattern was removed, it was possible to perform cell detection and tracking.

Cells were automatically detected using the LOG filter. Different methodologies were proposed in the past for the task of cell detection such as automatic thresholding

segmentation [24], active contours [25], and watershed segmentation. [26] However, the application of those methods to cell segmentation is not trivial requiring the separation of individual cells that might be overlapping or touching each other. [27] Also, it is known that there is a dependency between segmentation and interferences or changes in the image background, such as changes or distortions of image intensity or illumination. [16] The proposed software automatically performs the removal of the existing background patterns, therefore overcoming this difficulty.

Besides eliminating the user's subjectivity when performing manual analysis, the automatic tracking of the MobilityAnalyser software was significantly faster than the manual. Another relevant feature of the software is the ability to manually correct wrongly detected or tracked cells, as indicated by the user. Although this feature may increase the total time for analysis, it will still provide a more accurate analysis, in a shorter time. The possibility of obtaining results from cells mobility after visual inspection of the automatic tracking associated with background pattern removal were the basis for the development of the MobilityAnalyser software.

In addition, this tool includes all the mobility measures considered relevant for our study and that were not found in other available tracking tools. [28-31] A more extensive review on current methods and tools applied for cell migration analysis can be found in [32].

Given the tracking results with the location history of each cell, through the time-lapse videos, it was possible to perform cell mobility studies that included measurements on the trajectories, distance, migration velocity and persistence.

The results obtained from the automatic tracking show that the topographic cues influenced all parameters regarding cell mobility. Cell migration distance was significantly higher for the patterned substrates, as well as migration velocity. On the micropatterned lines surface cells trajectory was clearly guided through the lines patterns as cells displayed a directionality, moving mainly along the parallel grooves (Figure 5b). In addition, the highest cells velocity was detected on this type of surface, that may have caused accelerated cell migration, through the grooves.

hMSCs trajectory on the micropatterned pillars surface was not as directional as on the micropatterned lines surface. Still, the influence of the patterns is observed in a guided trajectory, a significantly longer travelled distance and higher velocity when compared to the flat control.

Regarding the cellular response to the flat surface, besides showing a shorter mean travelled distance and reduced velocity, cell trajectory was mainly randomized (occurring

in all directions) while being clear that cells tended to remain mostly around the same locations (Figure 5a).

Other authors have assessed the influence of micropatterns on cells migration. In agreement with our results, a number of studies have shown that cell migration speed is higher on microgrooved surfaces, when compared to flat ones. [33-35] Pillar patterns also increased cell velocity and migration. Frey *et al* concluded that fibroblasts cultured on pillar micropatterns showed a longer migration path, with increased linear speed and vectorial acceleration than cells on the flat substrate, mostly due to the higher surface contact area provided by the topographic cues, that guided cell migration. [36]

More often, line patterns induce cell alignment and migration along the grooves and ridges, as pillar patterns allow migrating cells to continuously encounter localized topographic stimuli. [36-38]

The MobilityAnalyser software was developed for automatic detection and tracking of cells on patterned substrates. The software successfully removed the periodic background patterns in brightfield time-lapse images and automatically detected and tracked the cells. Key parameters regarding cells migration distance, velocity, trajectory and persistence were obtained, as well as significantly faster and eventually corrected tracking.

In terms of the biological assessment, it was confirmed that the micropatterned surfaces clearly modulated cells adhesion and orientation, inducing increased migration at higher velocities than the flat surfaces. As previously shown, MSCs cultured on these surfaces showed an increased osteogenic differentiation, which helps to substantiate that the initial cell response to these substrates plays an important role in later stage processes such as MSCs differentiation.

Acknowledgements

This work was supported by FEDER funds through the Programa Operacional Factores de Competitividade (COMPETE and by Portuguese funds through FCT (Fundação para a Ciência e a Tecnologia) in the framework of the project PEst-C/SAU/LA0002/2013, as well as T. Esteves grant (SFRH/BD/80508/2011) and A. Carvalho grant (SFRH/BD/87624/2012), are acknowledged. P. Quelhas is a Ciência2008 awardee.

The authors would also like to acknowledge Mr. Rui Rocha (CEMUP) for the SEM images and Dr. Maria Lazaro and the Bioimaging Center for Biomaterials and Regenerative Therapies (b.IMAGE) for helping with the confocal microscopy.

Conflict of interest statement

The authors confirm that there are no known conflicts of interest associated with this publication and there has been no significant financial support for this work that could have influenced its outcome.

References

1. Curtis, A.; Wilkinson, C. Topographical Control of Cells. *Biomaterials* **1997,** *18*, 1573-1583.
2. Ito, Y. Surface Micropatterning to Regulate Cell Functions. *Biomaterials* **1999,** *20*, 2333-2342.
3. Mendonca, G.; Mendonca, D. B. S.; Aragao, F. J. L.; Cooper, L. F. Advancing Dental Implant Surface Technology - from Micron- to Nanotopography. *Biomaterials* **2008,** *29*, 3822-3835.
4. Berry, C. C.; Campbell, G.; Spadiccino, A.; Robertson, M.; Curtis, A. S. The Influence of Microscale Topography on Fibroblast Attachment and Motility. *Biomaterials* **2004,** *25*, 5781-8.
5. Kaiser, J. P.; Bruinink, A. Investigating Cell-Material Interactions by Monitoring and Analysing Cell Migration. *J Mater Sci Mater Med* **2004,** *15*, 429-35.
6. Geiger, B.; Spatz, J. P.; Bershadsky, A. D. Environmental Sensing through Focal Adhesions. *Nature Reviews Molecular Cell Biology* **2009,** *10*, 21-33.
7. Ventre, M.; Natale, C. F.; Rianna, C.; Netti, P. A. Topographic Cell Instructive Patterns to Control Cell Adhesion, Polarization and Migration. *J R Soc Interface* **2014,** *11*, 20140687.
8. Dalby, M. J.; Gadegaard, N.; Tare, R.; Andar, A.; Riehle, M. O.; Herzyk, P.; Wilkinson, C. D. W.; Oreffo, R. O. C. The Control of Human Mesenchymal Cell Differentiation Using Nanoscale Symmetry and Disorder. *Nature Materials* **2007,** *6*, 997-1003.
9. Watari, S.; Hayashi, K.; Wood, J. A.; Russell, P.; Nealey, P. F.; Murphy, C. J.; Genetos, D. C. Modulation of Osteogenic Differentiation in Hmscs Cells by Submicron Topographically-Patterned Ridges and Grooves. *Biomaterials* **2012,** *33*, 128-136.
10. Carvalho, A.; Pelaez-Vargas, A.; Hansford, D. J.; Fernandes, M. H.; Monteiro, F. J. Effects of Line and Pillar Array Microengineered Sio2 Thin Films on the Osteogenic Differentiation of Human Bone Marrow-Derived Mesenchymal Stem Cells. *Langmuir : the ACS journal of surfaces and colloids* **2016,** *32*, 1091-100.
11. Esteves, T.; Carvalho, Â.; Monteiro, F. J.; Quelhas, P. Periodic Background Pattern Detection and Removal for Cell Tracking. In *Image Analysis and Recognition: 11th International Conference, Iciar 2014, Vilamoura, Portugal, October 22-24, 2014, Proceedings, Part Ii*, Campilho, A.; Kamel, M., Eds. Springer International Publishing: Cham, **2014**, pp 123-131.
12. Esteves, T.; Oliveira, M. J.; Quelhas, P. Cancer Cell Detection and Morphology Analysis Based on Local Interest Point Detectors. *Pattern Recognition and Image Analysis, Ibpria 2013* **2013,** *7887*, 608-615.
13. Esteves, T.; Quelhas, P.; Mendonça, A. M.; Campilho, A. Gradient Convergence Filters and a Phase Congruency Approach for in Vivo Cell Nuclei Detection. *Machine Vision and Applications* **2012,** *23*, 623-638.
14. Li, K.; Chen, M.; Kanade, T. Cell Population Tracking and Lineage Construction with Spatiotemporal Context. *Med Image Comput Comput Assist Interv* **2007,** *10*, 295-302.
15. Essa, E.; Xie, X. Phase Contrast Cell Detection Using Multi-Level Classification. *International Journal for Numerical Methods in Biomedical Engineering* n/a-n/a.
16. Vovk, U.; Pernus, F.; Likar, B. A Review of Methods for Correction of Intensity Inhomogeneity in Mri. *IEEE Trans Med Imaging* **2007,** *26*, 405-21.

17. Madani, R.; Bourquard, A.; Unser, M. Image Segmentation with Background Correction Using a Multiplicative Smoothing-Spline Model. *2012 9th Ieee International Symposium on Biomedical Imaging (Isbi)* **2012,** 186-189.
18. Roy, S.; Carass, A.; Prince, J. L. In *Compressed Sensing Based Intensity Non-Uniformity Correction*, Biomedical Imaging: From Nano to Macro, 2011 IEEE International Symposium on, IEEE: **2011**; pp 101-104.
19. Zheng, Y. J.; Vanderbeek, B.; Xiao, R.; Daniel, E.; Stambolian, D.; Maguire, M.; O'Brien, J.; Gee, J. Retrospective Illumination Correction of Retinal Fundus Images from Gradient Distribution Sparsity. *2012 9th Ieee International Symposium on Biomedical Imaging (Isbi)* **2012,** 972-975.
20. Capel, D.; Zisserman, A.; Bramble, S.; Compton, D. An Automatic Method for the Removal of Unwanted, Non-Periodic Patterns from Forensic Images. *Investigation and Forensic Science Technologies* **1999,** *3576*, 274-284.
21. Xie, Y.; Chen, L.; Hofmann, U. Reduction of Periodic Noise in Fourier Domain Optical Coherence Tomography Images by Frequency Domain Filtering. *Biomedical Engineering/Biomedizinische Technik* **2012,** *57*, 830-832.
22. Tuceryan, M.; Jain, A. K. Texture Analysis. In *Handbook of Pattern Recognition and Computer Vision*, 2nd ed.; World Scientific: **2011**, pp 207-248.
23. Li, L.; Norrelykke, S. F.; Cox, E. C. Persistent Cell Motion in the Absence of External Signals: A Search Strategy for Eukaryotic Cells. *Plos One* **2008,** *3*.
24. Ali, R.; Gooding, M.; Szilagyi, T.; Vojnovic, B.; Christlieb, M.; Brady, M. Automatic Segmentation of Adherent Biological Cell Boundaries and Nuclei from Brightfield Microscopy Images. *Machine Vision and Applications* **2012,** *23*, 607-621.
25. Xing, F.; Yang, L. In *Unsupervised Shape Prior Modeling for Cell Segmentation in Neuroendocrine Tumor*, Biomedical Imaging (ISBI), 2015 IEEE 12th International Symposium on, IEEE: **2015**; pp 1443-1446.
26. Yang, X. D.; Li, H. Q.; Zhou, X. B. Nuclei Segmentation Using Marker-Controlled Watershed, Tracking Using Mean-Shift, and Kalman Filter in Time-Lapse Microscopy. *Ieee Transactions on Circuits and Systems I-Regular Papers* **2006,** *53*, 2405-2414.
27. Mosaliganti, K.; Gelas, A.; Gouaillard, A.; Megason, S. Microscopy Image Analysis: Blob Segmentation Using Geodesic Active Contours. **2009**.
28. Meijering, E.; Dzyubachyk, O.; Smal, I. Methods for Cell and Particle Tracking. *Methods Enzymol* **2012,** *504*, 183-200.
29. Barry, D. J.; Durkin, C. H.; Abella, J. V.; Way, M. Open Source Software for Quantification of Cell Migration, Protrusions, and Fluorescence Intensities. *The Journal of cell biology* **2015,** *209*, 163-80.
30. Bise, R.; Kanade, T.; Yin, Z.; Huh, S. I. Automatic Cell Tracking Applied to Analysis of Cell Migration in Wound Healing Assay. *Conference proceedings : ... Annual International Conference of the IEEE Engineering in Medicine and Biology Society. IEEE Engineering in Medicine and Biology Society. Annual Conference* **2011,** *2011*, 6174-9.
31. Debeir, O.; Van Ham, P.; Kiss, R.; Decaestecker, C. Tracking of Migrating Cells under Phase-Contrast Video Microscopy with Combined Mean-Shift Processes. *IEEE transactions on medical imaging* **2005,** *24*, 697-711.
32. Masuzzo, P.; Van Troys, M.; Ampe, C.; Martens, L. Taking Aim at Moving Targets in Computational Cell Migration. *Trends in Cell Biology* **2016,** *26*, 88-110.
33. Dalton, B. A.; Walboomers, X. F.; Dziegielewski, M.; Evans, M. D.; Taylor, S.; Jansen, J. A.; Steele, J. G. Modulation of Epithelial Tissue and Cell Migration by Microgrooves. *J Biomed Mater Res* **2001,** *56*, 195-207.

34. Kaiser, J. P.; Reinmann, A.; Bruinink, A. The Effect of Topographic Characteristics on Cell Migration Velocity. *Biomaterials* **2006,** *27*, 5230-41.
35. Kim, D. H.; Han, K.; Gupta, K.; Kwon, K. W.; Suh, K. Y.; Levchenko, A. Mechanosensitivity of Fibroblast Cell Shape and Movement to Anisotropic Substratum Topography Gradients. *Biomaterials* **2009,** *30*, 5433-44.
36. Frey, M. T.; Tsai, I. Y.; Russell, T. P.; Hanks, S. K.; Wang, Y. L. Cellular Responses to Substrate Topography: Role of Myosin Ii and Focal Adhesion Kinase. *Biophys J* **2006,** *90*, 3774-82.
37. Jeon, H.; Hidai, H.; Hwang, D. J.; Healy, K. E.; Grigoropoulos, C. P. The Effect of Micronscale Anisotropic Cross Patterns on Fibroblast Migration. *Biomaterials* **2010,** *31*, 4286-95.
38. Lim, J. Y. Topographic Control of Cell Response to Synthetic Materials. *Tissue Engineering and Regenerative Medicine* **2009,** *6*, 365-370.

CHAPTER IV

Femtosecond laser microstructured Alumina toughened Zirconia: A new strategy to improve osteogenic differentiation of hMSCs

Angela Carvalho[1,2,3,], Liliana Cangueiro[4,5], Vítor Oliveira[4,6], Rui Vilar[4,5], Maria H. Fernandes[7,8], Fernando J. Monteiro[1,2,3,*]*

1 i3S - Instituto de Investigação e Inovação em Saúde, U. Porto , Portugal

2 INEB - Instituto de Engenharia Biomédica, U. Porto, Rua Campo Alegre, 823, 4150-180, Porto, Portugal

3 Faculdade de Engenharia, Departamento de Engenharia Metalúrgica e Materiais, U. Porto, Rua Dr Roberto Frias, s/n, 4200-465 Porto, Portugal

4 Center of Physics and Engineering of Advanced Materials (CeFEMA), Instituto Superior Técnico, Av. Rovisco Pais, 1049-001, Lisboa, Portugal

5 Instituto Superior Técnico, Universidade de Lisboa, Av. Rovisco Pais, 1049-001, Lisboa, Portugal

6 Instituto Superior de Engenharia de Lisboa, Instituto Politécnico de Lisboa, Avenida Conselheiro Emídio Navarro No. 1,1959-007, Lisboa, Portugal

7 Laboratory for Bone Metabolism and Regeneration, Faculdade de Medicina Dentaria, U. Porto, Rua Dr. Manuel Pereira da Silva, 4200-393 Porto, Portugal

8 REQUIMTE/LAQV, U. Porto, Porto, Portugal

Applied Surface Science, 2018; 435: 1237-1245.

Abstract

The use of topographic patterns has been a continuously growing area of research for tissue engineering and it is widely accepted that the surface topography of biomaterials can influence and modulate the initial biological response. Ultrafast lasers are extremely powerful tools to machine and pattern the surface of a wide range of biomaterials, however, only few work has been performed on ceramics with the intent of biomedical applications, and the biological characterization of these structured materials is scarce.
In this work, relevance is given to the biological performance of such materials. A femtosecond laser ablation technique was used to modify Alumina toughened Zirconia (ATZ) surface topography, developing surfaces structured at the micro and nanoscale levels (μATZ), in a controlled and reproducible manner. Materials characterization was performed before and after laser treatment, and both materials were compared in terms of osteogenic response of human bone marrow derived mesenchymal stem cells cultured under basal conditions, expecting that the micro/nanofeatures will improve the biological response of cells. Cells metabolic activity and proliferation increased with the culture time and surface microtopography modulated cells alignment and guided proliferation. The modified surface, displayed significantly higher expression of osteogenic transcription factors and genes and, additionally, the formation of a mineralized extracellular matrix, when compared to the control surface, i.e. unmodified ATZ.

Keywords: Microstructured biomaterials, femtosecond laser, surface topography, osteogenic differentiation.

1. Introduction

Hard ceramics are widely used in biomedical applications, as an alternative to metals, due to their excellent mechanical and biological properties. [1-3] Alumina-Zirconia composites have been studied to avoid the single-phase ceramics disadvantages of ageing and inertness, while exhibiting improved strength and toughness. [4-6] Alumina toughened Zirconia (ATZ), composed by a zirconia matrix with evenly dispersed alumina particles, allows reaching strengths that significantly exceed the strength of ZrO_2. The presence of Al_2O_3 in the structure has also a positive influence on the material stability, resulting in a highly ageing resistant material. [7-8]

Ideally, the implanted biomaterial should replace the missing bone while stimulating osteoconduction for bone re-growth. It has been shown that micro and nanostructured surfaces are a good approach to improve biomaterials bioactivity and stem cells osteogenic differentiation. [9] In a previous publication we showed that hMSCs cultured on micropatterned SiO_2 surfaces, under basal conditions, exhibited a higher degree of osteogenic differentiation than cells cultured on a flat SiO_2 thin film. [10]

Materials texturing by ultrafast lasers has long been discussed as an alternative method for surface modification. [11] In recent years, ultrafast lasers have been successfully used to texture biomaterials surfaces. [12-14] These lasers have considerable advantages over other common techniques for surface modification because they can be applied to a wide range of metallic and dielectric materials, including materials transparent to low intensity infrared radiation and they allow creating surface textures, with features from nano to microscale, with high reproducibility and negligible surface contamination. [15-16]

Several researchers have evaluated the effect of laser texturing on the behaviour of cells cultured on metals and polymers. [17-20] However, on hard ceramics, most of the work developed focused on the laser processing methods and on the influence of laser processing on the ceramic properties. Wang *et al*, studied the effects of the laser processing parameters on alumina ceramics. The characteristics of the processed surface, cracking, heat affected zone, hole circularity and debris re-deposition were evaluated and the best laser processing parameters were identified. [21]

Barsch *et al* also studied the influence of the laser processing parameters on the development of surface microtextures on Zirconia (Y-TZP) ceramics and confirmed that femtosecond laser is a suitable tool to surface texture this material. [22]

Most of the work conducted on laser texturing of hard ceramics concerns alumina and zirconia. [23-26], and no detailed biological characterization of these surfaces was performed so far. Still, Dinca *et al* reported an improved adhesion and cytoskeleton organization of hMSCs cultured on droplet-shaped microcavities developed on zirconia by laser treatment as compared to the planar surface. [27] In what concerns Alumina-Zirconia composites, information is rare. Fiedler *et al* reported that structuring of ATZ with femtosecond laser is a promising technique to improve the ceramic surface for medical applications, but the biological response of the laser treated surfaces was not studied. [28]

In this work, we focused on the biological characterization of Alumina toughened Zirconia textured with femtosecond laser, an issue that, for the best of our knowledge, has not yet been addressed. Both the laser textured substrate and an untreated control were

characterized in terms of morphology, chemistry and topography prior to the *in vitro* cultures, in order to analyze the effects of the laser treatment on the surface properties and the influence of surface topography on human bone marrow derived mesenchymal stem cells attachment, morphology, proliferation and osteogenic differentiation.

2. Materials and Methods

2.1. Materials preparation

Alumina toughened Zirconia powder (ATZ) composed by 3% Yttria stabilized ZrO_2 with approximately 20% of Al_2O_3 (TZ-3Y20AB, TOSOH) was pressed and shaped as discs, using a uniaxial press at 40N. The discs were then pre-sintered at 1100ºC, polished and sintered at 1500ºC for 2h.

2.2. Femtosecond laser treatment

The laser treatments of the Alumina toughened Zirconia specimens was performed in air, using an Yb:KYW chirped-pulse regenerative amplification laser system (model s-Pulse HP, Amplitude Systèmes, Bordeaux, France). The pulse duration was 560 fs and the central wavelength 1030 nm. The laser beam cross-section was approximately circular, the intensity distribution Gaussian, and the beam radius ($1/e^2$) at the sample surface about 50 μm. The patterns were produced using a beam delivery system based on a Michelson interferometer, adapted from the one described by Oliveira *et al* [29] (Figure 1). In this optical set-up, the laser beam is split in two and the two partial beams reflected by mirrors M1 and M2, to a focusing lens FL of focal length L=75 mm, two partial beams on the sample's surface, where they interfere. The fringes spacing is given by $d=\lambda/[2\sin(\theta/2)]$, where λ denotes the radiation wavelength and θ the angle between the interfering beams, which depends on the distance between the two beams at the lens. The fringes spacing can be controlled by changing D by translating the mirror M2. In the present study, D=8 mm, leading to a fringe spacing d~10 μm. Total surface coverage was achieved by overlapping parallel laser tracks created by scanning the laser beam in the same direction at a speed of 1 mm/s, returning the laser beam to the origin of the track with the laser beam off and moving it in a direction perpendicular to the scanning direction of 0.05 mm (about 50% of a single track width). The tracks were produced with a pulse energy of 875 μJ and pulse repetition rate of 2 kHz.

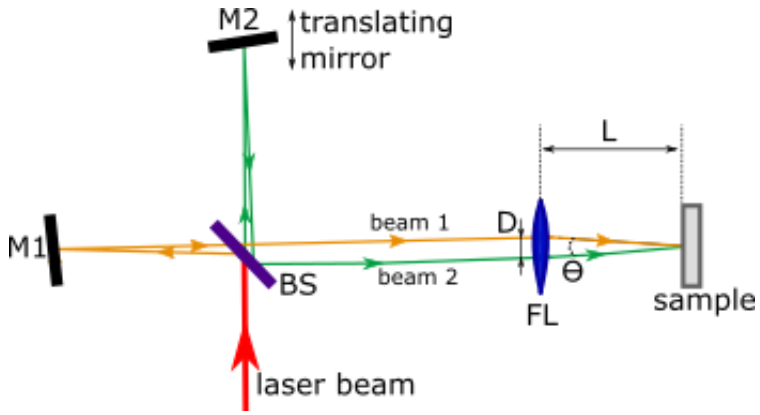

Figure 6 - Optical scheme for laser interference patterning. BS: beam splitter, M1 and M2: mirrors for beam 1 and 2, FL: focusing lenses.

2.3. Materials Characterization

2.3.1. Scanning Electron Microscopy

The microstructure of the ceramic and the topography of the laser treated surface were studied using a scanning electron microscope (SEM, FEI Quanta 400FEG ESEM/EDAX Genesis X4M) fitted with energy X-ray dispersive spectroscopy (EDS) for elemental analysis.

2.3.2. X-ray diffraction

X-ray diffraction was carried out with a Siemens D-500 Kristallofex 710 diffractometer to study the structures of the Alumina toughened Zirconia (ATZ) and the microtextured ATZ (μATZ) and possible phase transformation due to laser processing (D5000-Kristalloflex 710, Siemens).

2.3.3. Fourier Transform Infrared

The materials were characterized before and after laser treatment using a Bruker Tensor 27 FTIR spectrometer with an attenuated total reflection accessory (ATR Golden Gate, Specac). Analysis was performed in the wavelength range 4000-400 cm^{-1}, with 4 cm^{-1} steps with 2048 scans accumulated for each spectrum. The raw spectra were processed with a smoothing filter and baseline correction.

2.3.4. Atomic Force Microscopy

The surface topography of the ATZ and μATZ was studied by Atomic Force Microscopy in tapping mode (Veeco Metrology Multimode/ Nanoscope IVA). 3D topographic images of the surfaces were obtained using the apparatus software (NanoScope, Digital Instruments/Veeco). The nanoroughness parameters were obtained in terms of roughness average (Ra) and root-mean-square (Rq) on 3 boxes of 1 μm × 1 μm, measured on both the laser ablated grooves and the top areas on the μATZ and on ATZ untreated control.

2.3.5. Water Contact Angle

The surface wettability was evaluated by the sessile drop method using an OCA 15, DataPhysics Instruments GmbH apparatus. The measurements were performed with ultrapure water at 25 ºC and the contact angle was calculated by the Laplace–Young equation, using the SCA 20 software, DataPhysics Instruments GmbH.

2.4. Biological characterization

2.4.1. hMSCs harvest and culture

Human bone marrow stromal cells (hBMSCs) from human bone marrow were obtained from orthopaedic surgery procedures, after patient's informed consent. HBMSCs from different donors were characterized equally, as described in the following paragraphs. The bone was broken into small pieces and washed with alpha-minimum essential medium (α-MEM, Sigma) supplemented with 10 % fetal bovine serum (FBS, Gibco) and 1 % penicillin-streptomycin (3×10^{-4} mol/L and 5×10^{-4} mol/L, Gibco). The resultant cell suspensions were seeded in Petri dishes for 10 days. Afterwards, cell monolayers were washed with phosphate buffered saline (PBS, Sigma) twice and the media were changed. The cells tested positive for MSC markers CD105, CD146, and CD90 (surface markers expressed by mesenchymal stem cells) and confirmed to be negative for CD45 (surface marker of hematopoietic cells).

Due to MSCs ability to differentiate into several lineages, an initial experiment was performed to evaluate the preferred differentiation pathway of these cells under the experimental conditions used to address their response to the developed surface modification. Cells were seeded at a density of 2×10^4 cells/cm^2 on tissue culture polystyrene (TCPS) and cultured for 21 days in the basal medium described above. Then, histochemical staining was performed with ALP stain for osteogenesis, oil red stain for

adipogenesis, and safranin O for chondrogenesis. Cells stained positively for osteoblasts and negative for both chondrocytes and adipocytes.

When a high degree of confluence was reached, the adherent cells were washed with PBS, enzymatically released with 0.04% trypsin at 37 ºC, and sub-cultured. Cells of passage 4 were used in the experiments. Cells were seeded at a density of 2×10^4 cells/cm^2 on the thin films and on tissue culture polystyrene (TCPS) for culture control, and cultured for 21 days. The cultures were incubated in a humidified atmosphere of 5% CO_2 at 37 ºC and maintained with basal culture medium that was changed twice a week. Cultures were characterized throughout the culture time as follows.

2.4.2. Metabolic activity and proliferation

Cells metabolic activity was evaluated by the resazurin assay. Fresh medium with 10% of resazurin was added to the cells and incubated for 3 hours. Afterwards, 100µl was transferred to a 96-well plate and the fluorescence was quantified in a microplate reader (Synergy HT, BioTek) at 535 nm excitation wavelength and 590 nm emission wavelength. The results were expressed in relative fluorescence units (RFU).

DNA content was measured using the Quant-iT^{TM} Picogreen® DNA assay (Invitrogen) according to the manufacturer's instructions. Briefly, 100 µL of each cell lysate solution was added to 100 µL of PicoGreen reagent and incubated in the dark at room temperature for 5 min. Finally, the fluorescence intensity was measured with a microplate spectrofluorometer (Synergy HT, BioTek) at 530 and 590 nm (480–520 nm) emission (excitation), respectively. The results were expressed in ng of DNA per mL.

2.4.3. Cell Morphology

For focal adhesions immunostaining, fixed samples (3.7% paraformaldehyde, 15 min) were incubated for 5 min with 0.1% v/v Triton X-100 (Sigma) and 30 min with 1 wt% bovine serum albumin (BSA, Merck) at room temperature, to block nonspecific binding. Samples were then incubated with mouse anti-human vinculin mAb clone hVIN-1 (Sigma) at 1:100 for 1h at room temperature and then washed with PBS and stained with Alexa Fluor 488 rabbit anti-mouse IgG, F(ab')2 fragment (Molecular Probes) at 1:200 for 30 min at room temperature. Samples were subsequently washed three times and nuclei were counterstained with propidium iodide (Molecular Probes) for 10 min at RT. Cells

were observed with a Spectral Confocal Microscope Leica TCS-SP5 AOBS (Leica) after staining.

For the morphology evaluation via SEM (FEI Quanta 400 FEG/ESEM), the cells were dehydrated in graded ethanol solutions and hexamethyldisilazane (HMDS, Sigma) solutions from 50% to 100%, respectively. The samples were then sputter-coated (SPI-Module) with palladium-gold.

2.4.4. Quantitative real-time polymerase chain reaction (qRT-PCR)

qRT-PCR was performed to evaluate the osteoblastic differentiation of the hBMSCs cultured on the materials. At days 14 and 21 of culture, total RNA was isolated from the cell culture on the materials using the RiboPure^{TM} kit according to the manufacturer's instructions and quantified using a NanoDrop Spectrophotometer (NanoDrop Technologies). With iScript™ cDNA Synthesis Kit (Biorad), 40ng of RNA was converted into complementary DNA (cDNA).

qRT-PCR was performed using PrimePCR™ custom plate (Bio-Rad). PrimePCR assays consisted on the following genes: Alkaline Phosphatase (ALP), Collagen Type I (COL-I), Runt-related transcription factor 2 (RUNX2), Osteocalcin (OC), Osteonectin (ON), Osterix (OSX) and Osteoprotegerin (OPG). Glyceraldehyde-3-phosphate dehydrogenase (GAPDH) was selected as reference gene.

The PCR reaction mix contained PrimePCR assay, SsoAdvanced SYBR Green Supermix, cDNA and nuclease-free water. The 96-well plate was run on the CFX96 (BioRad) at 95°C for 120 seconds, then 95°C for 5 seconds and 60°C for 30 seconds (for 45 cycles).

Gene and transcription factors expression was calculated relative to GAPDH by the comparative ΔΔCt values method and fold change was calculated by normalizing the data to the values of the control surface, ATZ

2.5. Statistical analysis

Triplicate experiments were performed for all tested parameters. The results were expressed as the arithmetic mean ± standard deviation. The statistical analysis of the results was done using the one-way analysis of variance (One-way ANOVA) followed by the Tukey HSD *post hoc* test. Levels of $p \leq 0.05$ were considered to be statistically significant. The statistical analysis was performed using the SPSS statistical software (Statistical Package for the Social Sciences Inc., USA).

3. Results

3.1. Materials Characterization

3.1.1. Scanning Electron Microscopy

Figure 2 shows the ceramic surface before (a, b) and after (c, d) the treatment with the femtosecond laser. The laser treated surfaces exhibit parallel microgrooves with a periodicity of about 10 µm over their entire surface, which results from the imprinting of the two beams interference on the surface. At high magnification (Fig. 2 d), parallel ripples with a periodicity of between 300 and 400 nm can be seen on the laser treated surfaces. These ripples overlap the interference pattern and are oriented in a direction perpendicular to the direction of the microgrooves and perpendicular to the beam polarization direction. These ripples are laser induced periodic surface structures, or LIPSS, with high spatial frequency (HSFL) and were previously observed on surfaces of other ceramics materials. [30-31]

The EDS spectra of both specimens are identical, indicating that the surface composition was not affected by the laser treatment.

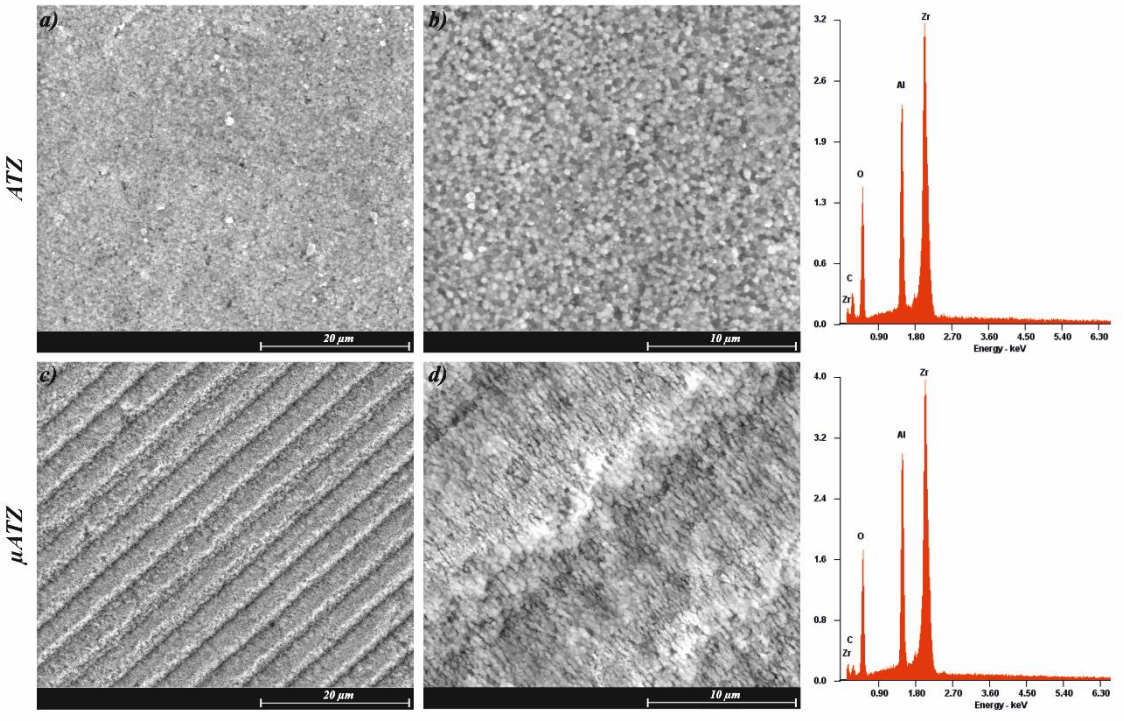

Figure 2 - SEM images and EDS spectra of ATZ (a, b) and µATZ (c, d) specimens. Images a) and c) were obtained at magnification of 5000x and b) and d) at a magnification of 10000x.

3.1.2. Atomic Force Microscopy

The AFM profiles of the untreated and laser treated surfaces are shown in figure 3 a). The interference pattern is observed in the laser treated surface. The peak-to-valley distance of the interference pattern on μATZ is about 2.6 μm. The high-frequency LIPSS are also clearly evident. This image confirms that these nanofeatures are perpendicular to the microtopography. On the ATZ, the grains are well distributed with no noticeable alignment.

The nanoroughness analysis (Ra and Rq parameters) revealed that the laser ablated microgrooves, with high-frequency LIPSS had a statistically significant higher average roughness (Ra = 140.8 ± 10.9 nm) when compared to those of both the top, untreated areas on the μATZ surface (Ra = 42.6 ± 0.8 nm) and the untreated control (Ra = 41.2 ± 0.9 nm).

The same results were obtained for the measurements of root-mean-square (Rq), where the micro/nanotextured grooves presented the highest values (Rq = 182.3 ± 12.8 nm), while the untreated areas of μATZ (Rq = 61.5 ± 3.7 nm) and the ATZ surface (Rq =53.2 ±.2.5 nm) presented significantly lower Rq values.

3.1.3. X-ray diffraction

The X-ray diffractograms of ATZ and μATZ are presented in figure 3 b). The same peaks were obtained for both specimens but the width of these peaks is larger for the laser treated sample, indicating a smaller crystallite size (according to Scherrer equation). [32] The peaks at 2θ = 25.7; 35.1; 37.8; 43.3; 52.6; 57.5; 66.5 and 68.3º can be ascribed to α-corundum, , while those at 30.1; 35.0; 50.1; 50.5; 59.7; 60.0 and 62.7º can be assigned to the tetragonal phase of zirconia. The monoclinic phase of Zirconia was not detected.

3.1.4. Fourier transform infrared spectroscopy

FTIR spectra of both specimens are displayed in figure 3 c). Five peaks are observed in the region 1400 cm^{-1} to 400 cm^{-1} in the spectrum of the untreated ATZ while after the laser treatment only three peaks are visible. The intensity of the bands is lower in the spectrum of the laser treated material as well as a small dislocation of the peaks, when compared to the initial material.

In the spectrum of ATZ, a small band at 773.1 corresponds to Al-O vibrations and the two peaks at 654.6 and 629.6 to the stretching modes of the AlO_6^{3-} octahedral. [33-34] The band at 615.9 in the spectrum of the treated sample can be ascribed to the same vibrational mode. Zr-O vibrations from tetragonal zirconia were identified at 501.7 in the ATZ and 492.1 in the μATZ. Zr-O bonds were also found at 360.7 and 373.3 for the ATZ and the μATZ, respectively. [35]

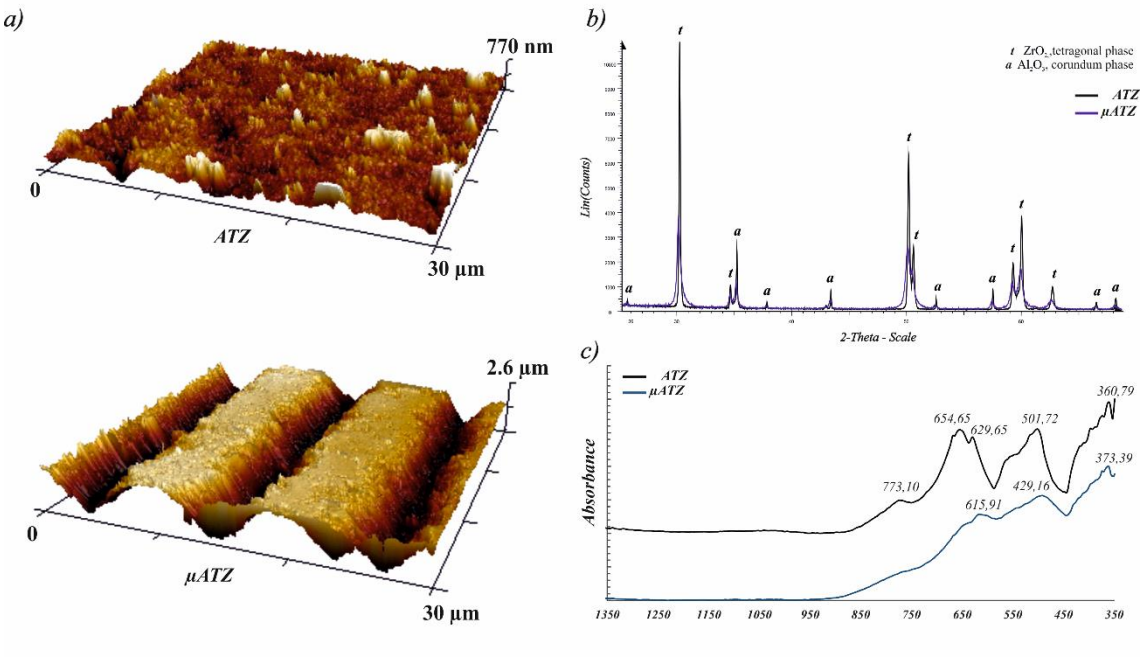

Figure 3 – AFM (a), XRD (b) and FT-IR (c) characterization of the ATZ and μATZ surfaces.

3.1.5. Water Contact Angle

In terms of wettability properties, the ATZ control surface displayed a hydrophilic value of 81.58 ± 1.08 while the microtextured surface exhibited a hydrophobic behaviour with a 98.71 ± 1.31 contact angle value.

3.2. Biological Characterization

3.2.1. Metabolic activity and proliferation

Figure 4 shows the metabolic activity and proliferation of the hMSCs during the 21 days of culture. On both surfaces, cells metabolic activity increased with the time of culture, with the characteristic lag phase of hMSCs between days 1 and 7. At day 14, cells on the textured surface showed a slight increase in the metabolic activity (~ 24%) compared to

the control surface. On day 21, the ATZ control increased to higher values (~ 11%) than the modified surface.

Cell proliferation exhibited the same tendency as the metabolic activity. An increased proliferation with the time of culture, with higher cell proliferation on the microtopography surface on day 14 (~ 26 %) and an increased proliferation on the control surface at day 21 (~ 7 %).

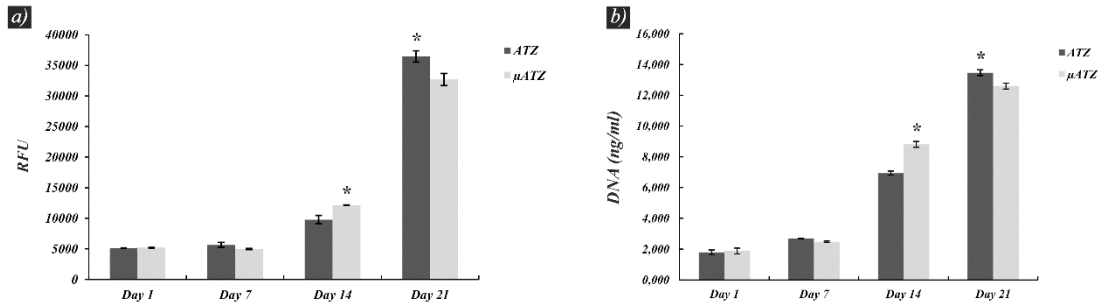

Figure 4 – Cell metabolic activity (a) and proliferation (b) of hMSCs cultured on ATZ and µATZ surfaces. * represents statistically significant differences ($p \leq 0.05$) between both materials, at each time-point.

3.2.2. Cell Morphology

hMSCs focal adhesions were observed by confocal microscopy at day 1 (Figure 5). Cells were well spread and adhered to the substrates. Focal adhesion points were found mostly on the hMSCs periphery. On the untreated ATZ control, cells were randomly organized and the focal adhesions were less, smaller and oriented in several directions, as showcased by the yellow arrows.

Cells adhesion to the µATZ was much stronger, oriented according to the microfeatures and displaying very mature focal adhesions with fillopodia well stretched, also completely aligned with the surface micropatterns, showing the directionality of cell migration, as indicated by yellow arrows and dashed line. To confirm this stronger interaction of cell with the micro and nanostructures, SEM observations were carried out. It is visible the fillopodia of cells connection with this surface, aligned with the microtopography and attached to the nanostructures.

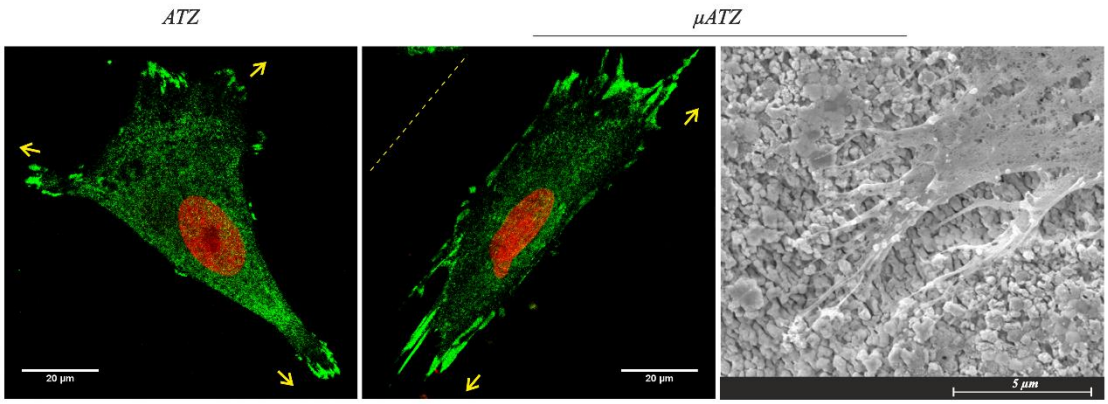

Figure 5 - Immunostaining of focal adhesions and cells morphology at day 1 of culture on the ATZ and μATZ and SEM of cells adhesion the micro/nanostrustures. hMSCs focal adhesions were stained for vinculin with Phalloidin 488 (green) and nuclei with PI (red). Yellow arrows display cell spreading directions and dashed yellow line the orientation of the micropatterns.

Scanning electron microscopy images show cell proliferation and organization during the time of culture (Figure 6). It can be seen that cells are modulated mostly according to the surface microtopographies on the μATZ, and randomly organized on the ATZ surfaces. At the earlier stages it is noticed that cells on the μATZ are mostly oriented according to the microtopography, although, some cells seem to align according to the nanofeatures direction. After 14 days, cells seemed completely aligned with the microtopography, covering almost all the surface. Cells on the ATZ substrate are well stretched and adhered and arranged in a random manner. At day 21, both materials were completely covered with cells. On ATZ cells were randomly organized, while on the μATZ cells remained aligned with the microtopography. The differences between cell morphology on both surfaces at day 21 are noteworthy (Figure 6 b). Cells on the ATZ are well spread with flat cytoplasmic membranes (1) while cells on the μATZ seem very well stretched, with clear stressed actin filaments, and the cytoplasmic membranes of the layer of cells is filled with vesicles and products from the mineralization process (2, 3). On the μATZ, at higher magnification, the beginning of the mineralization process was observed, with small vesicles all around the cytoplasmic membrane (2). In other zone in the μATZ surface (3), some small aggregates were found and confirmed to be mineralized calcium phosphate by EDS.

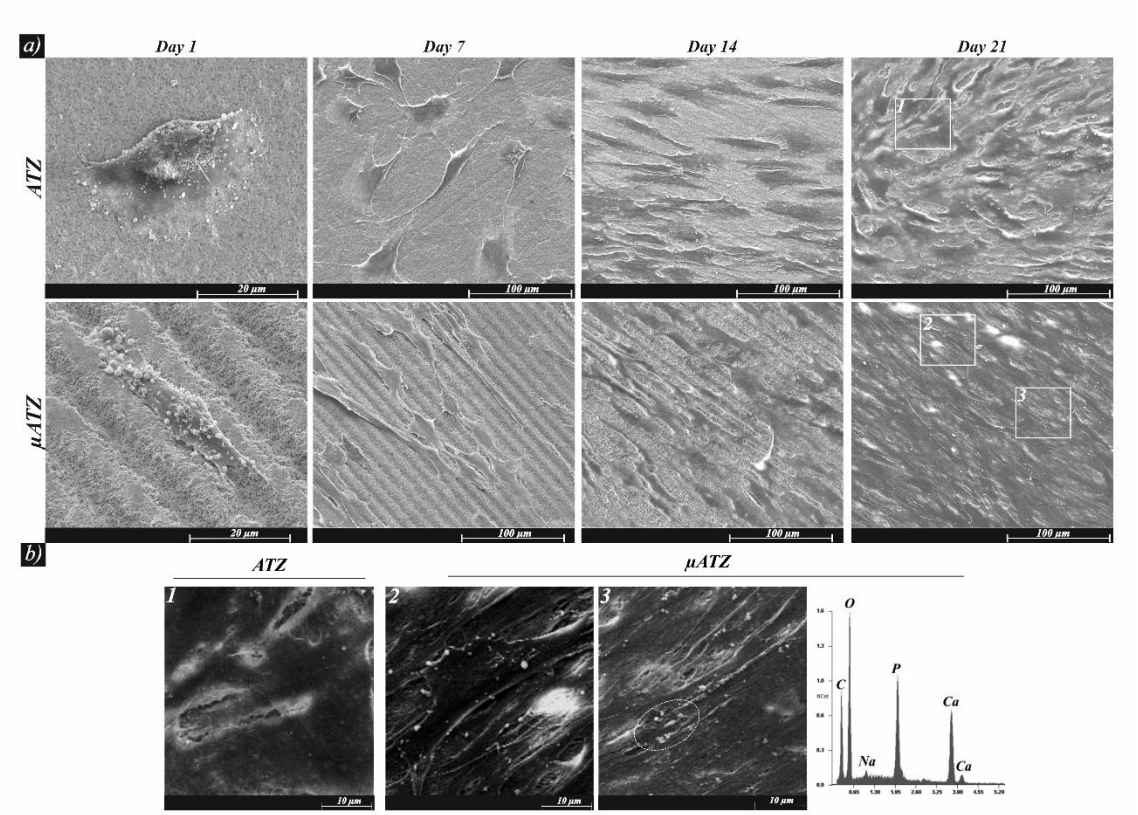

Figure 6 – SEM images of hMSCs morphology while adhered to the ATZ and μATZ, at 1, 7, 14 and 21 days of culture (a), and higher magnification images of hMSCs at day 21 (b).

3.2.3. Quantitative real-time polymerase chain reaction (qRT-PCR)

Real-time PCR assays were performed at days 14 and 21, to evaluate the degree of osteogenic differentiation of hMSCs on both surfaces (Figure 7). The values are expressed as fold change and were calculated by the ΔΔCt method to the reference gene GAPDH and normalized to the control surface, ATZ.

At day 14, the differences in gene expression on both materials are noticeable. All osteogenic-related markers were upregulated on the μATZ, with ALP displaying a significantly higher expression. In terms of osteogenic transcription factors, RUNX2 was upregulated by 97% in relation to the ATZ control while OSX displayed a 65% increased expression. All other osteogenic genes were upregulated, COL-I increased by 84%, OC by 42% and OPG was upregulated by 89%. A small increase was noticed for ON, with an increased expression of 21%.

At day 21, the tendency was maintained and all osteogenic-related markers were upregulated in the μATZ, with the exception of OSX. ALP expression lowered significantly, still with an increased expression when compared to the ATZ. Both COL-I

and RUNX2 were significantly upregulated in relation to the control. OC expression was upregulated by 50%, ON by 97% and OPG expression was 77% increased, when compared to the control, ATZ

Statistical analysis of gene expression on μATZ between days 14 and 21 revealed that ALP and transcription factor OSX expression were significantly higher at day 14, while RUNX2 and ON showed to be statistically significantly higher at day 21. The expressions of COL-I, OC and OPG were maintained, with no significant differences, between both time-points.

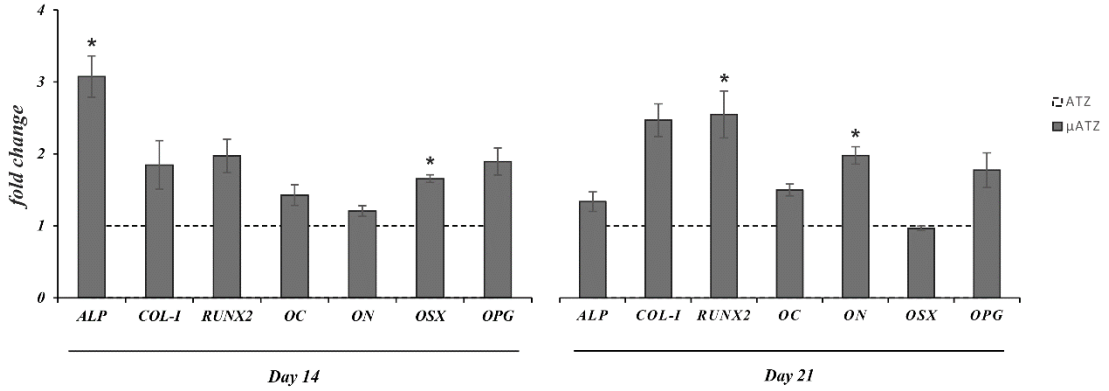

Figure 7 – Quantitative real-time polymerase chain reaction (qPCR) of osteogenic related genes and transcription factors for 14 and 21 days of culture. Quantitation of data was performed using the ΔΔCt method using GAPDH gene expression as an endogenous reference. Results were normalized to the control surface, ATZ, and are represented as fold change. * represents statistically significant differences between gene expression on the μATZ at 14 and 21 days of culture (p≤0.05).

4. Discussion

The new focus on tissue regeneration strategies is to develop biomaterials that can elicit specific biological responses at implantation.

It is well established that modifying the surface topography of a biomaterial has a positive effect on regeneration. Several authors have shown that biomaterials with topographic features in the micro and nanometer range present improved protein adsorption, cell adhesion, proliferation and increased differentiation. [10, 36-38]

In recent years, some authors used ultrafast lasers to structure the surface of a wide range of ceramics but the biological performance of the laser textured materials was only scarcely investigated. [39-40] In the present work, complex surface patterns consisting of high-frequency LIPSS overlapped to an interference grating were successfully created on the surface of Alumina toughened Zirconia.

SEM and AFM observations showed that, the high-frequency LIPSS present an orientation perpendicular to the microgrooves resulting from the laser interference. LIPSS can be formed in a wide range of materials and have been shown to considerably improve bioactivity and cells response. [41-42]

EDS, FTIR and XRD analyses showed that no changes occurred in the chemical composition of the materials due to laser treatment. In terms of structure, the broadening of the XRD peaks indicates a grain size refinement due to the laser machining. This conclusion is supported by the FTIR results, where the shift and lower intensity of the peaks on the laser treated surface indicate alterations in the structure organization and a less crystalline surface. [43]

The wettability test showed that, as expected, the textured surfaces exhibit higher contact angles as compared to the untreated ones. This influence of the microtopography on the surface wettability has been reported by several authors, who showed that the combination of micro and nanoroughness often leads to an increase of the contact angle, independently of the surface chemistry. [10, 44-45]

The *in vitro* cell culture was performed under basal conditions to evaluate the full impact of surface topography on hMSCs differentiation. Most studies that focus on evaluating the osteogenic differentiation of mesenchymal stem cells use supplemented media or soluble factors. However, and especially on studies with micro/nanostructured surfaces, the use of chemicals or soluble factors may potentially mask the real effect of the surface topography on cells behaviour.

Cell-surface interaction is a combination of multi-steps, from the initial events of protein adsorption and cell adhesion to cell proliferation, differentiation and matrix deposition and mineralization. Extracellular signals, such as surface topography, can regulate cell functions such as alignment, morphology, migration and differentiation. Cells interact with the surrounding topography through transmembrane proteins, integrins. When binding to the surrounding extracellular environment, the increasing recruitment of integrins forms focal adhesions. These facilitate cells migration, spreading and proliferation, and have been proved to regulate the osteogenic differentiation in some biomaterials. [46-49]

The hMSCs adhered on the ATZ displayed a lower number of focal adhesions following different directions. On the μATZ, mature focal adhesions were mainly modulated by the microtopography with a very distinguished alignment with cell morphology. Such results

confirm that cells are capable of establishing more and stronger cell-surface interactions in the presence of micro/nanofeatures. [50]

The surface topography modulated cell morphology, as it was observed that cells on the μATZ were able to spread and align according to the micropatterns and proliferated maintaining that orientation. Cells were found to align according to the microgrooves during all times of culture. On the untreated surface, cells were well spread, with no defined orientation and proliferated randomly organized.

The effects of micro and nanotopography are well described in the literature with divergent results that show to be dependent on the material, the size of the features and the cell type used. [51-52]

Martínez-Calderon *et al* studied cell adhesion and migration on stainless steel micro and nano textured by femtosecond laser. The focus of their study was to evaluate the influence of LIPSS on cells behaviour. Their results showed that the hMSCs aligned mostly according to the LIPSS orientation, when the LIPSS were parallel to the micropatterns, but when the LIPSS were perpendicular to the micropatterns, cells aligned according to the micropattern. In terms of adhesion, cells predominantly chose the site where the LIPSS nanopatterns were oriented parallel to the microstripes, but it could also be related with the different size of these microfeatures. [53]

In the present study, the high frequency LIPSS are perpendicular to the microgrooves direction and the cells aligned in the direction of the micropatterns, adhering preferentially in the microgrooves, despite the opposite direction of the nanotextures.

At day 21, there was evidence of osteoblasts in different stages of the mineralization process on the microstructured surface. The small vesicles that are formed all around the cytoplasmic membrane are an evidence of this process initiating. These membrane vesicles display a high ALP activity that hydrolyses organic phosphates providing phosphate ions that, together with calcium ions, initiate the mineralization process, being downregulated afterwards. [54] This evidence was also confirmed by qRT-PCR.

hMSCs cultured on both materials expressed osteogenic markers. On day 14, most were upregulated on the microstructured surface, with a noteworthy higher expression of ALP, COL-I, RUNX2, OSX and OPG, while OC and ON displayed an expression closer to the ATZ control values. At day 21, the expression levels of OSX were similar to the control, and all other osteogenic-related markers were upregulated on the μATZ, with noticeable higher expressions of RUNX2, COL-I, ON and OPG. On μATZ, RUNX2 and ON were statistically significantly upregulated after 21 days of culture.

Osteogenic differentiation is known to be mediated by RUNX2, a transcription factor that regulates the expression of osteoblast-specific genes like alkaline phosphatase, collagen type I, osteopontin and osteocalcin. [55-56]

ALP, type I collagen and OSX are considered early osteoblast markers. In our results, these genes were significantly highly expressed in the μATZ at day 14 and decreased at day 21, with the exception of collagen, responsible for matrix deposition, that continued to increase until day 21, with no statistical differences. [57-59] On the other hand, both OC and ON are genes expressed by mature osteoblast, at later stages of differentiation. [60]

The decrease of both ALP and OSX and slight increase in OC and ON may indicate that μATZ initiated the differentiation process earlier and advanced to a more mature phase at day 21. The expression of osteocalcin, which happens at the mineralization state of osteoblasts and is regulated by RUNX2, was increased by around 50% at both time-points, a slight increase in comparison to the control, which in turn may represent a small advance to the mineralization stage.

This, as noticed by Masaki et al, may be due to the degree of osteogenic differentiation, since the expression of OC occurs when osteoblasts are at a more mature stage of differentiation. [61] Moreover, at day 21, cells on the μATZ showed to be at different stages of the mineralization process, as confirmed either by the spotting of cells with the formation of transmembrane vesicles and by dots of already formed mineralization, as well as the decreasing of ALP and OSX and increase in ON. Also important, osteoprotegerin (OPG) is produced by developing osteoblasts and it can enhance the synthesis of bone matrix by blocking osteoclast bone resorption. The expression of this gene is important during the beginning of new bone formation by inhibiting bone resorption by osteoclasts, and it is expressed in similar levels at both time-points. [56]

In this work we developed a new Alumina toughened Zirconia material structured by femtosecond laser and performed adequate *in vitro* biological characterization. Nanostructured micropatterns were created in a reproducible and controlled manner. We proved that cells morphology, migration and proliferation were modulated preferentially by the surface microtopography and were not affected by the high-frequency LIPSS oriented perpendicularly to the microtopography features. hMSCs experienced a faster and higher osteogenic differentiation on these structured materials, than on the flat control surface, under basal conditions.

5. Conclusions

The surface topographical modification by femtosecond laser described in this work constitutes a simple, non-chemical, single-step process that can be applied to create precise and reproducible micro and nano textures on Alumina toughened Zirconia ceramics. It was confirmed that these materials are capable of modulating cell attachment, alignment and proliferation and that hMSCs undergo a faster and greater osteogenic differentiation, even when cultured with no supplemented media. These modified materials can constitute a biomaterial that is capable of inducing guided tissue regeneration and improved osteointegration that can be used in load-bearing conditions such as dental and maxillofacial applications and can withstand a long term shelf life.

Acknowledgments

This work was supported by FEDER funds through the Programa Operacional Factores de Competitividade (COMPETE) (POCI/01/0145/FEDER/007265) and by Portuguese funds through FCT (Fundação para a Ciência e a Tecnologia) under the Partnership Agreement PT2020 UID/QUI/50006/2013 and A. Carvalho grant (SFRH/BD/87624/2012). The authors would also like to acknowledge Rui Rocha (CEMUP) and Paula Magalhães and Tânia Meireles (CCGEN).

References

1. Kohal RJ, Att W, Bachle M, Butz F. Ceramic abutments and ceramic oral implants. An update. Periodontology 2000. 2008;47:224-43.
2. De Aza AH, Chevalier J, Fantozzi G, Schehl M, Torrecillas R. Crack growth resistance of alumina, zirconia and zirconia toughened alumina ceramics for joint prostheses. Biomaterials. 2002;23:937-45.
3. Wenz HJ, Bartsch J, Wolfart S, Kern M. Osseointegration and clinical success of zirconia dental implants: a systematic review. The International journal of prosthodontics. 2008;21:27-36.
4. Schierano G, Mussano F, Faga MG, Menicucci G, Manzella C, Sabione C, et al. An alumina toughened zirconia composite for dental implant application: in vivo animal results. BioMed research international. 2015;2015:157360.
5. Kurtz SM, Kocagoz S, Arnholt C, Huet R, Ueno M, Walter WL. Advances in zirconia toughened alumina biomaterials for total joint replacement. Journal of the mechanical behavior of biomedical materials. 2014;31:107-16.
6. Sequeira S, Fernandes M, Neves N, Almeida M. Development and characterization of zirconia–alumina composites for orthopedic implants. Ceramics International. 2017;43:693-703.
7. Faga M, Vallée A, Bellosi A, Mazzocchi M, Thinh N, Martra G, et al. Chemical treatment on alumina–zirconia composites inducing apatite formation with maintained mechanical properties. Journal of the European Ceramic Society. 2012;32:2113-20.

8. Kohal RJ, Bachle M, Renz A, Butz F. Evaluation of alumina toughened zirconia implants with a sintered, moderately rough surface: An experiment in the rat. Dental materials : official publication of the Academy of Dental Materials. 2016;32:65-72.
9. Kilian KA, Bugarija B, Lahn BT, Mrksich M. Geometric cues for directing the differentiation of mesenchymal stem cells. Proceedings of the National Academy of Sciences of the United States of America. 2010;107:4872-7.
10. Carvalho A, Pelaez-Vargas A, Hansford DJ, Fernandes MH, Monteiro FJ. Effects of Line and Pillar Array Microengineered SiO2 Thin Films on the Osteogenic Differentiation of Human Bone Marrow-Derived Mesenchymal Stem Cells. Langmuir : the ACS journal of surfaces and colloids. 2016;32:1091-100.
11. Young JF, Preston J, Van Driel H, Sipe J. Laser-induced periodic surface structure. II. Experiments on Ge, Si, Al, and brass. Physical Review B. 1983;27:1155.
12. Yada S, Terakawa M. Femtosecond laser induced periodic surface structure on poly-L-lactic acid. Optics express. 2015;23:5694-703.
13. Shukla P, Waugh D, Lawrence J, Vilar R. Laser surface structuring of ceramics, metals and polymers for biomedical applications: a review. Laser Surface Modification of Biomaterials: Techniques and Applications. 2016:281.
14. Cunha A, Zouani OF, Plawinski L, Botelho do Rego AM, Almeida A, Vilar R, et al. Human mesenchymal stem cell behavior on femtosecond laser-textured Ti-6Al-4V surfaces. Nanomedicine. 2015;10:725-39.
15. Wang JC, Guo CL. Numerical study of ultrafast dynamics of femtosecond laser-induced periodic surface structure formation on noble metals. J Appl Phys. 2007;102.
16. Rihakova L, Chmelickova H. Laser Micromachining of Glass, Silicon, and Ceramics. Advances in Materials Science and Engineering. 2015;2015:6.
17. Shinonaga T, Tsukamoto M, Nagai A, Yamashita K, Hanawa T, Matsushita N, et al. Cell spreading on titanium dioxide film formed and modified with aerosol beam and femtosecond laser. Appl Surf Sci. 2014;288:649-53.
18. Cunha A, Serro AP, Oliveira V, Almeida A, Vilar R, Durrieu MC. Wetting behaviour of femtosecond laser textured Ti-6Al-4V surfaces. Appl Surf Sci. 2013;265:688-96.
19. Duncan AC, Weisbuch F, Rouais F, Lazare S, Baquey C. Laser microfabricated model surfaces for controlled cell growth. Biosens Bioelectron. 2002;17:413-26.
20. Jun I, Chung YW, Heo YH, Han HS, Park J, Jeong H, et al. Creating Hierarchical Topographies on Fibrous Platforms Using Femtosecond Laser Ablation for Directing Myoblasts Behavior. Acs Appl Mater Inter. 2016;8:3407-17.
21. Wang X, Zheng H, Chu P, Tan J, Teh K, Liu T, et al. Femtosecond laser drilling of alumina ceramic substrates. Applied Physics A. 2010;101:271-8.
22. Bärsch N, Werelius K, Barcikowski S, Liebana F, Stute U, Ostendorf A. Femtosecond laser microstructuring of hot-isostatically pressed zirconia ceramic. Journal of Laser Applications. 2007;19:107-15.
23. Perrie W, Rushton A, Gill M, Fox P, O'Neill W. Femtosecond laser micro-structuring of alumina ceramic. Appl Surf Sci. 2005;248:213-7.
24. Sugioka K, Cheng Y. Ultrafast lasers-reliable tools for advanced materials processing. Light-Sci Appl. 2014;3.
25. Erdur EA, Basciftci FA. Effect of Ti:Sapphire-femtosecond laser on the surface roughness of ceramics. Lasers in surgery and medicine. 2015;47:833-8.
26. Delgado-Ruiz RA, Calvo-Guirado JL, Moreno P, Guardia J, Gomez-Moreno G, Mate-Sanchez JE, et al. Femtosecond laser microstructuring of zirconia dental implants. Journal of biomedical materials research Part B, Applied biomaterials. 2011;96:91-100.

27. Dinca V, Sima LE, Rusen L, Bonciu A, Lippert T, Dinescu M, et al. Bio-Interfaces Engineering Using Laser-Based Methods for Controlled Regulation of Mesenchymal Stem Cell Response In Vitro2016.
28. Fiedler S, Irsig R, Tiggesbaumker J, Schuster C, Merschjann C, Rothe N, et al. Machining of Biocompatible Ceramics with Femtosecond Laser Pulses. Biomedizinische Technik Biomedical engineering. 2013.
29. Oliveira V, Polushkin N, Conde O, Vilar R. Laser surface patterning using a Michelson interferometer and femtosecond laser radiation. Optics & Laser Technology. 2012;44:2072-5.
30. Höhm S, Rosenfeld A, Krüger J, Bonse J. Femtosecond laser-induced periodic surface structures on silica. Journal of Applied Physics. 2012;112:014901.
31. Dufft D, Rosenfeld A, Das S, Grunwald R, Bonse J. Femtosecond laser-induced periodic surface structures revisited: a comparative study on ZnO. Journal of Applied Physics. 2009;105:034908.
32. Cullity BD. Elements of X-ray Diffraction. 2001.
33. Cavalu S, Banica F, Simon V, Akin I, Goller G. Surface Modification of Alumina/Zirconia Ceramics Upon Different Fluoride-Based Treatments. Int J Appl Ceram Tec. 2014;11:402-11.
34. Sarkar D, Mohapatra D, Ray S, Bhattacharyya S, Adak S, Mitra N. Synthesis and characterization of sol-gel derived ZrO2 doped Al2O3 nanopowder. Ceram Int. 2007;33:1275-82.
35. Agarwal RK, Rastogi SC. Infrared and Thermal Studies of Oxozirconium(Iv) Complexes of 4-Cyanopyridine N-Oxide. Thermochim Acta. 1985;87:357-62.
36. Keller JC, Schneider GB, Stanford CM, Kellogg B. Effects of implant microtopography on osteoblast cell attachment. Implant dentistry. 2003;12:175-81.
37. Boyan B, Lossdorfer S, Wang L, Zhao G, Lohmann C, Cochran D, et al. Osteoblasts generate an osteogenic microenvironment when grown on surfaces with rough microtopographies. Eur Cell Mater. 2003;6:22-7.
38. Shou GH, Dong LQ, Wang XZ, Cheng K, Weng WJ. Enhanced biological performance on nano-microstructured surfaces assembled by SrTiO3 cubic nanocrystals. Rsc Adv. 2015;5:67896-900.
39. Vicente Prieto M, Gomes ALC, Montero Martín J, Alvarado Lorenzo A, Seoane Mato V, Albaladejo Martínez A. Effect of femtosecond laser treatment on effectiveness of resin-zirconia adhesive: an in vitro study. 2016. 2016;7:6.
40. Aivazi M, Hossein Fathi M, Nejatidanesh F, Mortazavi V, HashemiBeni B, Matinlinna JP, et al. The evaluation of prepared microgroove pattern by femtosecond laser on alumina-zirconia nano-composite for endosseous dental implant application. Lasers in medical science. 2016;31:1837-43.
41. Cunha A, Oliveira V, Serro AP, Zouani OE-F, Almeida A, Durrieu M-C, et al. Ultrafast laser texturing of TI-6AL-4V surfaces for biomedical applications. ICALEO 2013, LIA Pub 616: Laser Institute of America Orlando, FL, USA; 2013. p. 910-8.
42. Liang CY, Wang HS, Yang JJ, Yang Y, Yang XJ. Surface modification of cp-Ti using femtosecond laser micromachining and the deposition of Ca/P layer. Mater Lett. 2008;62:3783-6.
43. Lee SY, Regnault WF, Antonucci JM, Skrtic D. Effect of particle size of an amorphous calcium phosphate filler on the mechanical strength and ion release of polymeric composites. Journal of biomedical materials research Part B, Applied biomaterials. 2007;80:11-7.
44. Mills CA, Fernandez JG, Martinez E, Funes M, Engel E, Errachid A, et al. Directional alignment of MG63 cells on polymer surfaces containing point microstructures. Small. 2007;3:871-9.

45. Pelaez-Vargas A, Gallego-Perez D, Magallanes-Perdomo M, Fernandes MH, Hansford DJ, De Aza AH, et al. Isotropic micropatterned silica coatings on zirconia induce guided cell growth for dental implants. Dental materials : official publication of the Academy of Dental Materials. 2011;27:581-9.
46. Lim JY, Dreiss AD, Zhou Z, Hansen JC, Siedlecki CA, Hengstebeck RW, et al. The regulation of integrin-mediated osteoblast focal adhesion and focal adhesion kinase expression by nanoscale topography. Biomaterials. 2007;28:1787-97.
47. Yim EK, Darling EM, Kulangara K, Guilak F, Leong KW. Nanotopography-induced changes in focal adhesions, cytoskeletal organization, and mechanical properties of human mesenchymal stem cells. Biomaterials. 2010;31:1299-306.
48. Ye K, Wang X, Cao L, Li S, Li Z, Yu L, et al. Matrix Stiffness and Nanoscale Spatial Organization of Cell-Adhesive Ligands Direct Stem Cell Fate. Nano letters. 2015;15:4720-9.
49. Biggs MJ, Dalby MJ. Focal adhesions in osteoneogenesis. Proceedings of the Institution of Mechanical Engineers Part H, Journal of engineering in medicine. 2010;224:1441-53.
50. Biggs MJ, Richards RG, Dalby MJ. Nanotopographical modification: a regulator of cellular function through focal adhesions. Nanomedicine : nanotechnology, biology, and medicine. 2010;6:619-33.
51. Martinez E, Engel E, Planell JA, Samitier J. Effects of artificial micro- and nano-structured surfaces on cell behaviour. Annals of anatomy = Anatomischer Anzeiger : official organ of the Anatomische Gesellschaft. 2009;191:126-35.
52. Flemming RG, Murphy CJ, Abrams GA, Goodman SL, Nealey PF. Effects of synthetic micro- and nano-structured surfaces on cell behavior. Biomaterials. 1999;20:573-88.
53. Martinez-Calderon M, Manso-Silvan M, Rodriguez A, Gomez-Aranzadi M, Garcia-Ruiz JP, Olaizola SM, et al. Surface micro- and nano-texturing of stainless steel by femtosecond laser for the control of cell migration. Scientific reports. 2016;6:36296.
54. Fernandes MH, Gomes PS. Bone Cells Dynamics during Peri-Implantitis: a Theoretical Analysis. Journal of oral & maxillofacial research. 2016;7:e6.
55. Komori T. Regulation of osteoblast differentiation by transcription factors. Journal of cellular biochemistry. 2006;99:1233-9.
56. Kirkham G, Cartmell S. Genes and proteins involved in the regulation of osteogenesis. Ashammakhi N, Reis R, Chiellini E, editores Topics in Tissue Engineering. 2007;3.
57. Golub EE, Boesze-Battaglia K. The role of alkaline phosphatase in mineralization. Current Opinion in Orthopaedics. 2007;18:444-8.
58. Hayes JS, Khan IM, Archer CW, Richards RG. The role of surface microtopography in the modulation of osteoblast differentiation. Eur Cell Mater. 2010;20:98-108.
59. Nakashima K, Zhou X, Kunkel G, Zhang Z, Deng JM, Behringer RR, et al. The novel zinc finger-containing transcription factor osterix is required for osteoblast differentiation and bone formation. Cell. 2002;108:17-29.
60. Hayrapetyan A, Jansen JA, van den Beucken JJ. Signaling pathways involved in osteogenesis and their application for bone regenerative medicine. Tissue Engineering Part B: Reviews. 2014;21:75-87.
61. Masaki C, Schneider GB, Zaharias R, Seabold D, Stanford C. Effects of implant surface microtopography on osteoblast gene expression. Clinical oral implants research. 2005;16:650-6.

CHAPTER V

GENERAL DISCUSSION AND FUTURE WORK

GENERAL DISCUSSION

New strategies for reconstruction or replacement of bone with high mechanical strength are still extensively researched with one of the main goals being the development of biomaterials that can last for the remaining life of the patient.

As previously described, most common practices are based on the use of bone grafts or Titanium based biomaterials, even though both are still associated with risks and post-surgery complications. Titanium implants have been reported to cause certain post-implantation problems, such as allergic reactions, wear particles diffusion, poor osteointegration and infections.

In order to improve the reliability and duration of this type of bone implants, appropriate alternative biomaterials should be capable to provide mechanical strength while modulating cells response to improve tissue regeneration.

Bioceramics are a diverse category of materials that offer several interesting properties for bone tissue engineering and have been continuously used as bone fillers, scaffolds and components of dental and orthopaedic implants. However, as explained by Chevalier *et al* (2009), the biggest challenge with ceramics is that no tough ceramic can create a strong biologically relevant interface with bone, while bioactive ceramics, that can promote direct bone-implant adhesion, are all incapable of being used in load bearing applications.[1]

Alumina toughened Zirconia (ATZ) has been recently introduced as a bioceramic that combines improved mechanical strength and toughness when compared to the monolithic materials, higher resistance to low temperature degradation and easier processing/machining. [2]

Still, being a hard ceramic, ATZ lacks appropriate interfacial bonding with the surrounding tissues, thus requiring surface functionalization, to improve cell adhesion and tissue regeneration.

With such purpose aiming at bone substitution applications, it is essential to design biomaterials with improved surface properties, without compromising the material bulk characteristics, especially the mechanical strength, hardness and toughness.

Surface functionalization with physical cues offers several advantages over some chemical modifications. Topographic modifications are much more stable *in vivo* than surface chemistry modifications and may control cell behaviour at the specific site. The use of topographic features has been a continuously growing area of research for tissue

regeneration. Numerous studies have shown that both micro- and nano-scale topographical patterning can influence cell interactions with surfaces and enhance cell adhesion and proliferation, up-regulate specific cytoskeletal and extracellular matrix proteins, reduce the immunological response and increase osteogenic differentiation. [3-6]

Both surface modifications applied to improve Alumina toughened Zirconia biological properties were successfully developed. The micropatterned silica coatings are a versatile surface modification that can be applied to different materials, such as glass and ceramics, without altering the substrate mechanical or chemical properties. [7-9]

Likewise, the surface functionalization with the femtosecond laser didn't alter the ATZ surface chemistry.

As expected, the surface topography and roughness were clearly altered with both surface modifications. The increased micro- and nanoroughness led to increased hydrophobicity on both surfaces, a relationship that has been previously reported and was confirmed in our experiments. [10-11]

Topography-mediated fate determination of hMSC has enormous potential to allow the design of specific implant surfaces capable of promoting rapid and more effective osteointegration. [12] Still, it is common that researchers use chemical stimuli to evaluate the osteogenic differentiation of Mesenchymal Stem Cells. However, these results can't be translated to *in vivo* situations and some of the soluble factors used are known to cause adverse effects. [13-15]

The results obtained from both *in vitro* cultures show that a range of microtopographic features can promote osteogenic differentiation of hMSCs under basal conditions, and that this stimulation can be more or less enhanced depending on the geometric pattern arrangement. In addition, hMSCs showed to be greatly affected by well-defined microtopographic cues rather than by nanotexturing.

Other interesting finding was that mesenchymal stem cells behaviour and osteogenic differentiation were enhanced on both bioactive (silica) and bioinert (ATZ) surfaces, with distinct chemistry and surface reactivity, due to the presence of surface topographic cues. As expected in bioactive materials, the micropatterned silica coatings caused enhanced cell response, osteogenic differentiation and mineralization. With regard to the bioinert surface of ATZ, the developed microfeatures were capable of guiding cell adhesion, orientation and proliferation, in addition to improving the osteogenic response of the cells.

The obtained results allowed to establish that surface topography may be used to improve cellular response to bioinert ceramics, guiding cell adhesion and proliferation and differentiation pathway.

More than one approach can be pursued to satisfy different requirements of biomaterials or medical applications. In the end, the selection must take into consideration the processing method, applicability, reproducibility and *in vivo* reliability.

This being said, the laser textured material presents some advantages over the micropatterned silica coatings. Femtosecond laser processing is a single-step processing method with no chemical residues that can precisely pattern different materials with none or only residual surface contamination.

Moreover, it can be applied to different shapes and the final component contains only one type of material, being able to withstand higher forces, since there is no interface between two materials.

Being one final material, it is expected that it will be able to endure high mechanical stress and torque without compromising surface topography, nor inducing cracking or component failure due to unexpected fracture.

This is not the case for the silica coatings. Although the adhesion of the coating to the ceramic surface may be strong, certain types of procedures, as the implantation of a dental implant, for example, could exceed the adhesion strength of the film, causing its detachment or rupture.

This was one of the main reasons why the approach with ultrafast laser technology was introduced in this work, as a mean to overcome the difficulties arising from having a bioactive thin film, while keeping the advantages of introducing surface topography, capable of conditioning cell adhesion, proliferation and differentiation.

High performance ceramics with adequate mechanical characteristics and tailored surface, capable of modulating host-implant interactions, would greatly improve the current strategies.

The obtained results point towards the possibility of developing Alumina toughened Zirconia based biomaterials that might withstand long-term shelf-life and be used in load-bearing conditions such as dental and maxillofacial implants in order to produce guided tissue regeneration and enhance implant osteointegration.

FUTURE WORK

In terms of future perspectives, additional experiments should be performed, in order to strengthen the results described in this work.

To further improve the surface bioactivity, the addition of bioactive nanoparticles to the surface could be tested. Aggregates of bioactive nanohydroxyapatite (nanoHA) can be applied by using the same laser source as the one used to texture ATZ, with the technique of pulsed laser deposition (PLD). With this technique it is possible to create a discontinuous film of nanoHA particles on the previously textured ceramic. Certain parameters can be changed to adjust the amount of nanoparticles that can be deposited on the textured surface. This complementary technique would be interesting from the point of view of improving surface bioactivity while maintaining a simple process of surface functionalization.

Detailed mechanical characterization of the laser treated ATZ should be conducted, with the intent of evaluating possible interferences of the laser treatment on the mechanical properties of the bulk material. Such tests should provide an initial perspective to the material performance *in vivo* and its reliability to constitute different types of implants.

One of the drawbacks associated with Titanium dental implants is the possibility of bone infections, such as peri-implantitis and osteomyelitis. Particularly, when working with materials with increased roughness and surface area, this subject needs to be further considered.

In terms of bacterial adhesion and growth, there is still discrepancy in results regarding bacterial response to patterned surfaces. Adequate bacterial adhesion and biofilm formation tests should be carried-out, with different pathogens associated to bone and periodontal infections and distinct methodologies, for example both under static and dynamic flow conditions.

Finally, adequate *in vivo* experiments should be designed and performed. The proposed model is to compare the response of the laser textured ATZ *versus* the unmodified ATZ when implanted in an animal model. *In vivo* experiments will allow to observe the overall tissue response to ATZ materials implantation at bone/implant interfaces.

References

1. Chevalier, J.; Gremillard, L. Ceramics for Medical Applications: A Picture for the Next 20 Years. *Journal of the European Ceramic Society* **2009,** *29*, 1245-1255.
2. Yang, Y.; Kang, Y.; Sen, M.; Park, S. Bioceramics in Tissue Engineering. In *Biomaterials for Tissue Engineering Applications*, Springer: **2011**, pp 179-207.
3. Craighead, H. G.; James, C. D.; Turner, A. M. P. Chemical and Topographical Patterning for Directed Cell Attachment. *Curr Opin Solid St M* **2001,** *5*, 177-184.
4. Watari, S.; Hayashi, K.; Wood, J. A.; Russell, P.; Nealey, P. F.; Murphy, C. J.; Genetos, D. C. Modulation of Osteogenic Differentiation in Hmscs Cells by Submicron Topographically-Patterned Ridges and Grooves. *Biomaterials* **2012,** *33*, 128-136.
5. Ito, Y. Surface Micropatterning to Regulate Cell Functions. *Biomaterials* **1999,** *20*, 2333-2342.
6. Wilkinson, C. D. W.; Riehle, M.; Wood, M.; Gallagher, J.; Curtis, A. S. G. The Use of Materials Patterned on a Nano- and Micro-Metric Scale in Cellular Engineering. *Mat Sci Eng C-Bio S* **2002,** *19*, 263-269.
7. Laranjeira, M. S.; Carvalho, A.; Pelaez-Vargas, A.; Hansford, D.; Ferraz, M. P.; Coimbra, S.; Costa, E.; Santos-Silva, A.; Fernandes, M. H.; Monteiro, F. J. Modulation of Human Dermal Microvascular Endothelial Cell and Human Gingival Fibroblast Behavior by Micropatterned Silica Coating Surfaces for Zirconia Dental Implant Applications. *Science and technology of advanced materials* **2014,** *15*, 025001.
8. Carvalho, A.; Pelaez-Vargas, A.; Hansford, D. J.; Fernandes, M. H.; Monteiro, F. J. Effects of Line and Pillar Array Microengineered Sio2 Thin Films on the Osteogenic Differentiation of Human Bone Marrow-Derived Mesenchymal Stem Cells. *Langmuir : the ACS journal of surfaces and colloids* **2016,** *32*, 1091-100.
9. Pelaez-Vargas, A.; Gallego-Perez, D.; Magallanes-Perdomo, M.; Fernandes, M. H.; Hansford, D. J.; De Aza, A. H.; Pena, P.; Monteiro, F. J. Isotropic Micropatterned Silica Coatings on Zirconia Induce Guided Cell Growth for Dental Implants. *Dental materials : official publication of the Academy of Dental Materials* **2011,** *27*, 581-9.
10. Jung, Y. C.; Bhushan, B. Contact Angle, Adhesion and Friction Properties of Micro-and Nanopatterned Polymers for Superhydrophobicity. *Nanotechnology* **2006,** *17*, 4970.
11. Barthlott, W.; Neinhuis, C. Purity of the Sacred Lotus, or Escape from Contamination in Biological Surfaces. *Planta* **1997,** *202*, 1-8.
12. Hamilton, D. W.; Wong, K. S.; Brunette, D. M. Microfabricated Discontinuous-Edge Surface Topographies Influence Osteoblast Adhesion, Migration, Cytoskeletal Organization, and Proliferation and Enhance Matrix and Mineral Deposition in Vitro. *Calcified tissue international* **2006,** *78*, 314-325.
13. Murphy, W. L.; McDevitt, T. C.; Engler, A. J. Materials as Stem Cell Regulators. *Nat Mater* **2014,** *13*, 547-557.
14. Brammer, K. S.; Choi, C.; Frandsen, C. J.; Oh, S.; Jin, S. Hydrophobic Nanopillars Initiate Mesenchymal Stem Cell Aggregation and Osteo-Differentiation. *Acta Biomater* **2011,** *7*, 683-690.
15. You, M. H.; Kwak, M. K.; Kim, D. H.; Kim, K.; Levchenko, A.; Kim, D. Y.; Suh, K. Y. Synergistically Enhanced Osteogenic Differentiation of Human Mesenchymal Stem Cells by Culture on Nanostructured Surfaces with Induction Media. *Biomacromolecules* **2010,** *11*, 1856-1862.